Designing a Plasma Controlled UAV

AE3200 - Design Synthesis Exercise

Group 07

Algera E. G.	4158326
Bauer Y.	4210654
van Hauwermeiren A. E.	4171616
van 't Laar V. C.	4144481
Pronk E. J.	4094018
Roos T.	4209648
Saß K.	4131916
Sonneveld V. C.	4218426
Waars N. D.	4226275
Wang S.	4224671

Chief Supervisor: M. Kotsonis, PhD. ,

Assistant Supervisors: A. Sciacchitano, PhD. - J. Ellerbroek, PhD. - W. Yu, MSc.

Delft University of Technology

TU Delft Delft University of Technology

Challenge the future

Preface

In the past ten weeks we have run trough the process from a blank sheet of paper to the full design of a plasma actuated unmanned aerial vehicle. These ten weeks have been a combination of hard work and fun. We would like to mention a few persons that contributed significantly to the realisation of the plasma UAV.

First of all, we would like to especially thank our supervisors staff of the Faculty of Aerospace Engineering of the TU Delft: our tutor Marios Kotsonis, PhD. our co-tutor Andrea Sciacchitano, PhD. and both of our coaches Joost Ellerbroek, PhD. and Wei Yu, MSc. Not only the advice on the delivered work and weekly meetings helped us, but their shared expertise gave us a great additional benefit. We would furthermore like to thank Guiseppe Correale, MSc. for his great introduction on plasma actuators, Kitso Epema, BSc. for his view on the choices made in the design of the Dutch UAS drone and Jeroen Veerman, MSc. for sharing his database of reference UAVs.

Furthermore, we would like to thank Mirjam Snellen, PhD. of the Aircraft Noise and Climate Effects department for directing us to two valuable sources for estimating the noise that propellers induce. One of which was Lothar Bertsch, PhD. of the DLR. His insights on the propeller noise really gave us new insight. This was especially useful to us, since propeller noise still has quite some uncertainties; empirical models cannot be scaled and therefore do not apply to our design. Michael Arntzen, MSc of NLR and TU Delft helped us as well with the estimation of the noise of the propulsive system.

Finally, Ricardo Pereira, MSc. has helped us with the evaluation of the feasibility of a wing tip plasma actuator mechanism and Christos Kassapoglou, PhD. gave us advise about the approach of the structural analysis for composites.

Table of Contents

List of Figures

List of Tables

List of Symbols and Abbreviations

Abbreviations

AC	Alternating Current
AOA	Angle of Attack
BR	Baseline Review/Report
BW	Battery Weight
CAD	Computer-Aided Design
CAGR	Compound Average Growth Rate
CFD	Computational Fluid Dynamics
CFRP	Carbon Fibre Reinforced Polymer
CG	Center of Gravity
COG	Center of Gravity
CPU	Central Processing Unit
CW	Contingency Weight
DBD	Dielectric Barrier Discharge
DC	Direct Current
DC	Duty Cycle
DLR	Deutsches Zentrum für Luft- und Raumfahrt
DSE	Design Synthesis Exercise
EMI	Electromagnetic Interference
ESC	Electronic Speed Control
FBS	Functional Breakdown Structure
FFBD	Functional Flow Block Diagram
FR	Final Review/Report
GPS	Global Positioning System
HLD	High Lift Devices
HTOL	Horizontal Take-Off and Landing
LCA	Life Cycle Analysis
LE	Leading Edge
MTOW	Maximum Take Off Weight
MTR	Mid Term Review
NLR	Nationaal Lucht- en Ruimtevaartlaboratorium
OEW	Operational Empty Weight
PP	Project Plan
PS	Pressure Side
PV	Photo-Voltaic
PW	Payload Weight
R&D	Research and Development
RAMS	Reliability, Availability, Maintainability and Safety
RC	Rate of Climb
RPM	Revolutions Per Minute
S.M.	Safety Margin
SFC	Specific Fuel Consumption
SPL	Sound Pressure Level
SS	Suction Side
SWOT	Strength, Weakness, Opportunities and Threat Analysis
TE	Trailing Edge
TS	Tollmien-Schlichting
UAS	Unmanned Aircraft System
UAV	Unmanned Aerial Vehicle
ULM	Ultra Léger Motorisé
VTOL	Vertical Take-Off and Landing
WBS	Work Breakdown Structure
WFD	Work Flow Diagram

Symbols

α	Angle of Attack	[°]
$\bar{c}$	Chord Length	[m]
β	Side-slip Angle	[rad]
$\ddot{\theta}$	Angular Acceleration	[rad/s^2]
ΔC_l	Change in Lift Coefficient	[-]
ϵ	Twist Angle	[°]
η_0, ξ_0	Distance from Shear Centre	[m]
η_p	Propeller Efficiency	[-]
η_{eng}	Engine Efficiency	[-]
η_{esc}	Electrical Speed Controller Efficiency	[-]
η_{tot}	Total Efficiency	[-]
$\frac{d\epsilon}{d\alpha}$	Downwash Gradient	[rad/rad]
Γ	Circulation	[m^2/s]
Γ_w	Dihedral Angle of the Wing	[°]
Λ	Sweep Angle	[°]
λ	Taper Ratio	[-]
$\Lambda_{0.25c}$	Sweep Angle at Quarter Chord	[°]
ν	Kinematic Viscosity	[m^2/s]
ω	Rotational Velocity	[rpm]
ϕ	Roll Angle	[rad]
ψ	Yaw Angle	[rad]
ρ	Air Density	[kg/m^3]
ρ_0	Air Density at sea level	[kg/m^3]
ρ_∞	Free Stream Density	[kg/m^3]
σ	Normal Stress	[Pa]
σ_{xx}	Normal Stress in x direction	[Pa]
τ	Shear Stress	[Pa]
τ_{xy}	Shear Stress in $xy-$plane	[Pa]
θ	Pitch Angle	[rad]
A	Aspect Ratio	[-]
a	Speed of Sound	[m/s]
b	Wing span main wing	[m]
b_h	Wing Span horizontal tail	[m]
B_n	Area of Boom n	[m^2]
b_v	Wing Span vertical tail	[m]
C	Battery Capacity	[Wh]
C_D	3D Drag Coefficient	[-]
C_d	2D Drag Coefficient	[-]
C_L	3D Lift Coefficient	[-]
C_l	2D Lift Coefficient	[-]
C_m	Moment Coefficient	[-]
$C_{D,max}$	Maximum 3D Drag Coefficient	[-]
$C_{D,0}$	Zero Drag Coefficient	[-]
C_{D_i}	Induced Drag Coefficient	[-]
C_f	Skin Friction Coefficient	[-]
c_{HT}	Horizontal Tail Volume Coefficient	[-]
c_h	Horizontal Tail Chord	[m]
$C_{L,max}$	Maximum 3D Lift Coefficient	[-]
C_{L_α}	Lift Gradient	[deg^{-1}]
C_{l_β}	Roll Moment Coefficient due to Sideslip	[-]
$C_{L_{des}}$	Design Lift Coefficient	[-]
C_{m_α}	Moment Coefficient due to Angle of Attack	[-]
$C_{m_{ac}}$	Moment Coefficient about aerodynamic centre	[-]
c_{MAC}	Mean Aerodynamic Chord	[m]
C_{n_β}	Yaw Moment Coefficient due to Sideslip	[-]
c_r	Root Chord	[m]
c_t	Tip Chord	[m]
c_{VT}	Vertical Tail Volume Coefficient	[-]
c_v	Vertical Tail Chord	[m]
D_{δ_a}	Rolling Duty Cycle	[-]
D_{δ_e}	Pitching Duty Cycle	[-]
D_{δ_r}	Yawing Duty Cycle	[-]
D_i	Induced Drag	[N]
D_{prop}	Propeller Diameter	[m]
E	Endurance	[s]
e	Oswald factor	[-]
$E_{bat,tot}$	Total Energy Capacity	[-]
f	Frequency	[Hz]
F^+	Normalized Pulse Frequency	[-]
f_c	Control Pulse Frequency	[Hz]
f_{pulse}	Pulse Frequency	[Hz]
g	Gravitational Constant	[m/s^2]
h	Cruise Altitude	[m]
$I_{m,xx}$	Mass Moment of Inertia around the $x-$axis	[kg m^2]
i_w	Wing Incidence Angle	[°]
I_{xx}	Area Moment of Inertia about $x-$axis	[m^4]
K_{ic}	Fracture Toughness	[Pa/$\sqrt{\text{m}}$]
L	Lift Force	[N]
L'	Lift per Unit Span	[N/m]
l_h	Tail Length	[m]
m	Mass	[kg]
M_x	Moment about $x-$axis	[Nm]
n	Load Factor	[-]
P	Power	[W]
p	Roll Rate	[rad/s]
P_a	Power Available	[W]
P_{br}	Brake-Shaft Power	[kW]
P_{elec}	Electrical Power	[W]
P_{peak}	Peak Power	[W]
P_r	Power Required	[W]
q	Pitch Rate	[rad/s]
$q_s, q_b, q_{s,0}$	Total, Basic and at Cut Shear Flows	[Pa]
q_∞	Free Stream Dynamic Pressure	[Pa]
R	Range	[km]
r	Yaw Rate	[rad/s]
$R_{turn,min}$	Minimum Turning Radius	[m]
Re	Reynold's Number	[-]
S	Wing Surface Area	[m^2]
S_h	Horizontal Tail Surface Area	[m^2]
S_v	Vertical Tail Surface Area	[m^2]
S_x	Shear Force along $x-$axis	[N]
t	Skin Thickness	[m]

t/c	Thickness to Chord Ratio	[-]
T/W	Thrust to Weight Ratio	[-]
T_{max}	Maximum Engine Thrust	[N]
$t_{turn,min}$	Minimum Turning Time	[s]
U_∞	Wind Tunnel Airspeed	[m/s]
V	Electrical Potential	[V]
V	Velocity	[m/s]
V_∞	Free Stream Velocity	[m/s]
V_{cruise}	Cruise Speed	[m/s]
V_h/V	Tail Speed Ratio	[-]
V_{loiter}	Loiter Speed	[m/s]
V_{max}	Maximum Speed	[m/s]
$V_{parachute}$	Parachute Descent Speed	[m/s]
V_{range}	Range Speed	[m/s]
V_{stall}	Stall Speed	[m/s]
W	Weight	[N]
W/P	Power Loading	[N/W]
W/S	Wing Loading	[N/m^2]
x, y, z	Distance from Centroid or Neutral Axis	[m]
X_{act}	Distance between Separation Point and Actuator	[m]
x_{ac}	Aerodynamic Centre Location	[m]
$x_{cg,fuselage}$	Fuselage c.g. location from wing quarter-chord	[m]
x_{cg}	Centre of Gravity Location	[m]

Summary

In this final report the result of a 10 week Design Synthesis Exercise of a plasma controlled UAV is presented. When conventional control surfaces are used on small UAVs, they become very fragile and unreliable due to the many small moving parts they involve. To solve this, plasma actuators could be used to control small UAVs; they are lightweight, consume little power and are very simple and reliable. Up until now, only research has been done on the concept of plasma actuator control. In order to take the next step in this field, research needs to be put into practice by designing a proof of concept. The purpose of this Design Exercise is to come up with a design of such a flying prototype, which can be used to test some plasma control concepts in practice.

Project Overview

The report starts off with a conceptual overview of the project, in which the mission of the UAV is examined and the results of the plasma actuator research are presented. It is found that there are in total eight mechanisms with which plasma actuators can control the flow, each with their own advantages and limitations. As for the mission of the UAV, the top level requirements are defined and additional requirements regarding UAV operations are set. The main requirements are that the UAV shall have a range of 10 km, an endurance of 2.0 hours, a 1.0 kg payload and a maximum wing span of 3.0 meters. Some of the additional requirements are that the UAV shall be able to fly in rainy weather conditions and that it shall be operable with a certain amount of ease. The additional requirements were set using the functional breakdown of the UAV, in which the specific (sub)system functions were defined.

With the requirements set in the project overview, a constraint analysis was performed. This constraint analysis led to a design wing loading of 82 N/m^2 and a design power loading of 0.45 N/W. In addition, the stall speed was set to 10 m/s, the aspect ratio was taken to be 7.75, the maximum C_L was taken to be 1.4, and the climb rate was set to 1.25 m/s.

Technical Design

With the rough design parameters known, the detailed technical design of the UAV was started. The main parameters that came out of this are presented in Table 1. The engine was sized first, based on the outcome of the constrain analysis. With the engine power known, the battery was sized, taking into account a margin for the plasma actuator power. With the battery size known and the other fuselage components set in earlier reports, the fuselage was designed. This includes the placement of the parachute, which will be used in case of an emergency landing.

The aerodynamic design was performed next. This obviously revolved around the integration of plasma actuators, so first the control mechanisms discovered in the literature research were investigated further through a wind tunnel test and with several analytical solutions. From these investigations, it was found that the maximum change in lift coefficient for normal flight conditions is achieved on a blunt trailing edge airfoil. The results from this investigation were then used in the airfoil selection and wing planform design. It was decided to use two airfoils, to aid in the plasma actuator integration; the main wing mainly consists of a cambered airfoil, to increase the lift generation capability of the wing. At the tip, this airfoil transitions into a blunt airfoil, for which plasma actuators have the best performance. The tail also uses this blunt airfoil, for the same plasma dominated reasons. The main parameters of the wing can be found in Table 1.

With the main wing lay-out and dimensions known, the structural design of the UAV was started. The main priority of the structural design was to come up with the lightest possible design, since it is desirable to keep the UAV weight as low as possible. It was decided to use TeXtreme for the wing structure, a very strong and lightweight material. The core of the wing is made of PUR foam. After conducting a stress analysis, it was found that the wings are sufficiently strong if the minimum of 2 layers of fibre required to obtain an quasi-isentropic material are used. The tail will also be made of the TeXtreme-PUR material combination, while the tail booms will be made from hollow carbon rods, whereas the fuselage will be made with TeXtreme and Airex foam. The fuselage structure has been specifically designed to withstand the landing loads, and all other components also passed the stress analysis.

With the weight of the UAV now known and the aerodynamic UAV properties defined, a stability and control analysis was performed. The results of this analysis were used to size the different tail properties. These properties can again be found in Table 1. The aircraft is both statically and dynamically stable at all times, partly because of the rather long tail arm. From the structural analysis the mass properties of the aircraft were derived, and after combining these properties and the results of the aerodynamic analysis of the plasma actuators the obtainable control rates were calculated. These rates, which can be found in Table 1, were found to be similar to control rates that can be achieved with conventional control surfaces.

Operations

After the technical design of the UAV was done, the operational side of the project was investigated. First of all, a production plan was set up, in which the prototype production process is described in detail. This also led to an accurate estimation of the production costs. Subsequently an operational analysis of the aircraft was performed. This included the definition of the take-off and landing procedure; take-off will be performed using a launcher, which will propel the UAV to around 11 m/s, after which its engine will take over. For landing, the UAV will be brought very close to the ground, at which point it is pitched to an angle of 14 degrees, at which angle the HLD are activated. The UAV can then touch down (fuselage first) at a low enough speed to prevent structural damage.

Next, the UAV avionics were designed. A unique flight controller layout was required for the plasma actuator control. Every single flight motion requires it's own channel, and to achieve this the Pixhawk 3D autopilot was chosen. This autopilot is connected to the custom high voltage circuit, which provides the plasma actuator with the required high-voltage AC signal. This signal is generated using a Minipuls bridge board and automotive ignition coils. The rest of the flight control system, consisting of sensors, remote control and telemetry components, was also sized. For communications an antenna emitting a half sphere was used, the specifications of which can be found in Table 1. To provide an overview of the flight control and communications systems, wiring diagrams were made for both.

Up until this point the UAV performance was only know for a couple of flight conditions, so a performance analysis was performed. A typical UAV mission profile was analysed, and the turn and climb performance of the UAV were mapped. The results of the performance analysis can again be found in Table 1. From the performance analysis it was concluded the UAV performs up to par, and hence a mass, cost and power budget of the final design were established. In addition, the environmental impact of the UAV was assessed and found to be quite low. Finally, the impact and possibility of several system failures was assessed in a risk analysis. The acceptable risk for the UAV is quite high, since it is a prototype, but it was found that the design is fail-safe in most cases.

To complete the design process, this first iteration of the UAV design was assessed and several recommendations to improve the design were made. These include more time in the wind-tunnel to test aerodynamic and stability concepts, and a more optimal structural design.

Table 1: Summary of UAV parameters

	Parameter	Symbol	Value	Unit
Wing	Aspect ratio	A	7.75	-
	Main wing span	b	3.0	m
	Wing root profile		NACA63A-915	
	Wing tip profile		NACA64A-015	
	Wing span horizontal tail	b_h	0.70	m
	Wing span vertical tail	b_v	0.30	m
	Wing surface area	S	1.16	m^2
	Horizontal tail surface area	S_h	0.21	m^2
	Vertical tail surface	S_v	0.15	m^2
	Taper ratio	λ	0.5	-
	Quarter chord sweep	$\Lambda_{.25c}$	0	$^\circ$
	Twist angle	ϵ	0	$^\circ$
	Dihedral	Γ	3	$^\circ$
	Wing incidence angle	i_w	2	$^\circ$
	Tip chord	c_t	0.257	m
	Root chord	c_r	0.515	m
	Mean aerodynamic chord	c_{MAC}	0.401	m
	Horizontal tail chord	c_h	0.3	m
	Vertical tail chord	c_v	0.3	m
	Wing loading	W/S	82	N/m^2
	Power loading	W/P	0.45	N/m^2
	Max. lift coefficient	$C_{L,max}$	1.4	-
	Max. drag coefficient	$C_{D,max}$	0.1	-
	Zero drag coefficient	$C_{D,0}$	0.01	-
	Plasma actuator length	L_{plasma}	6.15	m
Propulsion	Propeller diameter	D_{prop}	0.33	m
	Max. rotation speed	ω	6500	rpm
	Max. shaft power (brake power)	P_{br}	211	W
	Max. engine thrust	T_{max}	16	N
	Thrust to weight ratio	T/W	0.17	-
	Max. sound pressure level	SPL	94	dB
Stability	Tail length	l_h	2.2	m
	Fuselage c.g. location from 0.25 chord	$x_{cg,fuselage}$	0.62	m
	Moment coefficient due to angle of attack	C_{m_α}	-1.73	-
	Roll moment coefficient due to sideslip	C_{l_β}	-0.04	-
	Yaw moment coefficient due to sideslip	C_{n_β}	0.21	-
Systems	Total energy capacity	$E_{bat,tot}$	326	Wh
	Peak power	P_{peak}	405	W
	Data range	R_{data}	22	km
	Data transfer rate	f_{data}	125	kbps
Performance	Maximum take-off weight	$MTOW$	9.96	kg_f
	Cruise altitude	h	300	m
	Stall speed	V_{stall}	10	m/s
	Cruise speed	V_{cruise}	13	m/s
	Loiter speed	V_{loiter}	13	m/s
	Range speed	V_{range}	17	m/s
	Max. speed	V_{max}	29	m/s
	Parachute descent speed	$V_{parachute}$	6	m/s
	Range	R	10	km
	Endurance	E	2.0	h
	Rate of climb	RC	1.25	m/s
	Min. turning radius	$R_{turn,min}$	17.7	m
	Min. time to turn	$t_{turn,min}$	5.6	s
	Max. roll rate	p	47	$^\circ$/s
	Max. pitch rate	q	55	$^\circ$/s
	Max. yaw rate	r	36	$^\circ$/s
	Reynolds number range	Re	250,000-550,000	-

Chapter 1 - Introduction

A Design Synthesis Exercise (DSE) work-group of ten Bachelors Aerospace Engineering students has been assigned with the task to design a fully plasma controlled Unmanned Aerial Vehicle (UAV). Instead of having movable control surfaces, such as a rudder and ailerons, the control of the UAV is to be done with the use of plasma actuators. In short, plasma actuators contain two electrodes, which can be attached to the wing and the empennage. When applying a high voltage over the electrodes, plasma will be generated which basically can accelerate the air in a direction, thereby altering the airflow. This feature can be used for control, although a fully plasma controlled UAV does not exist to this day. More in depth information on the concept of plasma actuation can be found in Section 2.1.

Recent research in plasma actuators has shown promise for their application in flow control [1]–[8], more specifically over airfoils [9] and specifically for UAVs [10], [11]. These promising plasma actuators have advantages over conventional control surfaces since they have no moving parts. This means that they are easier to maintain and therefore reduce the maintenance costs. Plasma actuators take away the complexity of servos and moving parts found in conventional control surfaces, and thereby increase the reliability. Next to that, the response of plasma actuators can be considered very fast. As of today, plasma actuation has not been applied in aircraft configurations to fully replace conventional control surfaces. The limited available experience in application and testing of plasma actuators in flight create an opportunity for innovation and therewith the design of a plasma controlled flying vehicle. Control with the use of plasma leads to fast responses of the flying vehicle, which makes it a promising concept. Plasma actuation is currently most effective at low operating speeds, thus a UAV is chosen for implementation and demonstration of this technology. The outline of the entire design process of such a plasma controlled UAV is to be reported.

The main purpose of this report is to present and elaborate on the design of a fully plasma controlled UAV. The design choices that were made in the mid-term report are used as basis for the final design. After the initial sizing and some preliminary design choices, the group continued on the design to end up with a plasma actuator controlled UAV. The main focus lies in the technical details where all design choices and methods are discussed. Furthermore, a project overview is given along with operational details.

A road map of the report structure is shown in Fig. 1.1. Chapter 2 provides an overview of the preliminary design that was drafted in the first stage of the project. This is explained in more detail in the Mid-Term Report [12]. The process that led to this preliminary design is split up in three chronological parts: literature study, mission analysis and top level concept. This provides a rough baseline and basic configuration, which sets for instance the weight, power and cost budget that have to be achieved in the detailed design phase. The baseline of the design is described thoroughly in Chapter 3. This will act as a base for the technical design details that will follow in Chapter 4, where each subsystem - fuselage group, aerodynamics, structures and control - of the plasma UAV is discussed in detail. The covered elements on the subsystems are the specifications, trade-offs, sensitivity on design, verification and validation. Note that once all subsystems have been worked out, the design as a whole is validated. Hence the technical details chapter ends with the detailed design of the plasma UAV. Moreover, Chapter 5 addresses to the operational aspects of the UAV, so everything that happens after design. This includes an operational and logistic concept, avionics and ground system set-up. Then the overall UAV performance and all technical risks are analysed. Finally, Chapter 6 presents a review of the whole project. Have all requirements been met? If more time was available, which parts would be explored in more detail and subsequently be improved? This chapter draws conclusions for the whole project.

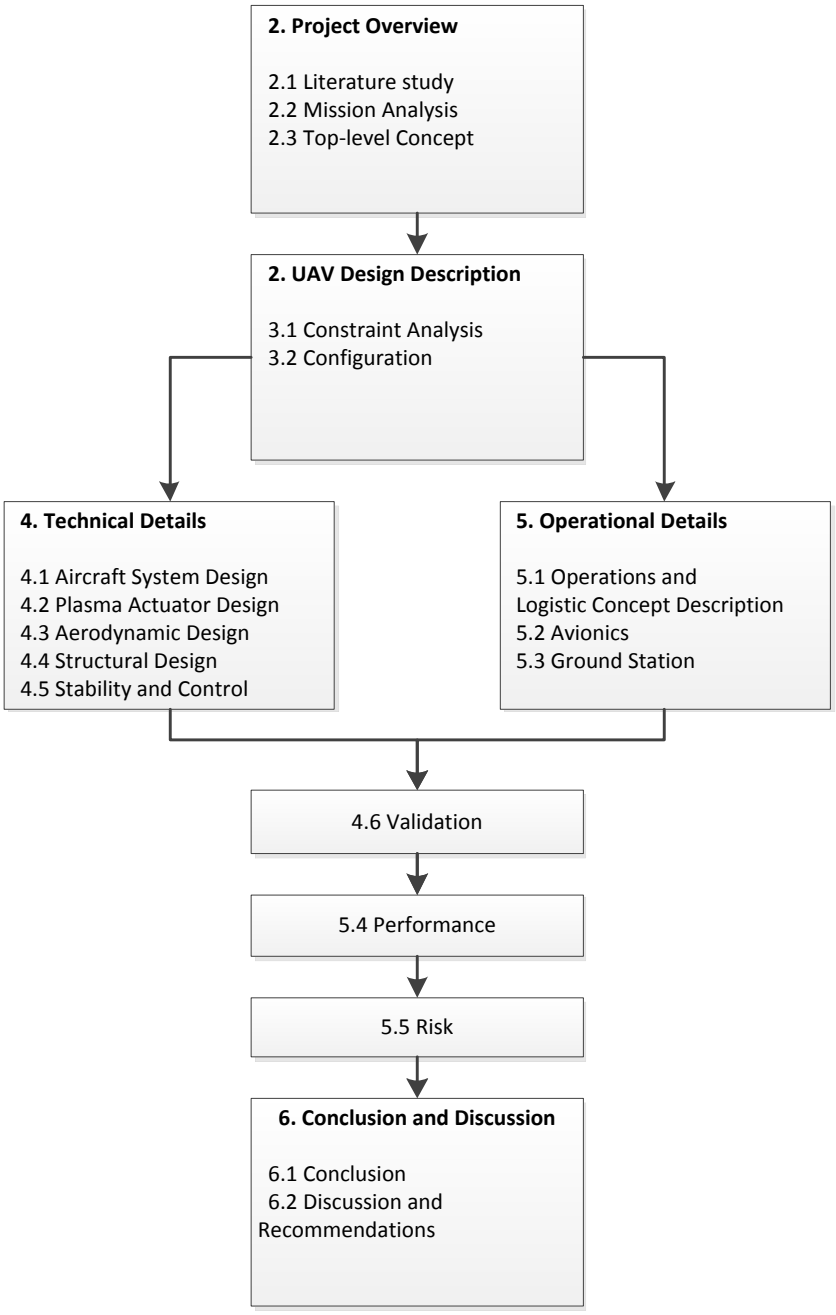

Figure 1.1: Road map of the report.

Chapter 2 - Project Overview

This chapter gives an overview of the whole DSE project. The goal is to design a plasma actuated UAV and this goal is explained in detail in two parts. The first section describes the literature study, consisting of the UAV market analysis and the principle and different mechanisms of plasma actuation are discussed. The second part, Section 2.2, explains the mission, which comprises the requirements, the functional breakdown and flow diagram. Once the project overview is clear at the end of this chapter, the top level concept is presented in Chapter 3.

2.1 Literature Study

The literature study provides background information in order to get a better insight on the plasma actuated UAV design. This information is divided into two parts. First the UAV market analysed, including a strength, weakness, opportunities and threats (SWOT) analysis. Secondly, Section 2.1.2 explains the principles of plasma actuation and eight distinguishable actuation mechanics.

2.1.1 Market Analysis

The plasma actuator is a recently new developed technology that can change the current market: the opportunity to use plasma actuators instead of conventional control surfaces renders less maintenance and more reliable aircraft. The scope of this UAV design restricts to research on the implementation of plasma actuators for control and developing a prototype. Hence, there is not a direct commercial opportunity. The product can however turn out to be of significant value for a specific purpose and therefore penetrate the market. For this reason the payload is designed to be modular, so that it can be easily adapted to a specific mission or purpose in the commercial, civil, military or scientific sector.

Specific applications require different mission profiles (a general mission profile is depicted in Fig. 5.13) in terms of requirements for i.e. agility, loiter time and endurance. Considering the performance requirements stated in Section 2.2.1 (range of 10 km, endurance of 2.0 hours, and payload mass of minimally 1.0 kg) the final product can be used for many applications, depicted in Fig. 2.1. Considering this wide range of applications, the UAV has to be adapted for every single application to meet specific requirements such as being able to continuously transmit live video footage, or autonomously analyse acquired data. Therefore, a collaboration could be set up with an external company that can implement a specific payloads.

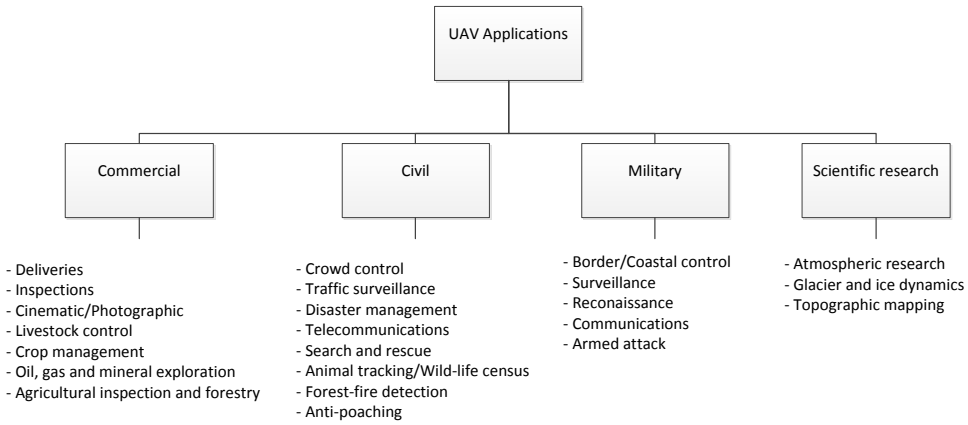

Figure 2.1: Selection of possible UAV mission options

Considering similar UAVs, a price of €10.000 would be a good estimation to not only cover the project price, production of the product and adaptation for the specific application, but also making some profit[1]. A breakdown of the costs can be seen in Table 5.9.

[1]RobotShop Distributon Inc., accessed on May 1, 2015: `http://wwww.robotshop.com/en/micropilot-mp-vision-uav-glider.html`

The market for UAVs is relatively new, but rapidly growing. According to the Teal Group, an aerospace consultant, the UAV market is expected to double within the next ten years. Global UAV expenditure will grow from "$6.4 billion annually to $11.5 billion, totalling almost $91 billion in the next ten years"[2], as can be seen in Fig. 2.2[3]. Furthermore, the market for micro and small UAVs is expected to reach $1.9 billion by 2020 and file a Compound Average Growth Rate (CAGR) 12.31% until 2020[4]. The global UAV market is still dominated with military UAVs, but civil UAVs is the growing segment: 11% nowadays to 14% in 2024. The United States still account for 65% of the global R&D expenditure.

With respect to market dynamics, Porter's five forces[5] are considered. The threat of new entry is quite low since the technology for plasma actuators has to be researched first. The threat of substitute products is present in the form of conventional control surfaces. Once the advantages of plasma actuators have been proven, the threat can be regarded to be small. The same goes for competitive rivalry. There are many UAV companies on the market at the moment, although none with plasma technology. Buyer power is high as the market is quite saturated. Supplier power is low as materials and products are not difficult to obtain.

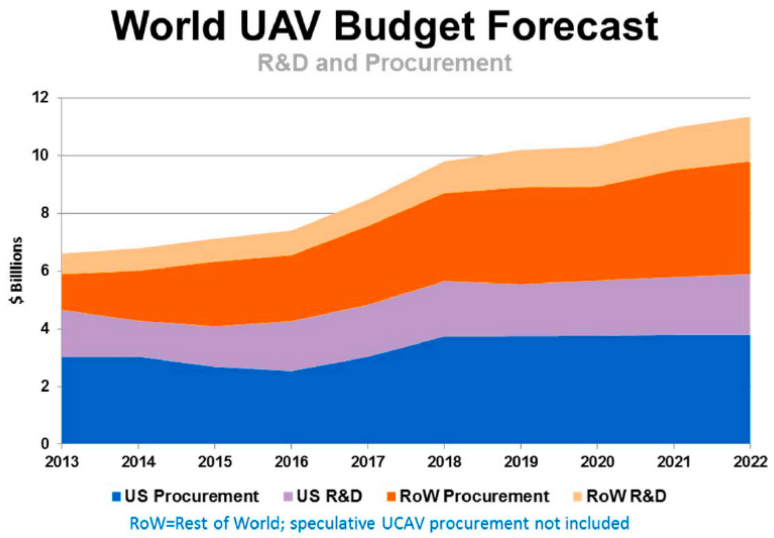

Figure 2.2: UAV market forecast

SWOT Analysis

To be able to analyse the positive and negative internal and external factors of the control of a UAV with plasma, a SWOT analysis is to be performed. The strengths, weaknesses, opportunities and threats are identified. In this analysis, strengths and weaknesses evaluate the UAV internally, while opportunities and threats look at potential external positive and negative influences.

Strengths:

- Successfully integrating a plasma actuator can significantly reduce structural weight of the wing.
- Since conventional control surfaces are no longer needed, there is no longer need for structural inspection of these complex control surface systems. Only electrical degradation should be assessed, which is simpler.
- Maintenance of the plasma actuators is easy, as they can be replaced easily.

Weaknesses:

- Current research has only yielded plasma actuators that are useful at low Reynolds numbers.

[2]Teal Group, accessed on April 23, 2015: `http://www.tealgroup.com/index.php/about-teal-group-corporation/press-releases/118-2014-uav-press-release`

[3]InvestingDaily, accessed on April 23, 2015: `http://www.investingdaily.com/17175/a-precision-investment-strike/`

[4]Markets forecast and analysis, accessed on April 23, 2015: `http://www.marketsandmarkets.com/Market-Reports/small-uav-market-141134567.html`

[5]Porter's five forces, accessed on June 25, 2015`http://www.cgma.org/Resources/Tools/essential-tools/Pages/porters-five-forces.aspx?TestCookiesEnabled=redirect`

- The plasma actuator is a working laboratory model, but it has never been successfully commercially implemented yet in aerospace industry.
- The creation of the high voltage AC signal for the operation of the plasma actuators still requires additional heavy electrical components, which keeps the weight-specific effectiveness low for now.

Opportunities:

- Once plasma actuators have proven to be effective for drag reduction, the additional weight of the electrical components has to be taken into account. As drag reduction method, they will definitely be implemented in slower aircraft, like ULMs.
- As soon as the legal issues around their implementation as control methods in manned aerial vehicles are solved, they can replace conventional control surfaces in aircraft.
- If plasma actuators are ever able to operate at higher Reynolds numbers, they will definitely replace control surfaces on commercial aircraft.

Threats:

- Since UAVs are relatively new to the general public, regulations for UAVs in general are changing frequently. This could influence the applicability of UAVs, and along with it the market and speed of innovation.
- Lack of experience and short operating time will refrain aircraft designers from implementing plasma actuators for roll, pitch and yaw control.

2.1.2 Plasma Actuators

In this subsection the working principle behind the plasma actuator is explained. This introduction will help understand the control mechanisms that can be employed by plasma actuators.

Principles

Plasma the most energetic of the four fundamental states of matter, after solid, liquid and gas. There are two ways to produce plasma, either by heating up a gas or by applying a high voltage between two electrodes . The easiest way is the second, where two electrodes ionize the air between them, Fig. 2.3. These electrodes are separated by a dielectric layer to obtain a Dielectric Barrier Discharge (DBD). In this type of plasma actuation, the discharge is not able to reach the other electrode and plasma will be present on the dielectric.

If it is assumed the top electrode is positive, the free electrons in the (metal) electrode will be pushed towards the dielectric by the electric field that is present. However, the negative ions in the ionized air will also start to move towards the dielectric, making it increasingly negatively charged. Because of this charge build-up on the dielectric, the field will become weaker and weaker, and at some point it will be too weak to create plasma. To prevent this from happening and create a self-sustaining plasma, AC current is used. After a certain amount of time (based on the AC frequency) the order of the current and thus the electric field is changed, reversing the direction of electron ion migration. This prevents the electric field from becoming too weak, hence creating a sustained plasma.

The principal effect of the plasma cloud (the area of ionized air) is the generation of a body force on the boundary layer and an acceleration of the air in the direction away from the upper electrode. The force is due to collisions between the highly energized plasma particles and the normal air particles. This force-phenomenon can be applied in three different ways on an airfoil. The plasma can be used to enhance or hinder the circulation around the airflow, change the transition point on the upper surface (which may result in controlled separation) or (partly) reattach a separated flow to achieve a higher lift coefficient. The exact mechanisms will be explained further in this section.

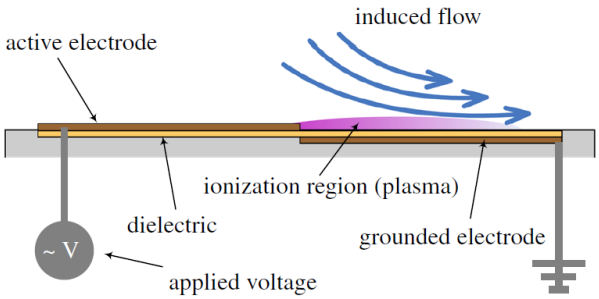

Figure 2.3: Layout of a plasma actuator [13]

Actuation Mechanisms

In order to control a UAV with a plasma actuator, a difference in lift coefficient, ΔC_L has to be achieved on one or more of its lifting surfaces. This is also the principal effect of a conventional control surface. In this section seven physical mechanisms are described, which could be used to create this difference in lift. The eight mechanisms can be grouped into two control modes, namely separation control and circulation control.

Separation Control Mode

The first mode plasma actuators can use to obtain a difference in lift coefficient, is to influence separation. One mechanism was identified that prevents separation and three were identified that promote it.

Mechanism 1:

The first mechanism to prevent separation or to reattach the flow, is to make the flow turbulent, ahead of the separation bubble. Turbulized flow has more energy and is less susceptible to separation, which makes sure it does not leave the airfoil as easily as laminar flow does. The turbulent flow therefore pushes back the separation bubble and/or makes it smaller. This more energized flow can be created by exciting the Tollmien-Schlichting (TS) waves present in the flow, provided that the plasma actuator is placed near the leading edge of the airfoil. At the trailing edge the flow is already separated, so plasma actuators placed here will not have any effect. This mechanism is comparable to passive leading edge vortex generators. The active vortex generation will perform well enough using plasma actuator pulsed at a predetermined actuation frequency. To pulse the signal with optimal effectiveness, the TS wave frequency could be determined during operation. This could be done by reactive control, but as it would imply some of heavy sensors, increased computational power and aerodynamics that are out of the scope of this project, only the passive mechanism will be considered in Section 4.2.3.

Mechanism 2:

The second mechanism promotes separation by keeping the flow laminar. This will make the flow separate earlier. When the flow is actively kept laminar until separation it will have less energy to withstand a pressure gradient, making it separate earlier and reducing the overall lift coefficient. This can be achieved by damping out the TS waves in the flow with the plasma actuator. To be able to use this mechanism effectively, the frequency of the TS waves has to be known coupled to the actuator. This requires a lot of sensors, and is therefore quite a heavy system.

Mechanism 3:

The third mechanism looks a lot like mechanism 1. Instead of amplifying the TS waves, it uses the actuator to produce a jet, which simply energizes the flow without taking into account frequency. In terms of the boundary layer, this can be seen as blowing the inflection point out of the boundary layer velocity profile and filling the profile up, making it more resistant to pressure gradient. This requires only open loop control, but is less effective and therefore consumes more energy than mechanism 1.

Mechanism 4:

A fourth mechanism is to actively detach the flow. This could be achieved by for example blowing upstream of the airfoil, to try and blow an inflection point into the boundary layer. This mechanisms can be seen as the opposite of mechanism 3. Instead of energizing the flow, the flow energy is decreased, so a pressure gradient will lead to separation sooner.

Circulation Control Mode

The second control mode consists of four mechanisms as well. Mechanism 5 and 6 directly change the circulation of the flow around the airfoil, using plasma actuators perpendicular to the flow. The main difference between the two is that the flow reattaches in mechanism 6, but not necessarily in mechanism 5. The last two mechanisms adjust the circulation in span-wise direction, by placing the plasma actuators parallel to the cord. Mechanism 7 shields the suction region and mechanism 8 corrects the velocity mismatch at the trailing edge of the wing.

Mechanism 5:

The Kutta condition states that the flow at the trailing edge coming from the upper side of the airfoil should be tangent to the flow from the lower side. The fifth mechanism directly changes the orientation of this tangency point with respect to the trailing edge. This can be done by installing a plasma actuator near the trailing edge on the upper or lower side of a sharp trailing edge airfoil. When switched on, the plasma actuators change the momentum of the flow and with that the Kutta condition location moves. If the plasma actuators push in the clockwise direction, a downward movement of the Kutta condition is achieved, increasing the circulation around the airfoil. This increase in circulation will lead to an increase of the lift produced by the airfoil.

The same mechanism can produce a decrease in lift in an analogous way, by pushing in the counter clockwise direction. This will move the Kutta condition upwards, decreasing the circulation and hence the lift of the airfoil.

Mechanism 6:

The sixth mechanism works like a Gurney flap, only with greater effectiveness. A Gurney flap is a small tab installed at a right angle to the main stream at the pressure side of the trailing edge. They are generally used on airfoils that have a separation bubble on their suction side in clean configuration. When the Gurney flap is deployed, it deflects the lower streamline of the flow downward. Since the flow is subsonic, this change will also make the airflow over the top move downward and the Kutta condition location is moved. This movement of the Kutta condition will prevent the separation bubble from forming and will increase the circulation around the airfoil. These changes again increase the lift round the airfoil.

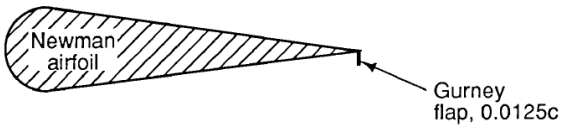

Figure 2.4: Layout of a Gurney flap [14]

Plasma actuators can mimic this Gurney effect, only they change the direction of the flow with a force instead of a change in the airfoil geometry. The top streamline is pushed down by the plasma actuator, reattaching it and moving the Kutta condition.

Proof that a plasma actuator can induce the Gurney effect can be found in literature. In reference [15], a plasma actuator is placed perpendicular to the chord line at the sharp trailing edge of a NACA 0012 airfoil and its effect is simulated. It was found that the actuator can produce an increase in lift coefficient of approximately 0.18, if positioned correctly. An even larger increase in lift was achieved for a blunt TE airfoil. The simulation in [8] shows that the lift coefficient increases dramatically when the plasma was actuated, from 0.086 to 0.904 at zero angle of attack.

The reason that blunt airfoils are more effective than sharp airfoils in achieving a ΔC_l lies in the type of Kutta condition they have. On a sharp airfoil, the flow around the top and the bottom are forced to come together at the end of the trailing edge, fixing the tangency condition to the airfoil. On a blunt airfoil, the flow cannot stay attached to the trailing edge in clean configuration, the curvature is too steep, so the streamlines will come together somewhere behind the TE. The Kutta condition is therefore not fixed to the airfoil and therefore easier to move. This will in turn lead to larger changes in the circulation and the lift of the airfoil.

Mechanism 7:

The third circulation mechanism operates similar to a winglet or tip tank. When a finite wing produces lift, the air will try to flow from the high pressure (lower) side towards the low pressure (upper) side around the wing tip. This motion creates a wing tip vortex, which can be counteracted by placing a winglet on the wing tip. This wing tip effectively increases the aspect ratio and hence the lift of the wing. Mechanism 7 can also counteract this 3D effect but in contrast to a winglet, which is always present, a plasma actuator can be turned on and off, and can therefore be used as a control mechanism. To investigate the effectiveness of this mechanism, the exact behaviour of a finite wing has to be researched more, starting with the lifting line theory.

As explained by Anderson [16], a wing can be represented by a 'bound vortex' and two 'free-trailing vortices', as illustrated in Fig. 2.5.

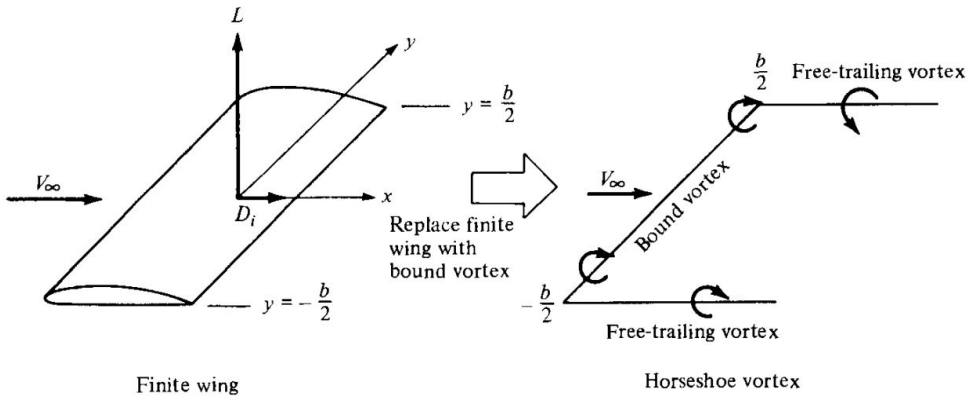

Figure 2.5: Lifting line representation of a finite wing [16]

The lift created by this vortex filament is proportional to its circulation, as determined by the Kutta-Joukowski theorem in Eq. 2.1.

$$L' = \rho_\infty V_\infty \Gamma \tag{2.1}$$

The circulation created by the bound vortex due to the generation of lift thus theoretically does not stop at the tips, but continues downstream via the free-trailing vortices until infinity. This gives rise to a horseshoe shaped vortex filament.

The single horseshoe model does not resemble reality, as the required downwash for this model to work approaches infinity at the bound vortex tips. A better representation is a number of superimposed horseshoe vortices, symmetrical around the middle of the lifting line, as shown on the left in Fig. 2.6. When the number of horseshoe vortices is increased further, the circulation Γ becomes a continuous function of the wing span location, as shown on the right of Fig. 2.6. Now the circulation and thus lift is maximum at the middle of the lifting line and zero at the wing tips and a continuous sheet of free-trailing vortices is leaving the lifting line. The density of this free-trailing vortex sheet is stronger, when the spanwise change in circulation $d\Gamma(y)/dy$ is larger. Therefore, when a realistic lift distribution is considered, the lifting line tip regions have very strong vortices attached to them.

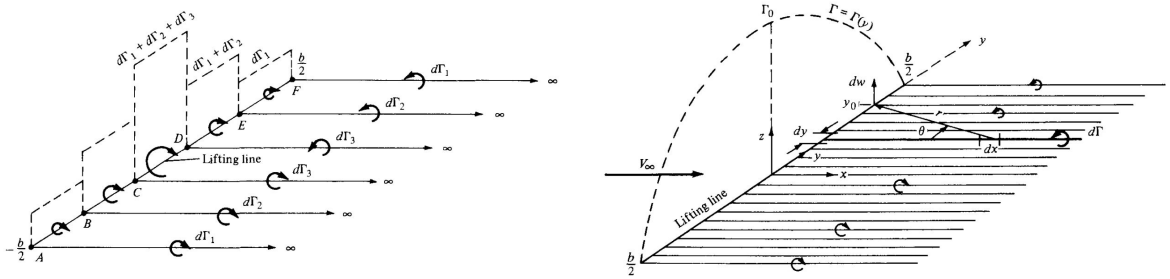

Figure 2.6: Lifting line representation of a finite wing [16]

The lifting line theory translates to reality remarkably well. Most prominently, the wing tip vortices can be observed. When the plasma actuators are placed in streamwise direction along the span, they create vortices that alter the sheet of circulation mentioned earlier. Near the wing tip, the plasma vortices should be able to shield the suction side from the flow trying to get around the wing tip. This is illustrated in Fig. 2.7a. The plasma actuator on the top pushes towards the wing, the actuator on the bottom pushes towards the root. These motions induce to small vortices, which form a sort of barrier for the flow. In addition, these small vortices accelerate the air from the top to the bottom, in the direction opposite to the flow. These two things will to a certain extent prevent the wing tip vortex from forming, reducing the 3D lift loss effect and temporarily increasing wing lift. The effect will be similar to that of a tip tank, as illustrated by two reference aircraft in Fig. 2.7b.

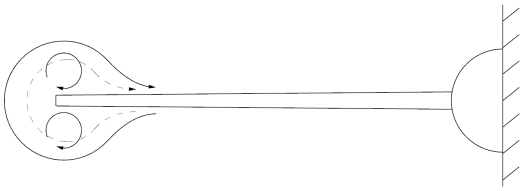

(a) Graphical representation of Mechanism 7

(b) Tip tanks on the Super Constellation

Figure 2.7: Systems influence the formation of wing tip vortices

To quantify the effectiveness of the winglet mechanism the difference between the 2D and 3D lift of the airfoil is considered.

Mechanism 8:

The last circulation mechanism, places the plasma actuators in the same streamwise direction as mechanism 7. Now the whole wing is covered with less powerful plasma actuators, to avoid concentrating their induced spanwise velocity.

To explain this mechanism the theory on the effect of a finite wing, explained in the previous section on mechanism 7, is applied in a different way. Apart from the wing tip vortices, the continuous sheet of circulation, decreasing in strength towards the middle of the lifting line, can also be observed in reality. The flow on the pressure side of the wing will tend towards the wing tips and the flow on the suction side is pushed towards the wing root. This creates a mismatch of their velocity vectors at the trailing edge, as can be seen in Fig. 2.8a. The layer of shear that is created, could be seen as the free-trailing vortex sheet translation to reality, culminating in the wing tip vortices, Fig. 2.8b.

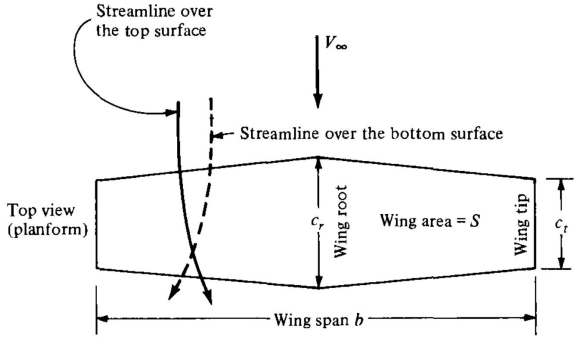

(a) The velocity mismatch between suction and pressure side of the wing[16]

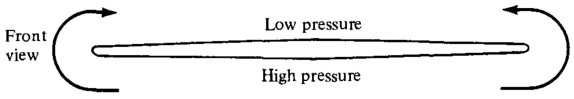

(b) Wing tip vortices [16]

Figure 2.8: A graphical representation of the 3D effect on a wing

Mechanism 8 fixes the mismatch in trailing edge velocities between the upper and lower surfaces, by adding a spanwise velocity component. Ideally, the trailing edge of the wing would have no circulation at all, like the bound vortex filament in Fig. 2.5 and all 'vortex shedding' could be removed. The more

the plasma actuators are placed and the more they are located near the wing tips, the more lift increase they should induce, as the velocity mismatch is the largest there.

A quantification of this mechanism is out of the scope of this project, because the ability of the plasma actuator to straighten out the flow is too uncertain. Intuitively the mechanism would be very effective and the ΔC_L large, if forcing of the flow could be achieved continuously over the whole wingspan. This would however imply a very large number of actuators, which is not desirable for a UAV.

2.2 Mission Analysis

The mission analysis consists of stating the requirements and analysing the UAV functions. Both the top-level and additional requirements are given in Section 2.2.1. The functional breakdown and functional flow diagram are schematic overviews which show how the UAV is built up with different systems and in which order the design of these systems occurs.

2.2.1 Top-level Requirements

Top-level requirements define the project and provide the first minimum and maximum constraints. A division can be made in functional requirements, performance requirements, system requirements, requirements on costs, sustainability and product development.

Functionality (TOP-FUNC):

1. The UAV shall have no moving control surfaces.
2. The UAV shall be controllable using plasma actuators.
3. The UAV shall have at least equal maximum pitch rates as similar conventional UAVs.
4. The UAV shall have at least equal maximum roll rates as similar conventional UAVs.
5. The UAV shall have at least equal maximum yaw rates as similar conventional UAVs.

Performance (TOP-PRF):

1. The UAV shall have a minimum range of 10 km.
2. The UAV shall have a minimum endurance of 2.0 h.
3. The UAV shall have a maximum wing span of 3.0 m.
4. The UAV shall have a minimum payload of 1.0 kg.

Systems (TOP-SYS):

1. The UAV shall have an autopilot with pre-programmed flight modes.
2. The UAV shall have a two-way telemetry compatibility.

Cost (TOP-CST):

1. The UAV program shall have a maximum cost of €10.000.

Sustainability (TOP-SUS):

1. The UAV shall produce equal or lower noise than similar UAVs.
2. The UAV shall have equal or lower emissions than similar UAVs.

Product Development (TOP-PD):

1. The UAV shall be designed by 10 students.
2. The UAV shall be designed within 10 weeks.

2.2.2 Additional Requirements

Apart from the top-level requirements given by the costumer, additional requirements have been set. The requirements are grouped into three categories: functionality requirements, performance requirements and system requirements.

Functionality (FUNC):

1. The UAV shall be able to fly in rain.
2. The UAV shall be able to be launched within 1 hour.
3. The UAV shall be stable.
4. The UAV shall have a fail-safe mode.
5. The UAV shall meet the Dutch regulations for UAVs [17].

Performance (PRF):

1. The UAV shall fly at an altitude of at least 150 m during cruise.
2. The UAV shall have a minimum cruise speed of 10 m/s.
3. The UAV shall have a maximum take off weight of no more than 10 kg.
4. The UAV shall have a minimum lifetime of 30 flight hours.

Systems (SYS):

1. The UAV shall have an airfoil with laminar stall.
2. The UAV shall have a battery that can be replaced within 15 minutes.
3. The UAV shall be able to store information on-board.
4. The UAV shall have a telemetry range of at least 10 km.

2.2.3 Functional Breakdown

Before the design phase, it is important to identify all the functions that the UAV has to perform. The Functional Breakdown Structure shows logical grouping of functions according to a predetermined set of criteria. The FBS is an AND-tree, therefore each element of the tree is the sum of elements below it [18]. The FBS is not laid out in a time-line manner as the Functional Flow Block Diagram (Section 2.2.4), but it gives a complete picture of the system functions.

The scope of this FBS is the complete plasma UAV system, containing the ground station (which determines the mission, programs the CPU, etc) as well as the UAV itself (landing, loitering, etc.). The first level FBS of the system (Fig. 2.9) is broken down into a second and third level in this section.

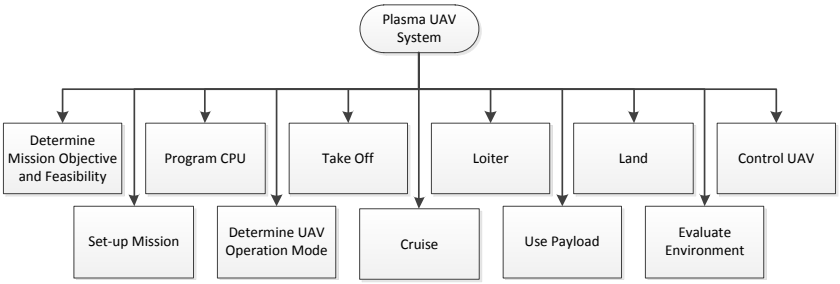

Figure 2.9: Functional breakdown structure, first level

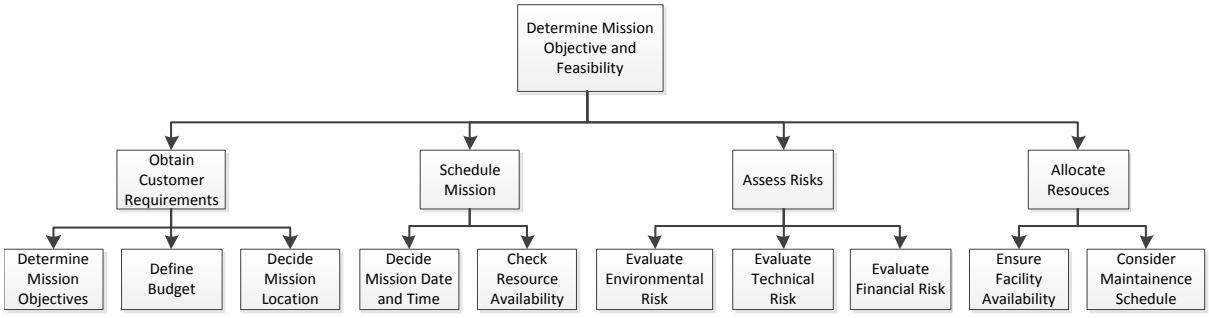

Figure 2.10: FBS: Determine mission objective

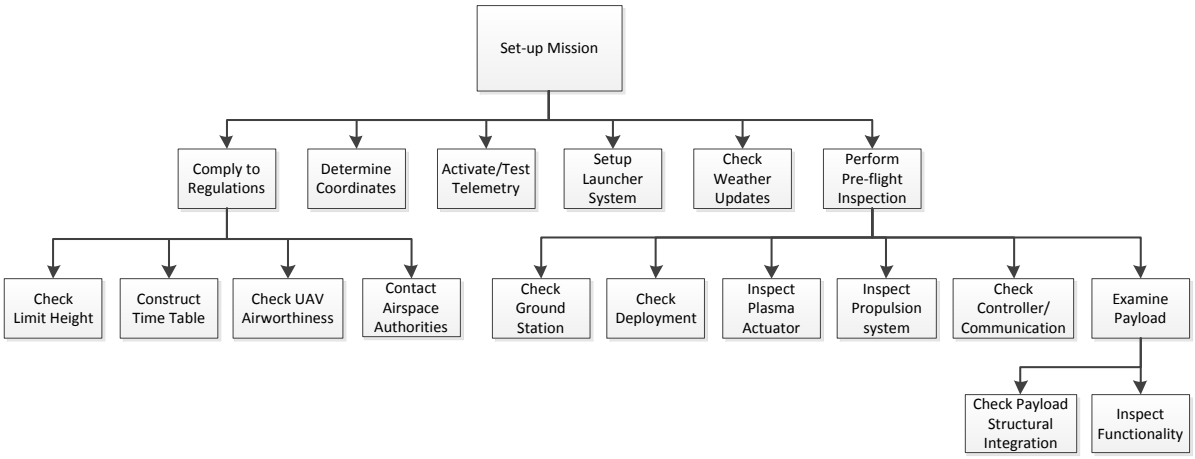

Figure 2.11: FBS: Set-up mission

Mission Set-Up

Before flight, it is crucial to set-up the mission, because the UAV must fly within safe and legal operation limits. In practice this means that before every flight several checks have to be performed. An important example is to check and test the telemetry, because the UAV shall be controllable. Moreover, it is important to keep in mind safety regulations, weather updates and the launch site. This is one of the most critical parts of every mission, since this makes sure that the mission will be safe and effective. An overview is given in Fig. 2.11.

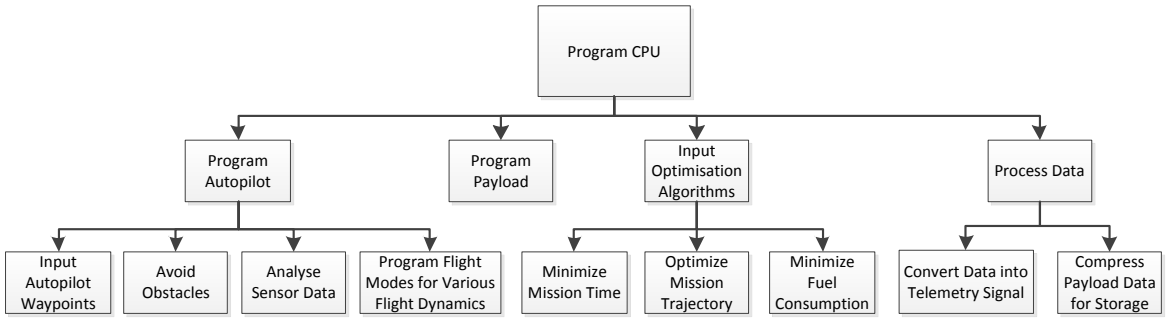

Figure 2.12: FBS: CPU programming

CPU Programming

The programming of the Central Processing Unit (CPU) includes four main activities, which can be seen in Fig. 2.12. The general programming is finished, but usually it is useful to have mission specific software. First of all the autopilot has to be programmed. It is necessary to input the way-points that it has to fly and obstacles have to be avoided. Furthermore the sensor data has to be analysed and several flight modes have to be programmed. In the case that payload is taken along it will have to take into account while programming the autopilot. The next is to apply optimisation algorithms. These can minimize the mission time, refine the mission trajectory and minimize the fuel consumption. Finally, the data has to be processed and converted into a telemetric signal or compressed for storage.

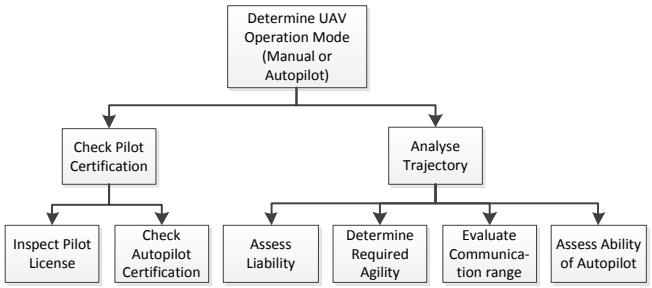

Figure 2.13: FBS: Determine operation mode

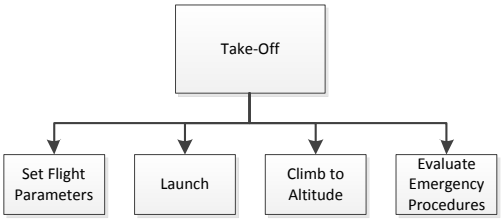

Figure 2.14: FBS: Take-off

Determine Mission Objective and Feasibility

The first step of the mission is always to identify its objective and feasibility (Fig. 2.10). The mission is defined by the customer requirements. They present the most general constraints, like the objective, budget and location of the mission. The scheduling of the mission depends on the availability of resources, such as personnel and the UAV system itself. To determine the feasibility of the mission several risks (environmental, technical and financial) have to be assessed. A definite allocation of the resources makes sure that all facilities are available and that the mission matches the maintenance schedule.

Take-Off

Take-off is the flight phase from standstill on the ground to the desired cruise or loiter altitude (Fig. 2.14). Launch may be from a runway, through the use of a (car-mounted) launcher or by hand launching.

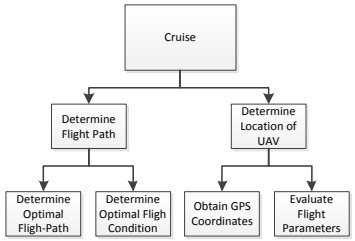

Figure 2.15: FBS: Cruise

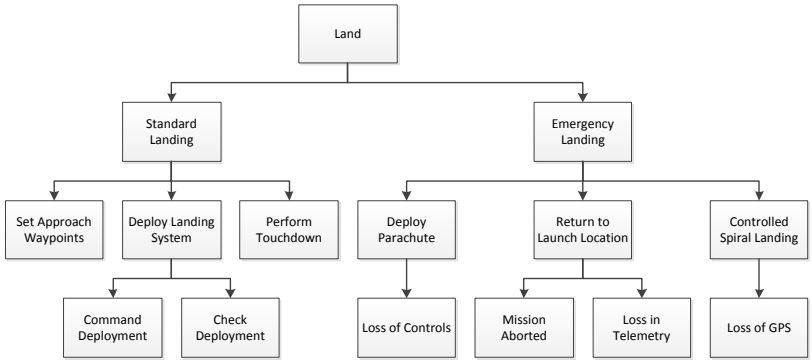

Figure 2.16: FBS: Land

Cruise

Cruise is the flight mode in which the UAV will fly to or return from the loitering location (Fig. 2.15). The UAV will determine the optimal flight path given the input coordinates and the evaluated environmental conditions, and will determine the optimal flight conditions. The optimization is either in terms of endurance or range, depending on the mission objective and subsequent profile.

Loiter

Loitering is the part of the mission where the UAV is circling around to scan for example the environment (Fig. 2.18). Loitering can be easily implemented by setting ground coordinates as a centre point, subsequently determining altitude, circle radius and the turning time.

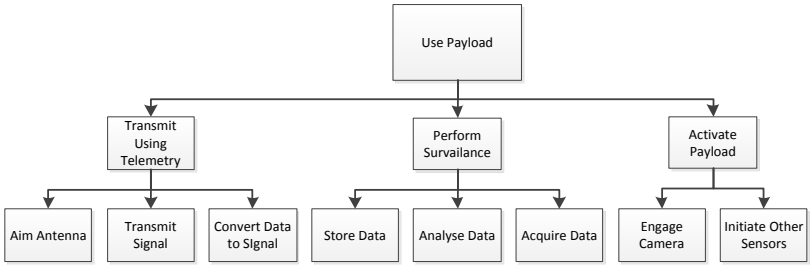

Figure 2.17: FBS: Use payload

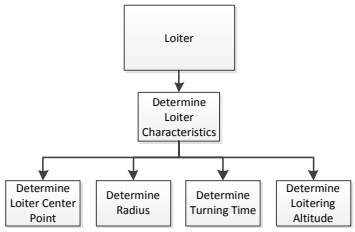

Figure 2.18: FBS: Loiter

Use Payload

The payload type has a considerable influence on the mission profile. A to be jettisoned payload requires a different approach than sensory equipment. For this report and mission profile, the latter form of use is assumed (Fig. 2.17). The possible payload sensory equipment (e.g. visual or thermal) will be activated when performing the mission objective. The data produced has to be processed and transmitted to a ground station. On board processing and storage, on board processing and transmission or direct data transmission are possibilities. The mission requirements will determine which option is used.

Land

In the case that everything goes as planned, the standard landing procedure is a relatively straightforward part of the mission. It encompasses going from cruise condition to a ground stand still (Fig. 2.16). The landing could be pre-programmed, in that case way-point coordinates to a designated landing area have to be determined. The landing procedure could also be carried out manually. In that case, the pilot has full control and he has to steer the aircraft to the landing location.

However, in case of an emergency, the UAV should be able to safely land as well, since failing to do so will probably lead to large repair costs. Four emergency scenarios have been thought of, each with an appropriate response procedure. In the case of loss of telemetry (the UAV can't be manually controlled anymore) a parachute will deploy, bringing the UAV to safety in a controlled manner. In the case that the telemetry link is broken for an extended period of time or the mission is aborted, the UAV should return to the launch location as fast as possible. Finally, if the GPS signal is lost for an extended period of time and the UAV is flying on autopilot (pilot cannot see the UAV) it will perform a controlled downward spiral until it has safely crash-landed.

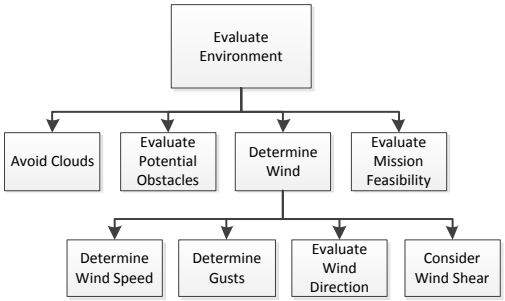

Figure 2.19: FBS: Evaluate environment

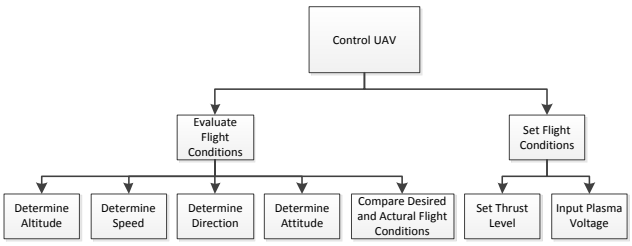

Figure 2.20: FBS: Control UAV

Evaluate Environment

A form of environment evaluation for a UAV is vital. For small and short range UAV systems this could be done visually by the pilot. For more complex systems with a form of autonomous flight, avoiding objects or conditions that could hinder the flight path or nominal operation becomes more complex (Fig. 2.19). At all times, the UAV shall be aware of its surroundings to the extent needed. If anomalies occur, it has to be determined whether the mission objective remains feasible and what measures have to be carried out. Next to that, determining the wind parameters is essential to maintaining a ground based flight path.

Control UAV

While the UAV is in flight, the current attitude of the craft needs to be evaluated. The parameters of interest are branched in Fig. 2.20 on the right hand side. The left hand side will use the previously evaluated parameters to provide the correct responses.

2.2.4 Functional Flow Diagram

The plasma actuated UAV has to be able to perform seven stages of a mission. Every stage is discussed separately in the following subsections. The Functional Flow Block Diagram is given in Fig. 2.21, which shows how the seven stages are split up into specific functions and the order in which they occur. Due to the complicated nature of the design of a UAV, this method will give additional insight on the design process and shows all mission related elements that have to be thought of during the design.

Plan Mission

Before operating the UAV, the mission needs to be planned beforehand. First of all, the requirements for the mission are obtained from the customers. Once determined, the available resources have to be allocated (i.e. human resources, UAV availability, etc.), and the risks of the mission are analysed. Finally, the date and location of the mission can be decided.

Mission Preparation

Preparing for the mission is essential to the success of the mission. The coordinates of the mission objective are determined in this stage, followed by contacting the authorities to comply with regulations. When the basic outline of the mission is determined, the choice between manual or autopilot control can be decided. Finally, the CPU of the UAV needs to be programmed for the payload, data processing and autopilot, if applicable.

Pre-Flight

Before the UAV takes off, a series of checks have to be performed. It is essential to check the weather and regulation updates before the mission. Standard pre-flight inspections are performed to ensure the functionality of each subsystem, such as checking of battery voltage level or testing of plasma actuators. Also, the telemetry system is to be activated and tested before the launch.

Take-Off

The flight parameters, such as GPS way-points, need to be entered in the flight computer. After launch, the UAV will climb to its cruising altitude to perform the mission. However, in case of emergency the UAV has to abort the mission enter the emergency procedure. In this event it is assessed whether to perform an emergency landing immediately or go home and land as close to the launching location as possible. Possible emergency scenarios are loss of control signal, engine failure or critically low voltage level. These events that activate the emergency procedure could not only occur during take-off phase, but anytime during the mission.

Mission

When the take-off procedure is completed, the autopilot system will evaluate the optimal cruising conditions at each given moment and initiate the flight to the desired loitering location. At this location of interest, the payload such as a camera is activated to save energy during cruise. At this point in time, the essence of the mission can be carried out (surveillance, inspection) and the data is transmitted through telemetry and/or stored on-board for later access. Once the mission has been completed, or the battery is drained, the UAV will fly back to the ground station.

Landing

Before initiating the landing procedure, the approach way-points have to be established. Once they have been set, the landing system is deployed and immediately checked with a feedback loop. Once deployment has been confirmed, touchdown is performed concluding the flight phase of the mission. In case of complications during the landing, a go around is performed.

Storage

When the UAV has completed the mission and landed at the ground station, it needs to be properly stored away for the next use. Firstly, the batteries have to be detached and recharged. Secondly, the landing system has to be retracted (manually if for instance a parachute is deployed). Finally, the flight and payload data has to be downloaded before the mission is evaluated and thus concluded.

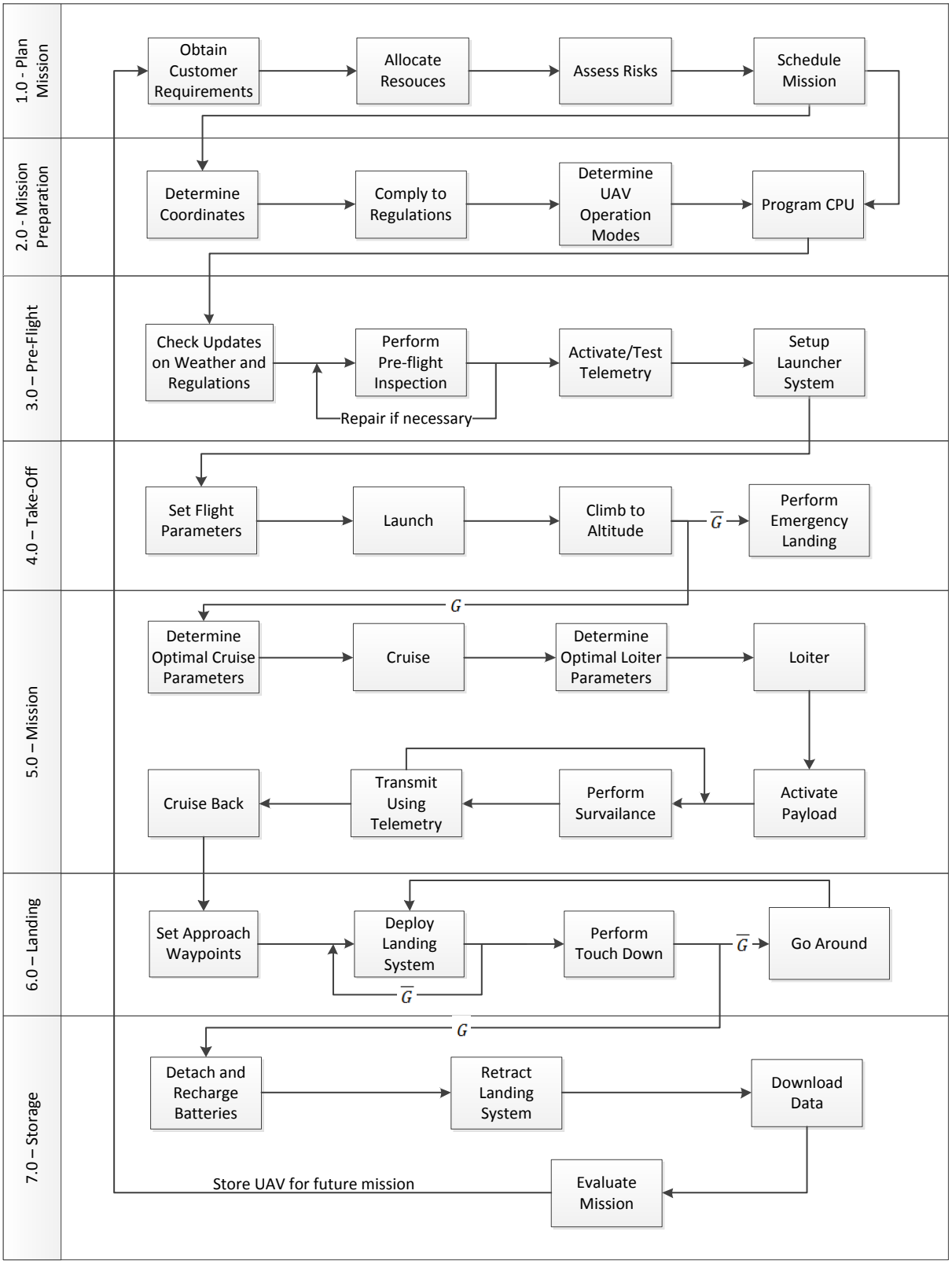

Figure 2.21: Functional flow block diagram

Chapter 3 - UAV Design Description

The following chapter will give an overall description of the factors that have been determined before the making of this report and that will act as a base for the technical details of the design that follow in Chapter 4. First an initial sizing was performed with which a constraint analysis was performed. This analysis can be consulted in Section 3.1. The final configuration is elaborated in Section 3.2 before the details of which can be presented further on.

3.1 Constraint Analysis

A constraints analysis is performed to determine two critical design values: the power loading and the wing loading. The output of this analysis is a diagram that gives an overview of the constraints set by several mission stages. Eventually a design point has to be chosen. This is a numerical value for both loadings that have to be accomplished during the next design stages.

The power loading and wing loading can be found by implementing required mission performance in a quantitative way. However, first some basic parameters need to be estimated, such as the propeller efficiency and the Oswald factor. These parameters are stated in Table 3.1. These values are included in the MATLAB script as well, along with the sea-level atmospheric parameters. Parameters like aspect ratio and maximum lift coefficient are varied. The sensitivity and validity of these initial values are discussed later.

Table 3.1: Inputs for initial sizing

Input parameter	Symbol	Value	Unit
Oswald factor	e	0.9	-
Propeller efficiency	η_p	0.75	-
Rate of Climb	RC	1.25	m/s
Endurance	E	2.0	h
Range	R	10	km
Specific fuel consumption	SFC	2.3×10^{-6}	kg/J
Wing span	b	3.0	m

Next, the mission properties are incorporated. Three mission stages have been included for the generation of the constraints diagram: cruise, climb and manoeuvring. Note that take-off and landing are not covered, because the concept design accompanies for a launched take-off and a belly landing.

Governing mission properties are design stall speed and design cruise speed. A constraint on the wing loading W/S follows directly from steady horizontal symmetric flight, formulated as:

$$\frac{W}{S} = \frac{\rho V^2 C_L}{2} \tag{3.1}$$

in which ρ is the air density, 1.225 kg/m^3 at sea level conditions, V is the stall speed, in the order of 10 m/s, and C_L is the (dimensionless) lift coefficient, ranging from 0.8 to 1.4 in this case.

Then, constraints for climb rate are implemented. Optimizing for climb rate eventually leads to maximizing the ratio (C_L^3/C_D^2). Hence, the following relation between power loading W/P and wing loading has been derived:

$$\frac{W}{P} = \frac{\eta_p}{V_C + \frac{(3C_{D0}\pi Ae)^{3/4}}{4C_{D0}}\sqrt{\frac{2W}{\rho S}}} \tag{3.2}$$

Here, η_p is the dimensionless propeller efficiency (0.75), V_c is the climb rate (1 m/s), e is the dimensionless Oswald factor (0.9) and A is the wing aspect ratio, ranging from 1 to 16 in the analysis. C_{D0} is the zero lift drag coefficient which is proportional to the skin friction coefficient ($\approx 1.328/\sqrt{Re}$ assuming laminar

flow) and to the wetted surface ratio (≈ 6 is reasonable value for conventional aircraft). Plausible values for the Reynold's number are in the range of 10^5 to 10^6 and the minimum drag coefficient C_{D0} has a 0.005 to 0.020 range.

For manoeuvring, the load factor $n = L/W = 1/\cos\phi$ for cornering is used as input. A bank angle ϕ of 45° results in a load factor of 1.41. A relation between power loading and wing loading has been established, where q is the dynamic pressure $\rho V^2/2$.

$$\frac{W}{P} = \left(\frac{C_{D0} q V}{W/S} + \frac{n^2 W/S}{\pi A e q} \right)^{-1} \tag{3.3}$$

The results of the constraint analysis are shown graphically in the constraints diagrams in Fig. 3.1 and 3.1. It shows how the input parameters lift coefficient and aspect ratio affect the required wing loading and power loading. The design point dictates what the values of those parameters should become. It is useful to have a high power loading and wing loading (thus low wing surface and low power requirements). However, this requires to implement a high lift coefficient and aspect ratio. A trade-off is required to choose a suitable and achievable design point.

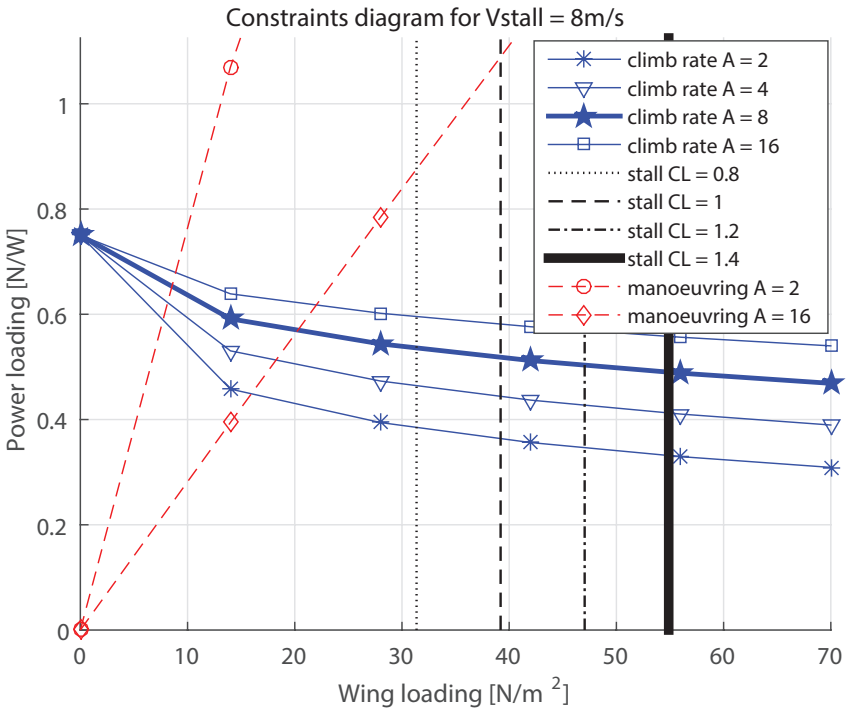

Figure 3.1: Constraints diagram showing the design space for stall speed 8 m/s

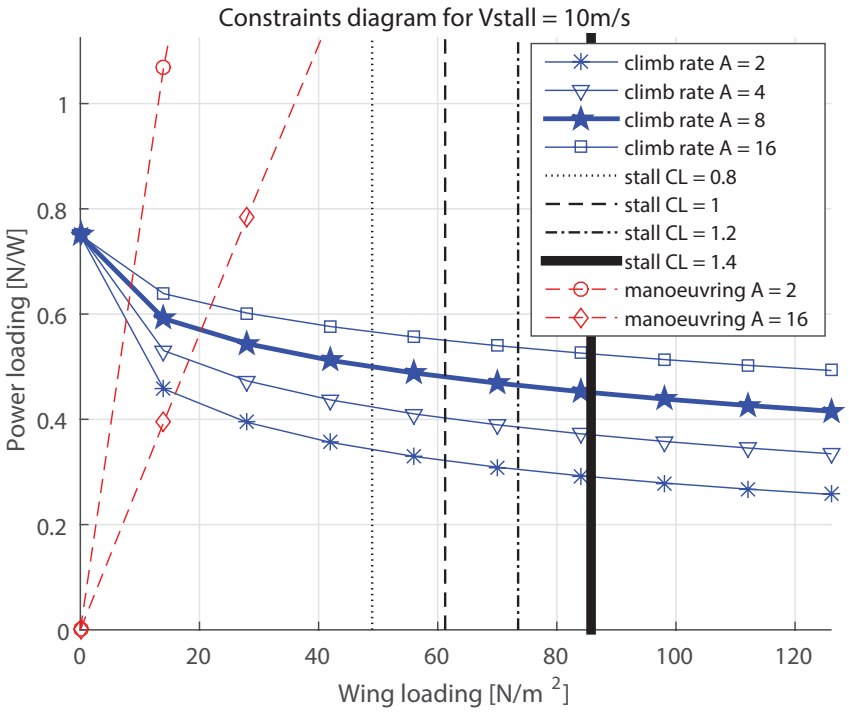

Figure 3.2: Constraints diagram showing the design space for stall speed 10 m/s

3.2 Configuration

For this DSE project, a UAV was to be designed which is controlled by plasma actuators instead of by moving surfaces as it normally is. This section discusses the configuration and lay-out of this UAV. Also, a generic substantiating will be given for the design choices that were made. This will be grouped in both aircraft systems, aerodynamics, structures and stability. The overall design of the plasma actuated UAV can be found in Fig. 3.3.

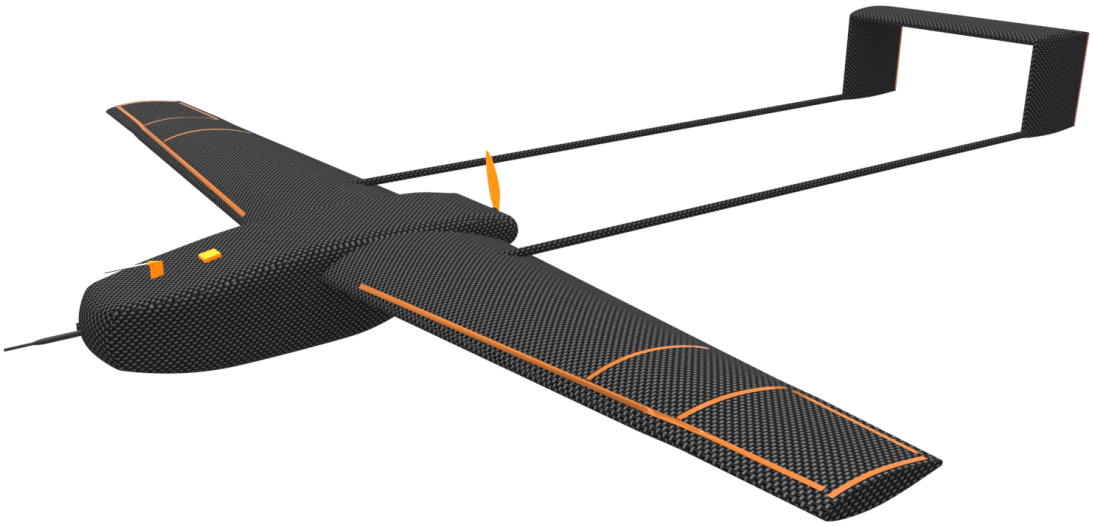

Figure 3.3: Overall design of the plasma actuated UAV

Aircraft Systems

For the propulsive system it had been decided before that an electrical motor with propeller will be used because it shows several advantages over a combustion engine. First of all, a large power system and battery is already available as this is needed for the plasma actuators. It therefore has to be scaled up slightly to account for the motor. A combustion engine would need an extra fuel system and fuel tanks, which would add to the weight. Since the UAV is already a rather small aircraft, the additional weight due to fuel and a combustion engine will have a large impact on the weight. This fuel will also shift the centre of gravity during operations, which will constrain the range for the centre of gravity. Furthermore, combustion engines are relatively heavy since the materials need to withstand high pressure and temperatures. Another reason to choose electrical engines over combustion engines is the omission of exhaust gasses. The propulsive system is placed relatively high in the fuselage in order to account for sufficient ground clearing for the propeller.

The plasma actuators, the motor and other systems need electricity in order to work. Currently, a number of different types of power sources exist that could be feasible for a UAV design: photo voltaic cells, fuel cells or batteries. Although recent improvements in efficiency of photo voltaic cells give promising perspective for application in aeronautics, it has some significant disadvantages for the plasma UAV design. First of all, it requires a large of amount of surface area on the UAV that is already being used for plasma actuators. Furthermore, its use constrains the weather conditions in which the UAV can be operated. Fuel cells have a relatively high efficiency and energy density that would benefit the UAV. However, they are relatively expensive and suffer from a limited lifetime [19].

Plasma actuator control has only been tested in the lab and yet is a fairly unproven concept in practice. Therefore, it was decided to include a parachute in the UAV to accommodate for an emergency landing in case of loss of control or another emergency situation. This will significantly reduce the chances of damage, both collateral and of components. The parachute will be stored such that the cables will not get tangled in the propeller and it will be anchored such that the load is properly transferred throughout the structure.

Finally, the UAV will use an autopilot with relevant sensors and a telemetric system that is capable of transferring data from the ground station to the UAV and vice versa. Furthermore, it should be able to control with a remote control. The details on the aircraft systems that the UAV uses can be read in Section 4.1. An overview of the systems within the UAV can be found in Fig. 3.4.

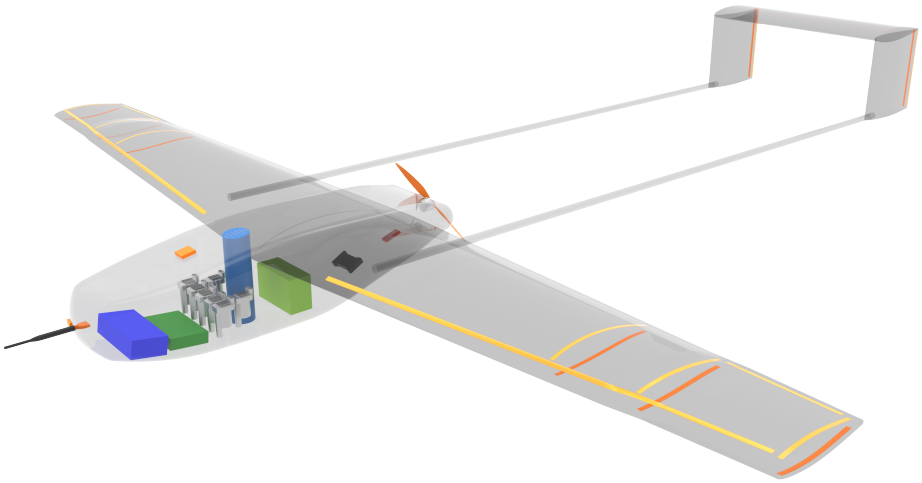

Figure 3.4: Overview of the systems within the plasma actuated UAV

Aerodynamics

When selecting an airfoil for the UAV, certain aerodynamic characteristics that follow from the constraint analysis have to be taken into account. First of all, the UAV will fly at sub-sonic speeds, with a stall speed in the range of 10 m/s. Furthermore, from Section 3.1, it follows that the lift coefficients will range from 0.8 to 1.4. At last, it has to be taken into account that plasma actuators have to be installed on the wing and this mechanism must be used for control.

The main wing of the UAV consists of two different airfoils. For the inner section of the wing, along the greatest part of the span, the NACA63A-915 airfoil will be used. This is a sharp trailing edge and cambered airfoil, ideal to produce high lift coefficients as needed. It has a rather large thickness to chord ratio of 15%. This is an advantage, since thick wings stall first at the trailing edge, which is needed for the plasma actuator application. At the wing tips an other airfoil will be used, the NACA64A-015. The reason for this is that there is more reliable data available of this airfoil in combination with the plasma actuators. Therefore, integration of these actuators on the airfoil will be easier and the effect will be more predictable. This second airfoil has a blunt trailing edge and is symmetrical. It will therefore also be used at the tail, since lift creation at zero angle of attack, i.e. camber, is not needed here.

The plasma actuators will be integrated on both the main wing as the empennage. The strips installed on the main wing will be used for roll control, a positive pitch moment (nose up) and some will also function as high lift devices. Four actuators will be installed on the wing in order to counteract the formation of a wing tip vortex. The actuators on the horizontal tail will help in the negative pitching moment. For yaw control, the plasma actuators will be installed on the vertical tails. The exact location of these actuators can be found in Fig. 4.14 in Section 4.2.3

A more detailed description of the integration of the plasma actuators and the aerodynamic design of the UAV will be given in Section 4.2.2 and Section 4.3.

Structures

The structure of the UAV has the sole purpose to distribute the forces throughout the UAV. The requirements of the structure arise from decisions made with respect to aerodynamic, stability, systems and operations.

The configuration of the structure of the UAV can be split up in the wing, tail and fuselage configuration. The first two essentially are structures composed of airfoil shapes. The wing, mounted on top of the fuselage houses two booms just next to the propeller. These booms both house a vertical tail which are connected at the top with a horizontal tail surface, resembling a 'pi-tail'. The structure of the wing and tail consists of a CFRP skin filled with a foam core, which is possible since no subsystems are housed in these structures apart from cabling. The rods connecting the tail to the wing are circular CFRP tubes filled with a foam core. The fuselage however is a plastic monocoque that houses all subsystems of the UAV and is placed under the wing. A detailed description on the structures of the UAV can be found in Section 4.4.

Stability and Control

In order to have longitudinal stability a horizontal tail is used. This tail is located behind the wing and fuselage For lateral stability two vertical tail surfaces are used. The horizontal surface is placed on top of these vertical surfaces in order to evade the prop wash. Due to this the tail results to be a so called 'pi-tail'. By using a pi-tail, both the horizontal and vertical tail surfaces profit from the shielded edges, so less drag is induced due to tip vortices. This design choice also allows to group the heavier components of the UAV, such as the wing, engine, batteries and transformers, close to the wing which is favourable to the stability. Since the centre of gravity will not shift during flight, the tail can be sized as small as possible, yielding a lighter tail. The tail is attached to booms, which are attached to the wing. Using boom enables the tail to be sized quite effectively by not adding lots of weight when the tail length changes.

To control the UAV fifteen plasma actuators are used, which are depicted in Fig. 5.5. To control these the flight controller drives a high voltage switch that send the AC signal that was converted from DC signal to the respective actuators, which induced a motion of the UAV. Details about both stability and control can be read in Section 4.5.

Chapter 4 - Technical Design of the UAV

Now that an overview of the DSE project has been given, the technical details and the way they were determined can be elaborated. This chapter starts with the design of the systems that the UAV consists of, such as the engine, battery and fuselage layout in Section 4.1. Hereafter, the analysis of the performed wind tunnel tests and the corresponding conclusions are reported on in Section 4.2.2. Then, the aerodynamic design will be explained in Section 4.3, in which the airfoil is selected, the wing planform is discussed and the integration of the plasma actuators is shown. Section 4.4 gives the stress analysis, the material selection and the characteristics of the used materials. The sensitivity analysis then investigates the sensitivity of the design for changes in major system parameters. The design of the tail, analysis of stability and control and the range of the centre of gravity can be found in Section 4.5. In each section, a sensitivity analysis is performed and the process is verified. Finally, the found values are validated in Section 4.6.

4.1 Aircraft System Design

In the following section the systems of the UAV are elaborated. First of all, the propulsive system, i.e. the electrical motor and propeller, is selected in Section 4.1.1. When this is known, the battery can be sized since the motor is one of the most important power drains. The sizing and selection of the battery can be read in Section 4.1.2. One important system to recover the UAV if something failed, is the parachute. About the parachute is reported in Section 4.1.3. The fuselage layout is discussed in Section 4.1.4.

4.1.1 Engine Selection

As mentioned in Section 3.2, it was decided to have an electrical propulsive system. When sizing and selecting the engine, the starting point was the power loading determined earlier as can be read in the Mid-Term Report [12]. The determined design power loading has been changed to 0.45 N/W, due to a lower climb speed. This is the highest power loading the UAV will encounter. This will be during climb. Regarding a MTOW of about 10 kg, it can be calculated that the required power is equal to 211.46 W, which is the shaft power P_{sh}.

Veerman states that three different efficiencies have to be taken into account: the Electrical Speed Controller efficiency, the Engine efficiency and the propeller efficiency. Based on statistical data these three and hence the total efficiency equal [20]:

- $\eta_{esc} = 97\%$
- $\eta_{eng} = 90\%$
- $\eta_{prop} = 85\%$
- $\eta_{tot} = 74\%$

This can then be used to calculate the required thrust with equation 4.1, where V is set to the stall speed 10 m/s, to end up with a conservative solution.

$$T = \frac{P_{br} \cdot \eta}{V} \tag{4.1}$$

This yields a required maximum thrust force of 15.69 N and therefore a thrust to weight ratio of 0.159. To calculate the power and therefore thrust needed during specific stages of the mission, equation 4.2 is used, which can be derived to end up with 4.3 with which the required power for different flight stages can be calculated. With this required power, the thrust can be determined with the thrust equation 4.1. For these different flight stages different values for velocity and lift coefficient are being used. The air density is at sea-level and S equals 1.1605 m^2. These different engine settings are depicted in Table 4.1.

$$P_{req} = D \cdot V \tag{4.2}$$

$$P_{req} = \frac{1}{2}\rho V^3 S \cdot C_D \tag{4.3}$$

An important thing to notice is the difference between the dissimilar powers P_{elec}, P_{sh} and P_a. The electrical power P_{elec} is the power the electrical motor consumes, i.e. the product of the voltage and

current. The shaft power (or brake power) P_{sh} is the power the motor transfers to the shaft and propeller and finally, the power available P_a is the power the propeller transfers to the air to propel it.

Table 4.1: Engine settings for different flight settings

Flight phase	Velocity [m/s]	Lift coefficient [-]	Required shaft power [W]	Required thrust [N]	Approximated throttle setting
Stall	10.0	1.300	69.05	5.12	50%
Loiter	13.0	0.859	66.71	3.79	40%
Cruise	13.0	0.900	71.21	4.07	45%
Range	16.2	0.468	69.05	3.02	35%
Max. speed	27.4	0.184	211.46	15.19	95%

With the partial efficiencies and the maximum required shaft power, the maximum electrical power of the engine is to be determined to be able to select a suitable electrical motor and propeller. According to the engine efficiency the electrical power should be 242.22 W.

The electrical motor to be used is the Antigravity 4006 380KV[1], produced by T-Motor. Using a T-MOTOR 13×4.4CF propeller[2], it produces 16.02 N of thrust at 100% throttle to allow for some contingency. It operates at a low operating temperature of $30°C$. N.B. the operating temperature is specified as the motor surface temperature after ten minutes running at 100% throttle. Further specifications are shown in Table 4.2. It can be noticed that the calculated required electrical power of 242.22 W exceeds the power the motor actually uses at 100% thrust, which is 232.8 W. This small difference can be explained due to the fact that Veerman's efficiencies are based on statistics. The Antigravity 4006 motor is a state of the art electrical motor and therefore has a higher electrical efficiency η_{eng}.

The size of the motor is 40 mm in diameter and 27 mm in height, weighing 0.066 kg. The propeller will form a cylinder with a diameter of 0.3302 m and is estimated to weigh 0.0157 kg. Finally, an Electronic Speed Control (ESC) unit is needed to transform the throttle input by the flight controller into a current to the electronic motor. The unit to be used is a T-Motor Air 20A, weighing 14 grams[3]. More about the ESC can be read in section 5.3.3.

Table 4.2: Specifications of a Antigravity 4006 380KV motor installed with a T-MOTOR 13×4.4CF propeller

Throttle	Current [A]	Elect. power [W]	Thrust [N]	RPM	Efficiency [N/W]	Torque [Nm]
50%	2.0	48.00	5.337	3719	0.111	0.096
55%	2.5	60.00	6.435	4528	0.107	0.108
60%	3.1	74.40	7.387	4840	0.099	0.123
65%	3.7	88.80	8.368	5155	0.094	0.139
75%	5.1	122.40	10.418	5451	0.085	0.172
85%	6.8	163.20	12.615	6327	0.077	0.208
100%	9.7	232.80	16.019	6515	0.701	0.267

Sensitivity Analysis

To finalise the selection for the engine, a sensitivity analysis is performed to check how changes in the parameter inputs change the thrust and power required for the motor. Assuming that the efficiency η and ρ does not change, it can be seen from equation 4.3 and 4.1 that, $P_{req} \propto V^3, S, C_D$ and $T \propto V^2, S, C_D$. From this it can be seen quantitatively, that the velocity is the most sensitive factor, as the used velocity is cubed to calculate the required power and squared to calculate the required thrust. Furthermore, the required power and thrust are simply proportional to S and C_D. In the unlikely case that the thrust force happens to be either insufficient, the propeller could be simply upgraded with the T-MOTOR 14"4.8CF propeller to achieve a maximum thrust force of 19.375 N[1].

[1]T-Motor, accessed on June 11, 2015: `http://www.rctigermotor.com/html/2015/Antigravity_Motors_0212/289.html`
[2]T-Motor, accessed on June 11, 2015: `http://www.rctigermotor.com/html/2013/prop_0904/31.html`
[3]T-Motor, accessed on June 11, 2015: `http://www.rctigermotor.com/html/2014/esc_1223/284.html`

4.1.2 Power System

To provide power for the engine and plasma actuators, a power source is needed. In the MTR [12], the battery had already been chosen over fuel cells or photo voltaic cells as type of power source. In this subsection, first a type of battery is chosen. Then, a power budget is made to estimate the amount of power and energy needed and subsequently, the power source is sized.

Battery Selection

The most simple solution is the use of batteries. They can be used in any weather condition and do not require high initial costs. Different types of batteries exist:

- Lead-acid
- Nickel-Cadmium
- Nickel-metal hydride
- Lithium-Ion
- Lithium-Polymer

Lithium based batteries have proven to have superior performance to the other batteries [21]. This can be explained by their high specific energy [Wh/kg] and energy density [Wh/l], which is visualized in Fig. 4.1[4]. From this figure, it can also be seen that lithium-polymer batteries have a higher specific energy than regular lithium-ion batteries. In fact, they contain the same substance as any lithium-ion batteries, but instead of a hard cylindrical or prismatic shape they are packed in a soft plastic pouch. This plastic pouch is lighter, increasing the specific energy. Therefore, lithium-polymer batteries have been selected as energy source for the plasma UAV.

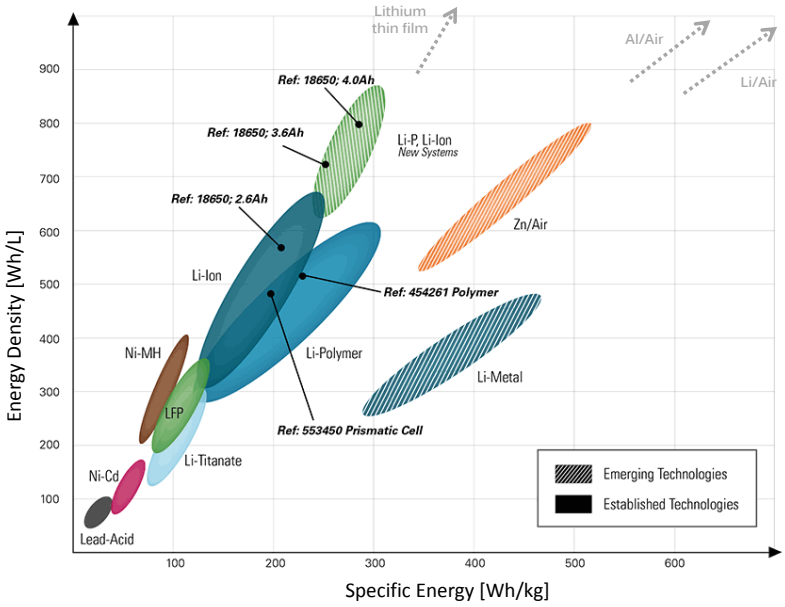

Figure 4.1: Comparison of energy density for various battery chemistry

Power Budget

To estimate the amount of battery needed, the required power and subsequently the required energy is budgeted in Table 4.4. For this, the following mission was assumed: The UAV is launched and climbs to an altitude of 300 m with a rate of climb of 1.25 m/s. Then, it either loiters for 2 hours, or flies over a range of 10 km.

While budgeting the energy required for propulsion, it was found that the 2 hours of loitering is more critical for the design, so in the power budget the loitering was accounted for. The required shaft power that is required in the conditions of climb and endurance from Section 4.1.1 are converted to electrical consumed power using the product of the engine and ESC efficiency factor of 0.90 and 0.97.

[4]Energy Densities, accessed on June 23, 2015: `http://www.iccnexergy.com/battery-systems/battery-energy-density-comparison/`

An estimation has been made on the amount of power that the plasma control system averagely consume, based on power per unit length, the length of plasma actuators for each control mode and the estimated time activated in the mission of two hours. The total plasma actuator length is found to be 6.15 m. The exact reasoning behind this can be found in Section 4.2. The power per unit length of plasma actuators is estimated at 30 W/m [5]. Table 4.3 summarizes the estimation of plasma actuator power consumption.

Table 4.3: Power consumption of the plasma actuators

Control mode	Actuator Length [m]	Time [min]	Power [W]
Roll (L/R)	0.3/0.3	40	3
Pitch (U/D)	1.25/0.7	40	12.5
Yaw (L/R)	0.6/0.6	10	1.5
HLD	2.4	10	6
Average power	-	-	23

As a reference for flight controller, the Lisa/M v2.0[6] was taken. This flight controller, which also provides the power for the communication and navigation systems carried on board, consumes a maximum of 2.5 W of power.

For a potential camera that that could be used, a GoPro[7] camera is taken as reference. This camera averagely consumes 2.9 W of electric power.

Adding all energy consumptions of each element, gives an energy of 235 Wh. To allow for a margin of safety, for instance when a go-around has to be performed when landing, a contingency of 20 % is introduced. Also, lithium-polymer batteries show a significant voltage drop when approximately 80 % of the capacity is used. For this, another contingency of 20 % is implemented, resulting in a total of 40 % energy capacity contingency and a total energy capacity of approximately 329 Wh.

Table 4.4: Power budget

	$P_{electrical}$ [W]	Time [s]	Energy [Wh]
Climb (propulsion)	242	300	20
Loiter (propulsion)	78	7200	157
Flight controller	2.5	7500	5
Camera (potential)	2.9	7500	6
Plasma actuators	22	7500	46
Subtotal			235
Contingency			94
Total			329
Peak power	405		
Average power	107		

Battery Sizing

The selected engine requires between 4 to 6 cells of 3.7 V each in series. Since voltage drop caused by internal resistance is dependent on the applied current, the highest possible voltage should be used to require less electrical current, while producing the same amount of power. Consequently, a lithium-polymer battery of 22.2 V, i.e. 6 cells of 3.7 V, is chosen.

The energy capacity in combination with the battery voltage give the required battery capacity C_{batt} [Ah]. This was estimated to be approximately 14.8 Ah.

The maximum power the battery has to deliver at an instance, te peak power, is also calculated. Together with the battery voltage, this is used to estimate the amount of current that the battery has to deliver.

[5] Value obtained from personal communication with project tutor Marios Kotsonis

[6] Paparazzi: The Free Autopilot, accessed on June 1st, 2015: `http://wiki.paparazziuav.org/wiki/Lisa/M_v2.0`

[7] GoPro, accessed on June 1st, 2015: `http://gopro.com/`

Using a margin of safety of 50%, the peak power is estimated to be approximately 405 W. This gives a peak current of 18.2 A. Lithium-polymer batteries are characterized in terms of C-rating. This is the product of the battery capacity in Ah and the maximum continuous current in Amps it can deliver. This requires a C-rating of only 1.23 C.

Higher C-rating of lithium-polymer batteries generally decreases the specific energy. Looking at available lithium-polymer batteries, the minimum C-rating is 5 C. In Table 4.5 characteristics of three types of battery configurations are given with different C-ratings. Manufacturers deliver battery packs in certain sizes, so to obtain the required capacity of 14.9 Ah more than one battery pack has to be used in the design. For the sake of easy operations, a requirement has been set that when using two or more battery packs in the aircraft, these have to be equal. Although higher C-ratings usually correspond to higher cost, it can be observed that the cost decreases with increasing C-rating. This is due to the fact that the 5 C and 10 C batteries are specifically designed for high specific energy.

Table 4.5: Battery configuration characteristics

Name/brand	Turnigy nano-tech	Multistar	ZIPPY Flightmax
C-rating	5 C	10 C	20 C
Number in series	2 x 11.1 V	1 x 22.2 V	1 x 22.2 V
Number in parallel	6 x 2.5 Ah	3 x 5 Ah	3 x 5 Ah
Total voltage [V]	22.2	22.2	22.2
Capacity [Ah]	15	15	15
Mass [g]	1764	1929	2352
Price	€170.76	€139.41	€149.25

The mass of the battery configurations in Table 4.5 increases significantly with the C-rating. Because a higher C-rating is not necessary, the Turnigy Nano-Tech[8] battery configuration as the most lightweight solution is chosen as opposed to the Multistar[9] and ZIPPY Flightmax[10]. The Turnigy configuration consists of a total of 12 battery packs, 2 in series and 6 in parallel.

Future Battery Developments

The sizing of the battery mass is influenced by a number of parameters. First of all, the electrical power required for the engine and in particular the power during loiter has a significant influence on the battery weight. Furthermore, the specific energy of batteries has a large effect on the battery weight and is rapidly improving.

A battery configuration could be found with sufficient specific performance, yielding a weight of 1.764 kg, well below the 2 kg limit. Although this battery suffices to prove that plasma control can actually be applied to a UAV, a weight reduction would have a big impact. Due to the great research effort, some new configurations are likely to be available in the near future. As a reference, the specific energy of the selected battery 'Turnigny nano-tech' is 189 Wh/kg. Lithium thin film (260-400 Wh/kg), Al - air (6,000+ Wh/kg) and Li - air (10,000+ Wh/kg) are only a few of the possible candidate battery technologies [22].

4.1.3 Parachute

Plasma actuated control is an unproven concept. To account for the unlikely event of a loss of control, it was decided to include a parachute in the UAV for emergency landings. When the control is not functional or another failure happens, the parachute can be deployed in order to recover the UAV. Off the-shelf parachutes are widely available in Internet web stores.

The system consists of the Skycat X68 Series, all-in-one Package. This launcher has a large spring inside the container, that is triggered by an electrical impulse. The parachute will be shot out of the container/fuselage rather rapidly and the parachute is fully released within split seconds. The system's

[8] Turnigy nano-tech LiPo battery, accessed on June 17th, 2015: `http://www.turnigy.com/batteries/nano-tech/`

[9] Multistar LiPo battery, accessed on June 17th, 2015: `http://www.hobbyking.com/hobbyking/store/uh_viewItem.asp?idProduct=65269`

[10] ZIPPY Flightmax LiPo battery, accessed on June 17th, 2015: `http://www.hobbyking.com/hobbyking/store/uh_viewItem.asp?idProduct=8582`

trigger unit relies on a separate battery. Therefore, the parachute can also operate during a loss of power. Finally, the package includes 20 fuse materials such that it is re-usable at least 20 times. Its dimensions and weight are 68 mm diameter, 215 mm height and a total weight of 0.417 kg, costing €479[11].

The parachute is to be installed at (or at least very close to) the centre of gravity location, in order to have a descent in which the UAV remains horizontal. A disadvantage of this is the fact that the parachute and its cables are in front of the propeller. Therefore, the propeller will be shut down before deploying the parachute. The propeller will obviously still rotate a bit, but in short footage provided by Skycat, it can be clearly seen that the parachute is deployed in such short time, that there should be no worries about the cables being tangled in the propeller[12]. Furthermore, if the parachute is attached slightly in front of the centre of gravity, the drag force induce in the first moments, will create a small moment due to which the UAV will slightly pitch up, decreasing the chance of parachute-propeller interference.

According to the manufacturer's website, the UAV loses 3-10 m altitude during the process of fully deploying the parachute. Once the parachute has been deployed, the drag of the chute decreases the vertical velocity of an 9.7 kg UAV up to 6.1 m/s. Skycat estimates the energy of the impact at 167 Joule, which is equivalent to a free-fall of 1.90 m. The trigger could also be connected to two devices to slow down the descent even more[13].

4.1.4 Fuselage Layout

This section accounts for the fuselage aerodynamic design and the space for its components. Section 4.4 then explains the structural design, accounting for the belly landing and other loads. Finally, Section 5.2 shows the integration of wing and fuselage.

The fuselage carries and protects the main components that have been discussed in the previous sections: the engine, the batteries, the parachute, the communication and avionics. An overview of their weights and dimensions is given in Table 4.20. Note that the UAV fuselage design is more straightforward than passenger aircraft because no passengers are on board and thus no pressurisation is needed. This then simplifies the structural design of the fuselage. Also, the nose of the fuselage does not have to take pilot visibility into account. Finally, due to the low cruise speed, design for drag is less critical than for transonic aircraft, for which wave drag occurs. It is however paramount to avoid sharp edges in the fuselage design to prevent high form drag.

Four criteria that have to be considered are low drag production, small aerodynamic instability, easy manufacture, assembly and disassembly (loading and unloading) and robust structure. The fuselage slenderness ratio - i.e. the ratio between cross section diameter and fuselage length - governs the zero-lift drag. Bluff bodies generate pressure drag, slender bodies generate friction drag. A minimum of zero-lift drag is produced at slenderness ratio around 0.3 [23]. Practically, all aircraft apply a lower value for stability purposes. However, the plasma UAV uses booms to achieve a high tail moment arm. A tail cone decreases the drag, so its suggested length is between 2 and 3 times the fuselage diameter [24]. In order to reduce pressure drag, the tail cone (divergence) angle is advised to not exceed 24 degrees. Reasonable nose lengths for subsonic aircraft vary from 1 to 2 times the fuselage diameter.

Fuselage cross sections are usually circular. This has the advantage that it is the best shape structurally for a pressurised cabin. Also, the aerodynamic performance is high. On the other hand, a squared cross section allows more convenient packing and can be manufactured more easily, i.e. a less expensive design. Finally, the UAV fuselage can be shaped as an airfoil. This design produces more lift, but also more drag and its production is more complex [25]. Considering packing and production convenience and the fact that the UAV does not need a pressurised cabin or particularly high aerodynamic performance, the squared cross section is the best option for the plasma UAV. Additionally, all edges are rounded to prevent extreme stress concentrations and high form drag.

4.2 Plasma Actuator Design

In this section it is attempted to translate the mechanisms presented in Section 2.1.2 from theory to practice. To do this, first a trade-off is made between the different mechanisms to identify which ones are to be investigated further.

[11] Skycat, accessed on June 4, 2015: `http://www.skycat.pro/shop/skycat-x68-all-in-one-package-for-4-8kg-up-to-11-kg-uavs`
[12] Skycat.pro Vine Account, accessed on June 4, 2015: `https://vine.co/u/1153831314600914944`
[13] Skycat, accessed on June 4, 2015: `http://www.skycat.pro/tech-specs`

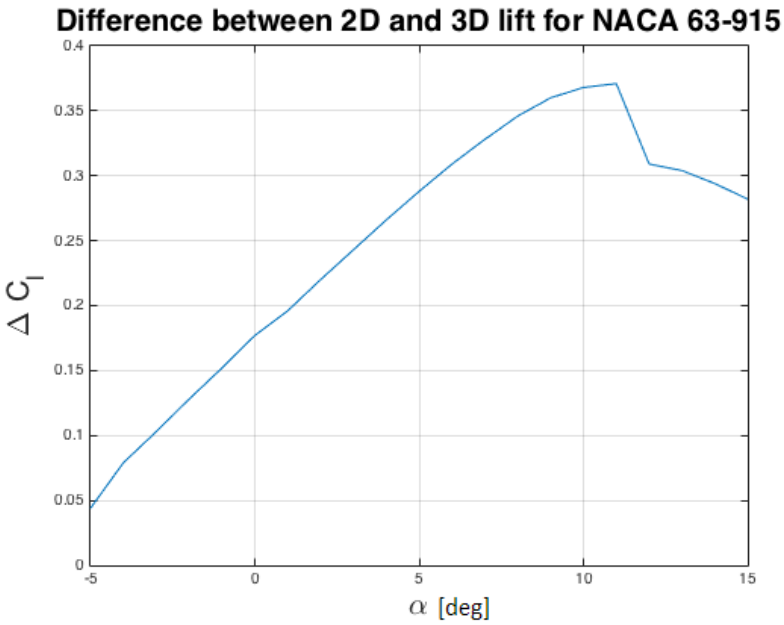

Figure 4.2: Difference between 2D and 3D lift for the NACA63A-915 airfoil

As was mentioned in the section on plasma actuators, there are two main types of control, circulation control and separation control. Since the latter type requires separated flow, it is not practical to use this mechanism for control during nominal operating conditions. It does have potential to be used as a high lift device however, so it is decided to test the effectiveness of a separation control mechanism.

The specific mechanism that is to be tested is the non-optimum form of mechanism 1. The plasma actuators will be pulsed, however the pulse frequency will be derived from literature instead of being measured. This is due to the fact that the equipment required for measurements is very heavy and therefore not suitable to be carried aboard the UAV. The other mechanisms presented in Section 2.1.2 are not as effective as mechanism 1 and are therefore not tested. The non-optimum form of mechanism 1 is essentially a more advanced form of mechanism 3, and mechanisms 2 and 4 are meant to decrease lift instead of enhancing it. This is not very convenient if separation control is to be used as a high lift device, and therefore these two mechanisms are not tested.

For control during nominal operating conditions, circulation control will be used. Since data for a rounded trailing edge airfoil, mechanism 6, is already known from literature [13], it is decided not to test this mechanism. The data in [13] is obtained at conditions similar to the operating conditions of the UAV and it is therefore valid to use this data in the UAV design. No useful data is available for mechanism 5 however, so this mechanism will have to be tested. Section 4.2.2 covers the windtunnel test that is performed to quantify the effectiveness of mechanisms 1 and 5.

As for mechanism 7, it is rather hard to test this control concept with the resources available, so it is attempted to quantify this mechanism analytically in Section 4.2.1. As was mentioned in Section 2.1.2 mechanism 8 is hard to quantify and requires a lot of plasma actuators for implementation. It is therefore decided not to test it in the current project, however it is a very promising concept for the future that will definitely have to be investigated. This will be touched upon again in Section 6.2.

4.2.1 Wing Tip Quantification

In this section of the report, it is attempted to quantify the effectiveness of control mechanism 7, the so-called 'virtual wing-tip'. The results of this quantification will be used to assess whether mechanism 7 will be incorporated into the UAV control system layout.

As was mentioned in Section 2.1.2, the purpose of the virtual wing-tip is essentially to counteract the wing-tip-induced lift loss for a 3D wing. In an attempt to obtain a ΔC_l value for the wing tip mechanism, the difference between the 2D and 3D $C_l - \alpha$ curve is therefore considered, Fig. 4.2. The C_l difference in this graph is the maximum obtainable increase in C_l for the wing tip mechanism. The mechanism is

not 100 percent effective however, so the change in C_l that is available for control will be lower. Rather advanced calculations are required to accurately quantify the obtainable ΔC_l, and these calculations are beyond the scope of this project. After consulting an expert[14] and adding a margin to be conservative during the design, it was decided that an efficiency of 50% should be feasible for the virtual wing-tip. This is of course a very rough estimate, so it is suggested to actually test the virtual wing-tip mechanism in the future.

For now the 50% efficiency is used in the quantification of mechanism 7. As can be seen in Fig. 4.2, the C_l that can be used for control depends on the angle of attack of the airfoil. Most aircraft cruise at an angle of attack of around 2-4 degrees, leading to an obtainable change in lift coefficient of 0.11- 0.13. This change in lift is quite large and effective enough to be used for airplane control. It is therefore decided to use mechanism 7 in the control of the UAV. The exact mode of deployment of the mechanism will be decided upon in Section 4.2.3.

4.2.2 NACA63-618 Testing with Plasma Actuators

In this section, the wind tunnel test done in week 6 of the project will be discussed and the results will be shown. The main purpose of the tests is to find out what effect plasma actuators can have on the lift coefficient of an airfoil when activated. Therefore, several tests were performed at varying angles of attack, wind speeds, pulse frequencies, voltages and duty cycles. In addition, different locations for the plasma actuators were evaluated.

First the test set-up will be given, such that the experiment can be reproduced. This will be followed by the method. Later the obtained test results will be shown and several conclusions will be drawn from these results.

Test Set-up

For the testing, a wind tunnel had to be used in combination with a force balance, an airfoil and self-made plasma actuators. A picture of the test setup can be found in Fig. 4.3.

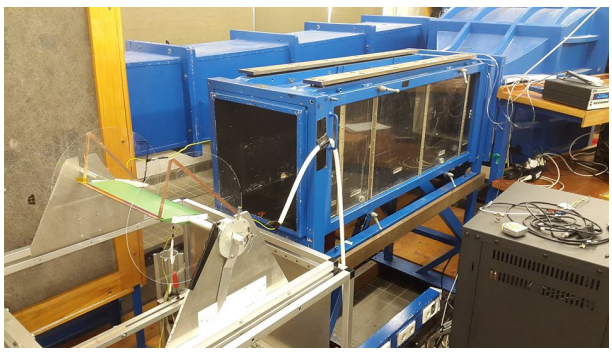

Figure 4.3: Test set-up

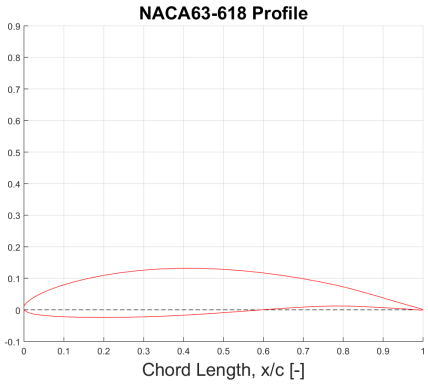

Figure 4.4: NACA63-618 airfoil

Flow facility The aerodynamic tests were all done in the M-tunnel. This is a low speed open circuit wind tunnel located at TU Delft. The test section has a diameter of 0.4 m by 0.4 m. The contraction ratio is 1:6.25. Since it is an open wind tunnel, the effective angle of attack changes. This will be discussed in more detail in the aerodynamic verification in Section 4.3.4.

External force balance The external force balance is located in front of the open wind tunnel. It is needed to measure the forces and to carry the airfoil that is installed. The balance consists of in total four S-shaped strain gauge load cells. These are needed to measure both aerodynamic forces, the lift and drag. For lift, only one strain gauge is needed, which measures the forces in the vertical direction. For drag, this is done by three of these strain gauges, measuring the forces in the horizontal direction. When

[14] Personal communication with Ricardo Pereira, MSc

starting a measurement run, the balance has to be biased. This means that all forces are set to zero, so that the actual testing can be done.

Airfoil The airfoil that is installed on the external force balance is the NACA63-618, which is shown in Fig. 4.4. This is a cambered airfoil with a sharp trailing edge. The airfoil is made out of non-conducting plastic, which is favourable to accommodate the high voltage installation of the plasma actuator. The span of the airfoil is 400 mm and it has a chord of 150 cm. The airfoil is clamped by two circular side plates. These plates prevent most of the tip vortex from appearing and therefore ensure a 2D flow.

Plasma actuator The plasma actuators are hand made and have to be installed on the airfoil as follows. For the electrodes, copper strips were used with a width of 10 mm. At first, one copper electrode strip was placed on the pressure side of the airfoil, about 10 mm of the leading edge. One side was placed about 100 mm from the end of the airfoil. Also the end had to be cut round, removing the angles, in order to prevent the electrode from sparking. The other side of the electrode was stuck along the clamping sheets, so that it could be connected to the amplifier. Then four layers of insulating Kapton® tape with a thickness of 0.05 mm, were placed on this electrode and acted as a dielectric between both electrodes. Care was taken as to leave no bubbles under the tape, since this might lead the plasma actuator to burn through when put under high voltages. When this was done, the second electrode was place on the layers of tape, just about 1 mm next to the first electrode. It is important that they do not overlap each other, since this might cause the electric field to alter in strength. The second electrode also has one long end taped on the clamping sheet so that it can be connected to the copper wires that lead to the amplifier. The effective span-wise length of the plasma actuator is 350 mm. This means that along this length actual plasma is generated. For the last three tests, the plasma actuator strip was removed, re-made and then installed on the trailing edge. The exact location of the plasma actuator for each test will be discussed later and can be found in Table 4.6

Method

In order to find out what effect plasma actuators can have on airfoil lift, eight different tests are performed. The first six tests serve to determine the effect of an actuator installed at the upper side of the airfoil at the leading edge. For the last three tests, the plasma actuator was removed from the leading edge and installed on the trailing edge.

The tests with the plasma actuator on the leading edge serve to assess the applicability of separation control. Separation control can be done using either a constant or a pulsed signal, so part of the test objective is to determine which signal type performs best. From literature [26], it is known there is an optimal pulse frequency, however the optimum value varies with Reynolds number so the optimum pulse frequency is determined first. This is done for different actuation voltages, to obtain a complete overview of the effectiveness of separation control.

To give more insight to circulation control as a control mechanism, the plasma actuator was placed on the trailing edge of the airfoil. At this location, actuators were placed on both the suction and pressure side of the airfoil. The flows over these sides have different characteristics, and one might be more susceptible to flow control than the other.

An overview of all tests is given in Fig. 4.5. The different categories within separation and circulation control can be clearly distinguished. For convenience, the test number corresponding to every case is given in the figure; test 1 is used to assess direct signal separation control, test 2-5 are used to characterize pulsed signal separation control, and tests 6-8 serve to test circulation control. More details about these tests are given below.

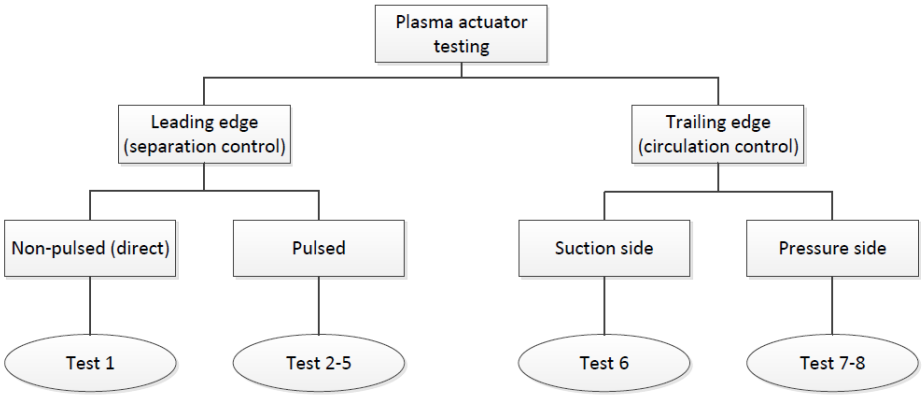

Figure 4.5: Overview of the plasma actuator test cases

In order to draw conclusions at a later stage, the results that came out of the tests have to be analyzed. Therefore it is important that test can be compared to each other; this means that for each test only one parameter can be changed, in order to find what effect it has on the $C_l - \alpha$ curve. Therefore, the angle of attack (α), the airspeed in the tunnel (U_∞), the duty cycle (DC), the electrical potential (V), the pulse frequency (f) and the location of the plasma actuator. The location is either at the leading or trailing edge (LE or TE), and on the suction or pressure side (SS or PS). An overview of the test plan can be found in Table 4.6 below.

Table 4.6: Overview of test plan

Test number	Tested parameter	α [°]	$U_\infty [m/s]$	DC [%]	V [kV]	f [Hz]	Location PA
1	-	varying	20	100	18	n/a	LE SS
2	F sweep	24	20	100	18	varying	LE SS
3	DC	varying	20	50	18	160	LE SS
4	V	varying	20	50	10	160	LE SS
5	F sweep	24	20	50	10	varying	LE SS
6	F	varying	20	50	10	80	LE SS
7	location actuator	varying	12	100	18	n/a	TE SS
8	location actuator	varying	12	100	18	n/a	TE PS
9	U_∞	varying	24	100	18	n/a	TE PS

Separation control
For the first test, a $C_l - \alpha$ curve is generated, showing both the clean configuration (plasma actuator off) and the active plasma actuator configuration with a constant signal.

The second test was performed at a constant angle of attack and the voltage signal was pulsed at different frequencies to find the optimum pulse frequency. Here the frequency was varied between 60 and 270 Hz, which correspond to a non-dimensionalized pulse frequency F^+ of 0.5 to 2.0. This is the region for F^+ where plasma actuators create the highest ΔC_l [26].

The optimum pulse frequency obtained from the previous test is used to generate another $C_l - \alpha$ curve, this time with the most optimum pulse frequency.

The tests that are outlined above were all done at a voltage of 18 kV. However, in order to see what happens at lower voltages, the voltage was lowered to 10 kV in test 4. A new frequency sweep plot is generated in test 5, which is then used to build yet another $C_l - \alpha$ curve in test 6.

Circulation control
All separation control tests made use of a plasma actuator installed at the trailing edge. To retain the flow similarity, i.e. the same Reynolds number and Mach number as before, the first two tests were performed at a lower airspeed of 12 m/s instead of 20 m/s. Also for all circulation control test, $C_l - \alpha$

curves are generated to determine the actuator effect. In test 7, the actuators were located on the upper or the so-called suction side of the trailing edge, pushing the air downstream. Later for test 8 and 9, the actuator was placed on the lower side of the airfoil, called the pressure side, pushing upstream. For the latter location, two different wind speeds were tested.

Results

The results of the nine tests outlined in Section 4.2.2 are highlighted best in two different plots: the $\Delta C_l - \alpha$ curve and a ΔC_l-frequency sweep plot. All plots have a box with information about the test parameters, i.e. the angle of attack, the wind speed, the voltage, the frequency and the position of the plasma actuator on the airfoil. For every test, the resulting plot is presented below and it is briefly analysed.

Separation control

The results of the first tests can be found in Fig. 4.6. From the figure, it follows that an activated plasma actuator delays the stall angle by about 5 degrees. This amounts to a maximum difference in lift coefficient ΔC_l of 0.5 at an angle of attack of about 24 degrees. At such a high angle of attack, a lot of drag is generated, which is in this case favourable, because the UAV will be able to fly at low velocity during landing manoeuvres while also slowing down due to the large drag forces.

The second test in Fig. 4.7 is a frequency sweep plot, used to determine the optimum pulse frequency. It is performed at an constant angle of attack of 24 degrees, since at this angle the plasma actuators have the highest effect on the ΔC_l. The plot shows that the ΔC_l does not depend on the tested pulse frequency range; it stays rather constant. The plot is most constant for the frequency range of 140 Hz to 220 Hz. According to [26], the best frequency for optimal effect of plasma actuators is about $F^+ = 1$, or 160 Hz for the tested case. This value is therefore used in later tests.

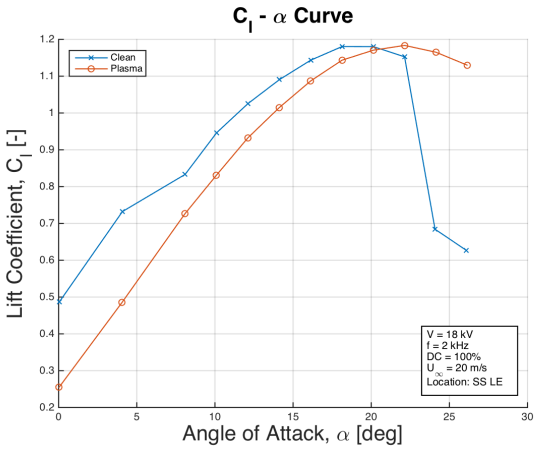

Figure 4.6: Test 1 - plasma on vs off

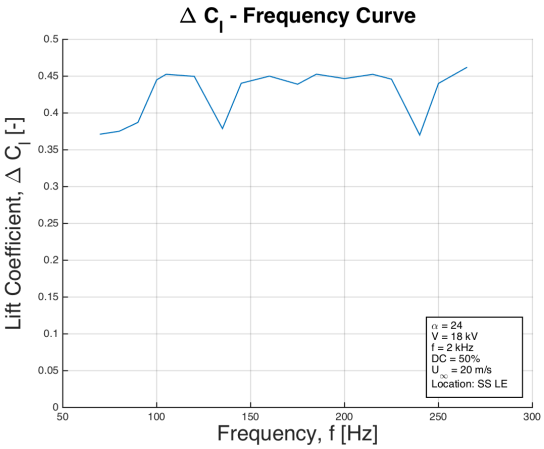

Figure 4.7: Test 2 - frequency sweep

Fig. 4.8 shows a $C_l - \alpha$ curve similar to the one generated in the first test. However, in this plot the duty cycle was set to 50%, such that the effect of the pulse can be seen. When looking at the ΔC_l, about the same value can be achieved with a pulse as without pulsing. The effect of pulsing can therefore be considered quite small.

Test 4 is the same test as test 3, but then performed at a lower voltage of 10 V instead of 18 V. The resulting $C_l - \alpha$ curve can be found in Fig. 4.9. Lowering the voltage does have an effect on the curve, in the way that it stretches the curve.

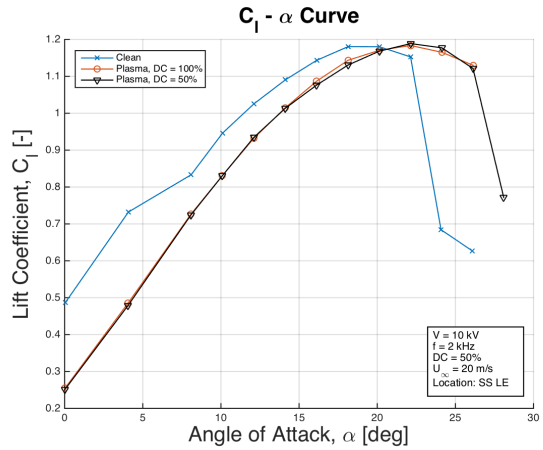

Figure 4.8: Test 1 and 3 - change in duty cycle, DC

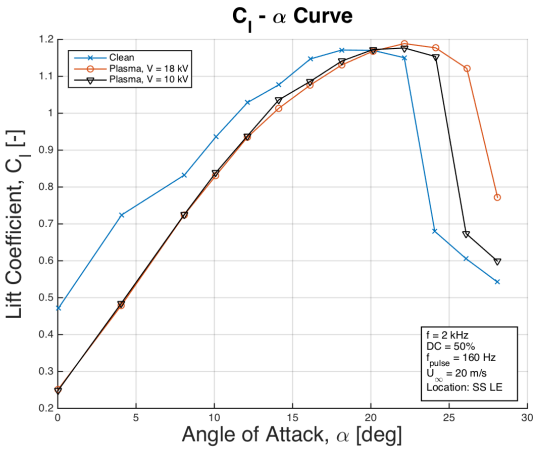

Figure 4.9: Test 4 and 5 - change in voltage, V

To determine the pulse-effect for lower voltages, a frequency sweep plot is also made for an actuation voltage of 10 kV. The result is shown in Fig. 4.10. Two main peak can be distinguished, one around 160 Hz as was used before. The other peak lays at 80 Hz. Therefore in test 6 and 7, the $C_l - \alpha$ curves at these two frequencies are generated. As can be seen in Fig. 4.11, a change in the frequency does not have a significant effect on the $C_l - \alpha$ curve.

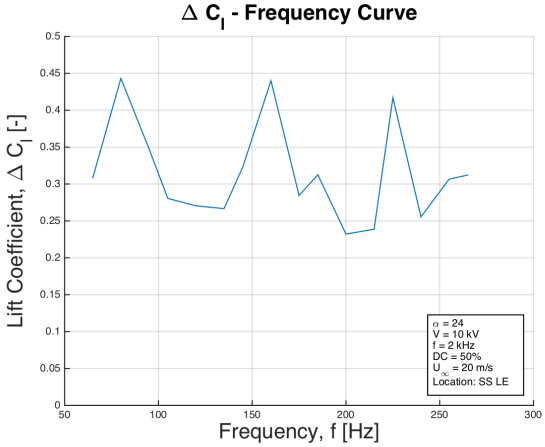

Figure 4.10: Test 5 - frequency sweep

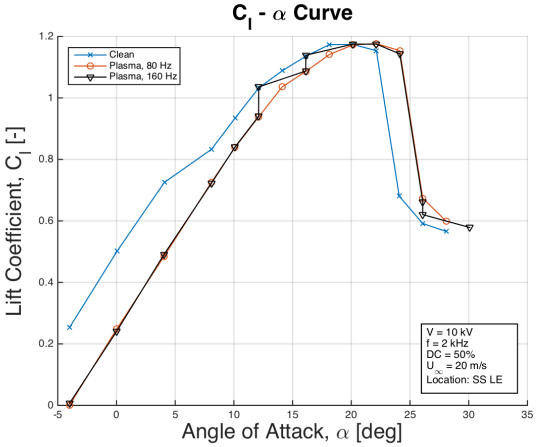

Figure 4.11: Test 6 and 7 - change in frequency, F

Circulation control

The results from the last three tests are shown in Fig. 4.12 and Fig. 4.13. Test 7 shows the $C_l - \alpha$ curve for a plasma actuator pushing downstream on the suction surface, while test 8 and 9 show the same curve, with the actuator placed on the pressure side and pushing upstream. Two different velocities are evaluated for the latter lay-out, namely 12 m/s and 24 m/s. As can be seen, the effect of circulation is not very pronounced. For most cases plasma actuators even decrease the lift, only for the highest tested speed a slight lift increase is observed. For the case of 24 m/s, it was decided not to go past the stall point, since circulation control is only used at cruising angles of attack in the design. This is because separation control yields a much larger ΔC_l at high angles of attack.

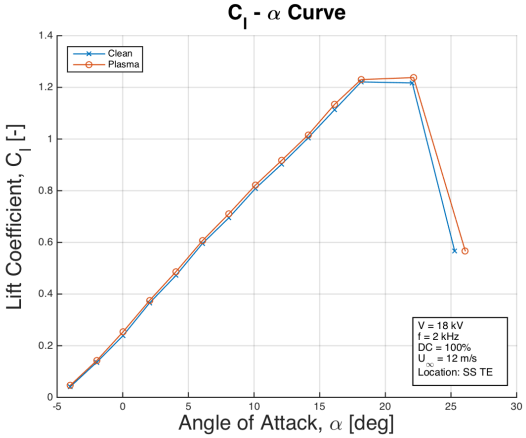

Figure 4.12: Test 7 - circulation control on a sharp TE

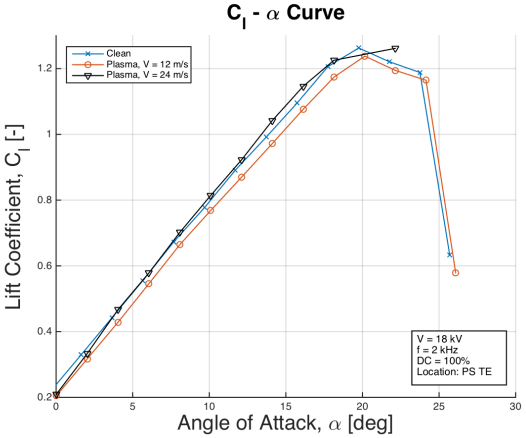

Figure 4.13: Test 8 and 9 - change in airspeed, U_∞

Conclusion

Now that the results, obtained from the wind tunnel test, have been shown and discussed, some conclusions can be drawn. Table 4.7 sums up all parameters and their corresponding values that have been found during the wind tunnel tests.

Table 4.7: Parameter effects

Parameter	Symbol	Values	Test	ΔC_l [-]	α_{stall} [°]	$\alpha_{\Delta C_{lmax}}$ [-]
Clean configuration	-	-	1	-	19	-
Pulse	DC	100%	1	0.50	22	24
		50%	3	0.51	22	26
Frequency	f	160 Hz	2	0.48	22	24
		80 Hz	6	0.34	22	26
Voltage	V	18 kV	4	0.51	22	26
		10 kV	4	0.48	22	24
Speed	U_∞	12 m/s	8	-0.055	20	26
		24 m/s	9	0.05	22	2

Clean configuration

To begin with, the use of plasma actuators delays the stall angle from 19° to 22°. As can be seen in Fig. 4.6, after stall of the clean configuration, a configuration with plasma actuators can still create a ΔC_l of about 0.5. These values show that separation control is possible, since the flow stays attached longer along the chord when the plasma actuators are on. This actually means that it can be used as a high lift device during landing configurations. The fact that the rather high angle of attack causes a lot of drag is in such a case acceptable, since low velocities are preferred during landing.

Pulse

Introducing a pulse to the actuator as in test 4, does not have a significant effect on the amount of the ΔC_l. A certain pulse frequency can be activated by switching the initial setting to e.g. 50%. The effect is so small that it can be neglected.

Frequency

The effect of frequency has been evaluated by performing two ΔC_l versus frequency range plots. Test 2 has a maximum ΔC_l at a frequency of 160 Hz, test 5 also showed a peak for a frequency of 80 Hz. However, when comparing these, 160 Hz seems to be the optimum frequency in order to produce the highest ΔC_l.

Voltage

Changing the voltage does not have a visible effect on the parameters as listed in Table 4.7. However, the

difference can be seen when looking at the $C_l - \alpha$ curve as shown in Fig. 4.9. The same lift coefficient is reached for both 10 kV and 18 kV, though the actual stall is more stretched out at a higher voltage. This is an advantage, as the UAV will not stall immediately when not flying at the exact correct speed.

Speed
As can be seen in Table. 4.7, the change in speed does indeed have an effect on the lift coefficient. This small effect is shown clearly in Fig. 4.13. When increasing the cruise speed to 24 m/s there is a significant value for ΔC_l, though this value is achieved at a very small angle of attack of 2°. This means that at high speeds, the difference in lift coefficient can already be achieved at small angle of attacks, which is preferable.

4.2.3 Plasma Actuator Integration

Now that the wing planform is defined, the integration of the plasma actuators into the wing and empennage can be considered. The working principle of the eight mechanisms was already explained in Section 2.1.2. The integration is discussed for each of the three manoeuvring rates that have to be achieved: roll, pitch and yaw. The effectiveness of plasma actuators as high lift devices is also presented.

Roll Control
In conventional aircraft, asymmetric deflection of ailerons generate counteracting changes in lift, causing it to roll. The same can be achieved using plasma actuators, because they can also provide lift differences.

It has been decided to use mechanism 6, the blunt TE Gurney flap mechanism, which is a circulation control method. Wing tip stall is a prerequisite for separation control, which causes an unacceptable amount of extra drag. To improve the efficiency of the aircraft and reduce the power consumption, the circulation control method is therefore preferred over separation control.

In order to achieve the highest possible roll rate, the change in lift has to be as large as possible. The highest change in lift is achieved using a blunt TE Gurney flap, so this mechanism is chosen. This is also explained in Section 2.1.2. A symmetric blunt airfoil is used at the wing tips, because more data is available about it, which makes the design more reliable. It is decided to put the plasma actuator exactly at the end of the airfoil, since this actuator location gives the most consistent performance [13]. To achieve the required high design lift coefficient, a cambered airfoil is still used at inboard sections, meaning the airfoil transitions from blunt to sharp somewhere along the wing.

To summarize, a schematic representation of the selected roll control configuration is presented in Fig. 4.14. In this figure, plasma actuator location 1 is for roll. This is also where the symmetric airfoil is applied. At the wing tip, the lift arm is the largest, so the actuator is most effective for roll performance.

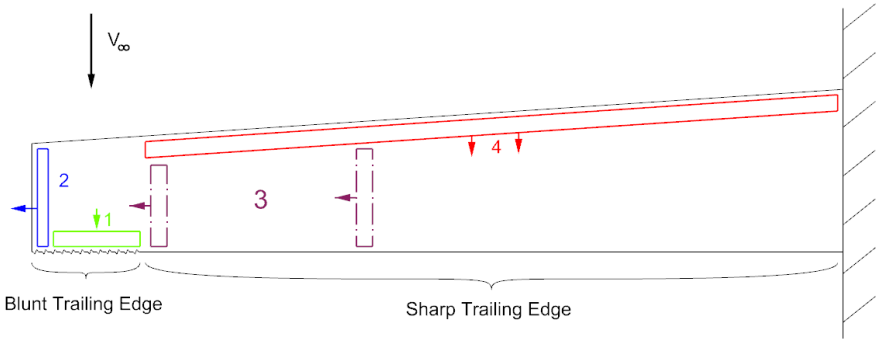

(a) Upper side

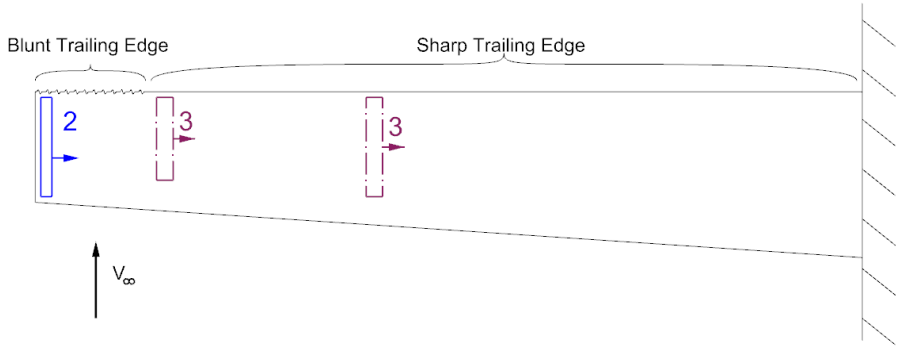

(b) Lower side

Figure 4.14: Schematic plasma actuator layout on the main wing

Pitch Control

Deflection of elevators typically controls pitch on a fixed wing UAV, but these moving surfaces can be replaced by plasma actuators as well. It has been decided to use the blunt TE 'Gurney flap' mechanism 5 on the horizontal tail and the 'winglet' mechanisms 7 and 8 on the main wing. They are explained in section 2.1.2

To induce a negative (pitch down) moment, the lift on the tail will be increased using a plasma actuator on the horizontal tail, Fig. 4.15. It is decided to use a rounded trailing edge airfoil for the symmetrical tail, since the ΔC_l obtained with a sharp tailing edge is too small to control the UAV effectively, as was found in Section 4.2.2. Again, the plasma actuators will be placed exactly at the end of the airfoil.

A positive (pitch up) moment can be created with plasma induced lift increase on the main wing. This can only be done if the centre of pressure of the wing is in front of the centre of gravity at all times, as is investigated in Section 4.5.3). The main wing lift increase could be obtained using the roll plasma actuators on location 1 in Fig. 4.14, operated symmetrically. However to decouple pitch from roll, the pitch up moment is created using plasma actuator mechanism 7 and 8. The actuators are placed in cordwise direction near the wing tip. Six actuators are used per wing on three different spanwise locations, namely 0 m, 0.375 m and 0.5 m from the tip. Per location, one is placed on the suction side and one on the pressure side of the wing, acting on the flow in opposite spanwise direction. This is done to increase the effectiveness of the control mechanism.

As shown in Fig. 4.14, the plasma actuators at location 2 shield the low pressure upper side of the wing from the high pressure lower side, a feature of mechanism 7. The plasma actuators at location 3 serve to counteract the formation of a wing tip vortex, but it is expected that it also solves the velocity mismatch at the trailing edge of the wing (i.e. mechanism 8). As was mentioned before, it is decided not to quantify this mechanism so the exact effect is not known, however a small effect will still be present and the lift of the wing will be enhanced just a little bit more than it would be for the case with plasma actuators only on the tip.

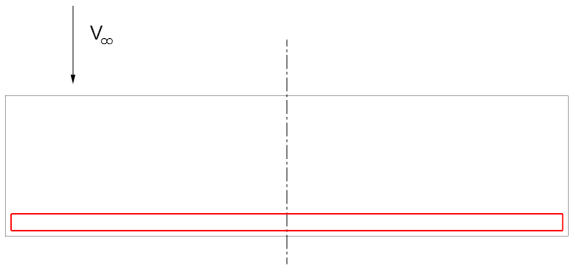

Figure 4.15: Schematic plasma actuator layout on the horizontal tail

Yaw Control

Yaw control is done with rudders on conventional aircraft. To control the yawing motion of the plasma UAV, a blunt TE circulation control mechanism is chosen. Yaw control is only important in case the roll control system fails, and in case it does, only small yawing moments are required. A schematic representation of the plasma actuator layout is presented in Fig. 4.16. A symmetric airfoil is used for the vertical tail, since it should not produce lift during normal flight conditions and it is desirable to have the lowest possible drag. As for all other blunt airfoils, the plasma actuator is placed exactly at the end of the airfoil.

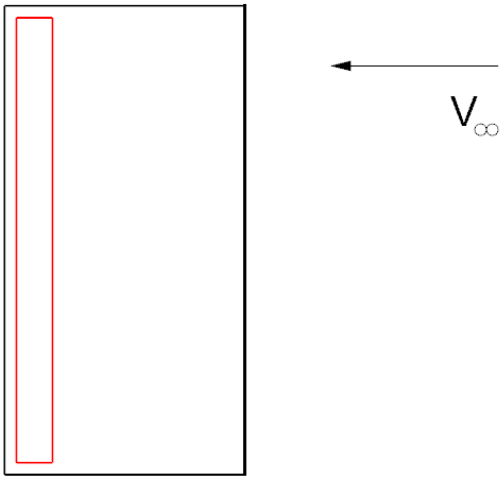

Figure 4.16: Schematic plasma actuator layout on the vertical tail

High Lift Devices

High lift devices (HLDs) are applied to achieve a higher maximum lift coefficient for take-off and landing. Although the take-off is achieved with a launcher and the UAV performs a belly landing, a higher lift coefficient can increase the wing loading, thus decrease the required wing surface area. This can even increase the aspect ratio (by having the same maximum wing span, but decreasing the chord length).

Since the HLD will only be used at landing, which occurs at low speed and high angle of attack, it is decided to use the separation control mechanism to generate the effect of HLDs. The actuators that are used as HLD are located at position 4 in Fig. 4.14. To have clean flow over the pitch and roll actuators at locations 1 and 2, the HLD actuators don't extend all the way to the wing tip.

4.2.4 Plasma Actuator Sensitivity Analysis

The plasma mechanisms used for roll, yaw, pitch and as HLD are designed to meet a set of requirements. In this section firstly the influence of a change in these requirements on their effectiveness and thus sizing

is assessed, considering a change in angle of attack (AOA), actuation voltage and frequency, UAV weight, airspeed and life cycle length. Secondly the sensitivity of the wind tunnel test is assessed.

Angle of Attack
Mechanism 1, used for the HLDs, is only effective at an AOA higher than the stall AOA, effectively shifting it with about 5°. The range of operation of the HLDs is between 20° and 26°, as can be seen in Fig. 4.8 in Section 4.2.2. If this range should be changed, another airfoil or mechanism should be selected.

Rolling, pitching down and yawing are accomplished using (Gurney flap) mechanism 6. This mechanism only operates at an AOA lower than the stall AOA. The ΔC_L achieved by the mechanism is increased when the AOA is higher, helping to stabilize the aircraft laterally and longitudinally.

Pitching up should work at all AOA, for as long as lift is created, the wing will produce wing tip vortices. These can then be countered by (winglet) mechanisms 7 and 8. The higher the AOA, the more lift is created and the more effective the pitch up control will become, limited by the stall AOA.

Weight Distribution
The HLDs are only influenced by the total weight and not by the weight distribution. They have to make sure the production C_L is maintained at higher angle of attack and thus lower airspeed. If the weight increases, so does the wing and the sizing of the HLDs, which always covers as much of the wing's leading edge as possible.

To keep the roll, pitch and yaw rates comply to the requirements, the moments of inertia I_{xx}, I_{yy} and I_{zz}, respectively are important parameters. If the rates were variable, they would change linearly with the inverse of I_m. However, as they are fixed requirements for the design of the UAV, the plasma actuator surface or effectiveness should be adjusted to react to a change in I_m.

The location of the CG is important for the stability of the UAV as well. If it diverts, the aircraft will tend to start rolling pitching or yawing. This movement can be countered by constantly activating the plasma actuators, which is quite expensive in terms of power.

UAV Airspeed
The two parameters that characterise the flow and determine the effectiveness of the plasma actuators are Reynolds number and Mach number. The AC-DBD plasma actuators used for this project are only effective up to relatively low Reynolds numbers. Plasma actuators still work efficiently around Reynolds numbers of 100.000-300.000, however their effectiveness decreases rapidly with Reynolds number [13].

The dominant effect is that of the Reynolds number, as the airspeeds and thus Mach numbers at which the plasma actuators might be applied, are too low for any compressibility effects to appear.

Applied Voltage and Frequency
The momentum added to the flow and thus the effectiveness of the plasma actuator is related to the applied voltage exponentially for rolling, pitching down and yawing. As the effectiveness of the HLDs is related to added momentum as well, the exponential relationship stands. The frequency doesn't seem to have an influence on the effectiveness of mechanism 6 [13].

For the pitching up mechanism, a separate assessment was made, as the generated blunt force is less important than the strength of the induced vortices. The starting vortex created by AC-DBD plasma actuators is assessed quantitatively by Whalley. It is concluded that an increase in voltage yields a small increase in the circulation and thus the size of the created vortex. No relationship with the frequency mentioned. When looking at the increase in momentum with voltage and frequency, a clear positive effect of the frequency can be seen [27].

Mission Time
When the mission time of 30 hours is extended, the performance of the plasma actuators might go down, due to deterioration of the high voltage switches and the dielectric layers.

4.2.5 Plasma Verification

In this section the verification method of the plasma actuator quantification is presented. It is split up into verification of the wind tunnel test and the verification of the analytical quantification process.

Wind Tunnel Test

This half of the plasma actuator design verification focuses on the verification of the wind tunnel test. The different sources of errors in the test data are determined and analysed, to verify whether the obtained results can be used in the overall plasma actuator design process.

Flow facility

For the wind tunnel test, the M tunnel was used which is an open circuit wind tunnel. The problem with such open wind tunnels is that the flow gets deflected downwards directly where the flow exits the tunnel. This means that the airfoil in front of the tunnel experiences a change in the effective angle of attack. In case the airfoil has been installed upside down (which was the case during the tests for the project), the airfoil experiences a larger angle of attack due to the deflected flow. The angle of attack at which the airfoil can be manually installed should therefore be corrected. This is done via an analytic correction method, which is based on the work of Brooks et al. [28].This corrected angle was already available in the interface that was used during the test, so the plots in Section 4.2.2 did not suffer very much from this defect.

External force balance

For the force balance setup, two correction have to be taken into account. First of all, the static forces that are present in the balance at the start of the test run have to be biased. This is analogous to a calibration of the load sensors. The static forces can be induced during for example mounting of the airfoil, and if they are not 'removed', the moment, lift and drag coefficient values will all be off. This was known in advance however, so care was taken to bias the force balance before every test and the test results did not suffer from this effect.

Airfoil

Even though the wind tunnel should represent a 2D configuration, it does not fully do so. The airfoil is clamped between two sheets in order to prevent any flow from the pressure side to the suction side of the airfoil. This flow normally leads to the tip vortices that are characteristic of a 3D flow. Even though the airfoil was clamped, the sheets were not large and solid enough to fully prevent this vortex generation. In addition, drag measurements were corrected for the effect of these side plates. Therefore, the wind tunnel does not give a perfectly 2D representation, and this has to be accounted for when using the test results in the design process. For the purpose of this project, the results are considered sufficient for plasma actuator design.

Plasma Actuator Quantification

This part of the verification method focuses on verifying the analytical mechanism quantification process. In this process, mechanisms 7 and 8 were quantified using different methods, see Section 4.2.1, and both of these methods will be verified here.

To verify the quantification of mechanism 7, the results could be checked against the known effects of real wing tip tanks. The aerodynamic principle behind both is the same, so it can be expected that their effect is also similar. The one complication in this is that it is very hard to determine what the size of the real tip tank should be. An initial estimate of the required size could be made by using the plasma starting vortex size from [27], however this is still a rudimentary calculation. It is therefore hard to verify the quantification calculation for mechanism 7, and it is suggested to immediately validate it instead, using a wind tunnel test. This will be elaborated on further in Section 4.6.

4.3 Aerodynamic Design

This section discusses the aerodynamic design of the plasma actuator controlled UAV. First an airfoil has to be selected. This selection is based on the data obtained from a JavaFoil[15] analysis and the wind tunnel tests discussed in the previous section. Next is the wing planform design, in which the wing configuration is discussed as well as some governing parameters such as taper and sweep. Finally, the integration of plasma actuator into the planform is explained. Its effectiveness is evaluated for roll, pitch and yaw control. The feasibility of plasma actuators used as high lift devices is also assessed.

[15] JavaFoil applies potential flow and boundary layer analysis and is a useful tool for simple flows. The tool is limited when separation occurs: it uses empirical corrections to find maximum lift.

4.3.1 Airfoil Selection

The aerodynamic design begins with selecting an airfoil. For this, a brief overview of the advantages and disadvantages of the following criteria is presented: Mach number, Reynolds number, camber, wing thickness, design lift coefficient and plasma actuator performance. NACA series are compared using JavaFoil to select promising airfoils. JavaFoil is then used to produce some aerodynamic data.

Given an airfoil geometry, its aerodynamic performance (i.e. lift, drag and moment coefficients) depends on Mach number, Reynolds number and angle of attack. It is convenient that the UAV flies sub-sonically. This simplifies the analysis in the sense that critical Mach number and compressibility effects do not have to be taken into account. A high Reynolds number allows the airflow to stay attached longer. This leads to a decrease of friction due to flow separation and an increase of maximum lift coefficient. The maximum lift coefficient also depends on camber and wing thickness.

Camber can be used to achieve higher design lift coefficient. Cambered airfoils produce lift at zero angle of attack. The location of maximum camber and maximum thickness is desired near the leading edge, as this increases the maximum lift coefficient for both parameters. This can also promote stall at lower angles of attack, which can be prevented using plasma actuators. The maximum lift coefficient is highest at a thickness to chord ratio of 14% [29]. Thicker wings stall first at the trailing edge of the wing. This is wanted for plasma actuator application. A disadvantage is that it also promotes drag.

The design lift coefficient is based on the mission phase that requires the most energy. This is the 2.0 h endurance mentioned in Section 2.2.1. For best performance in this stage, the (L^3/D^2) ratio should be maximised for propeller aircraft. This boils down to a lift coefficient of $C_{L_{des}} = \sqrt{3C_{D0}\pi Ae} = 0.9$. Another method is to estimate the required lift. A 10% compensation is suggested for the negative lift generated by the tail to trim the UAV, hence $C_{L_{des}} = 1.1/q \cdot W/S = 0.9$ yields a comparable result. The design lift coefficient is the same for 2D airfoils as for 3D wings, because the wing is unswept (see Section 4.3.2).

For the UAV wing design, the NACA 4-, 5- and 6-series provide promising airfoils. [24] The 4-series provides a general purpose airfoil. This series yields however relatively low maximum lift coefficients and high drag and pitching moment. Compared to the 4-series, the 5-series has a lower pitching moment in general. A reflexed camber line modification can be applied, which is generally only used for flying wings. The 5-series can thus be used for moment coefficient related solutions. More specifically, it can assist in simplifying the tail design. The 6-series generates less drag compared to the 4-series. This is achieved due to its emphasis on maximising laminar flow. Considering that more weight reduction can be achieved in the battery (due to lower drag coefficient) than in the tail design (due to lower moment coefficient), the 6-series is preferred.

In summary, the airfoil geometry needs the following characteristics: NACA 6-series, design lift coefficient of 0.9, maximum camber and thickness location near the leading edge and a thickness to chord ratio slightly higher than 14%. The maximum lift coefficient shall be at least 1.2 with aspect ratio 8 at Reynolds number range 2×10^5 to 5×10^5 based on the preliminary design in [12]. Finally, as the UAV flies sub-sonically, the Mach number is virtually zero.

A suitable airfoil is the NACA63A-915. This is a NACA 6-series, has maximum thickness to chord of 15% at 0.30 chord point, design lift coefficient 0.9. Note that the A-modification leads to a less cusped trailing edge region. Also, the NACA64A-015, a symmetric airfoil with the same thickness to chord is used at the wing tips and tail, because more reliable data of the plasma actuator performance is available for this airfoil. This was found in the previous section on plasma actuator integration. Thus, the fist wing profile is mainly used for lift generation, the second one for plasma integration. An overview of the selected airfoils can be found in Table 4.8.

Table 4.8: Airfoil selection

Airfoil	t/c [%]	C_{lmax} [-]	Camber	Position
NACA63A-915	15	1.5	yes	inner section wing
NACA64A-015	15	0.9	no	wing tips and empennage

Finally, JavaFoil is used to determine the aerodynamic characteristics. Fig. 4.17 shows the lift, drag and

moment polar of the NACA63A-915, Fig. 4.18 shows these polars for the NACA64A-015. The polars have been drawn for the expected Reynolds number range and aspect ratio of 8. The surface finish is assumed to contain irregularities (e.g. bugs and dirt) and the transition model is the Eppler standard. From the figures it becomes clear that when the Reynolds number decreases the sudden decrease in lift and increase in drag and moment coefficient occurs at progressively lower angles of attack. In addition, it can be seen that the design lift coefficient of 0.9 is reached at an angle of attack of around 2 deg. This is therefore the optimum cruise angle of attack. From Section 4.2.2, the optimum angle for the HLDs is right around the stall angle of the airfoil. From Fig. 4.17, stall is reached at around 14 degrees, therefore this is the optimum angle for landing.

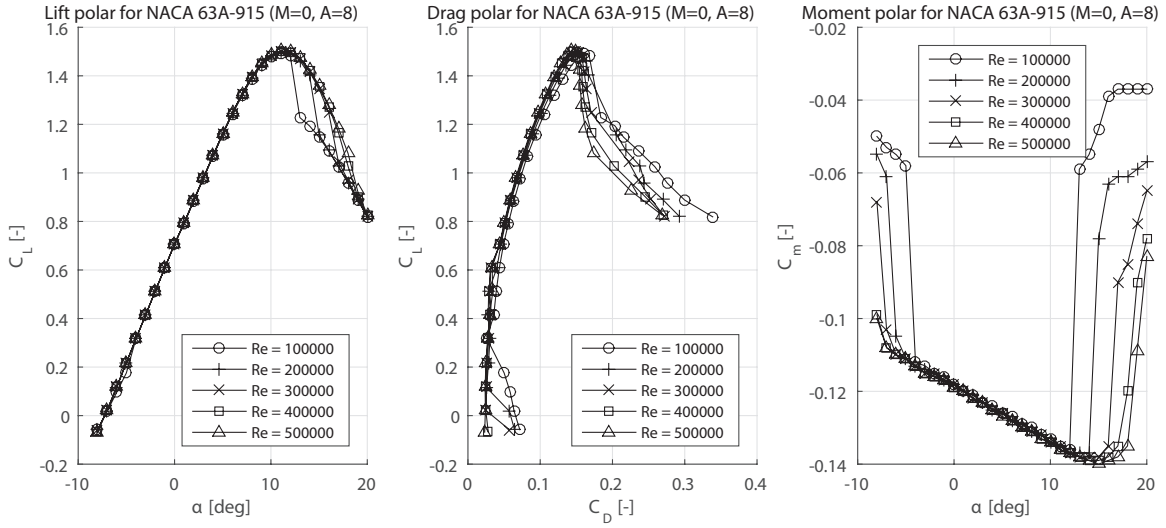

Figure 4.17: The aerodynamic polars of the NACA63A-915.

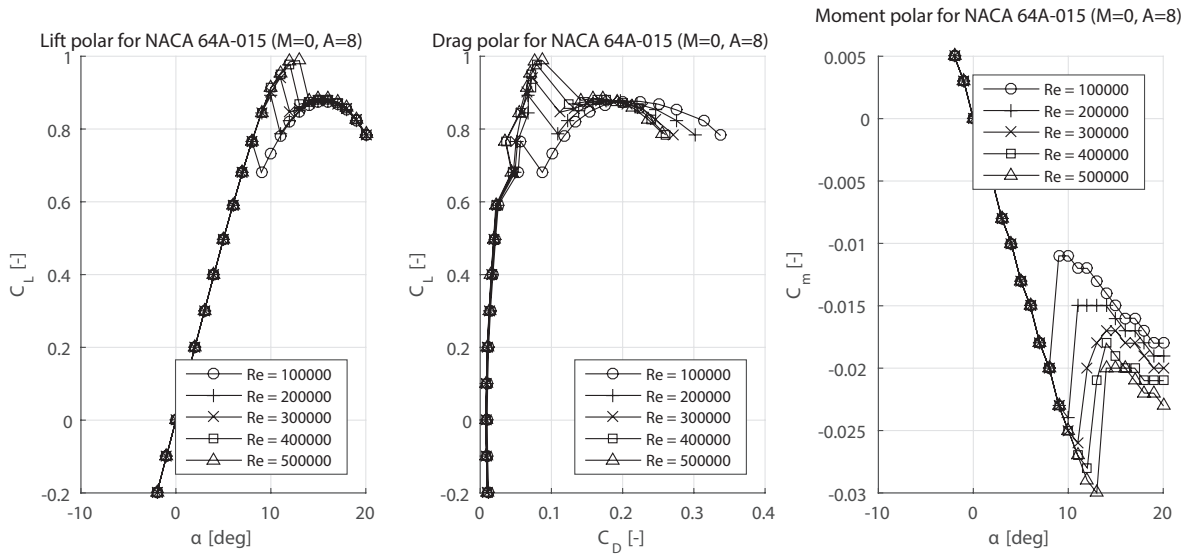

Figure 4.18: The aerodynamic polars of the NACA64A-015.

4.3.2 Wing Planform

Now that the airfoil has been defined, the wing planform can be designed. First several wing configurations are evaluated. Then, in order to define the wing planform, the following parameters have to be determined: taper ratio, quarter-chord sweep angle, wing twist angle, dihedral angle and the wing incidence angle. These parameters can be estimated using Raymer's method [29]. The results of the preliminary wing sizing are presented in Table 4.9. A small description of the main design decisions is given below.

Wing Configuration

The wing configuration can be high, mid or low. A high wing configuration was chosen to ensure enough ground clearance during the belly landing. This configuration is also more stable compared to a low or mid wing configuration, because it features a stabilising dihedral effect. Furthermore, possible payload instruments, such as a camera, enjoy better visibility when faced downwards.

Taper Ratio and Twist Angle

Taper ratio is defined as the ratio of tip chord c_t and root chord c_r and this parameter influences the lift distribution of the wing. An elliptical planform is desired to achieve the highest possible Oswald factor. This is unfortunately relatively expensive to construct. It can however be resembled by a trapezoidal area with a taper ratio of 0.45 [29].

A wing with elliptical lift distribution stalls uniformly over the span. Wing twist can be introduced for stall to occur first on inboard sections, such that roll control devices on tip sections are still effective. However, wing twist makes the manufacturing process more complex, thus more expensive. Tip stall can also be prevented by choosing a slightly higher taper ratio than required for elliptical lift distribution, without the disadvantage of the additional manufacturing complexity. Therefore a taper ratio $\lambda = 0.5$ is chosen, without twist. The root, tip and mean aerodynamic chord are now fixed, respectively $c_r = 0.47$ m, $c_t = 0.24$ m and $\bar{c} = 0.37$ m.

Sweep, Dihedral and Wing Incidence

The UAV operates at a very low Mach number so no sweep angle is necessary to reduce transonic effects. Positive (aft) sweep angle could still be used to create a tolerance for gusts, when a sudden increase in lift of the wing causes a pitch down torsion of the wing that decreases the incidence angle. However, gusts do not have to be taken into account in the design, because the UAV is designed as a prototype to demonstrate the use of plasma control. A positive sweep angle also provides stability through the dihedral effect. Nonetheless, introducing sweep angle for this effect is not as effective as introducing a dihedral angle. Roughly, a 1° dihedral angle has the same dihedral effect as a 10° sweep angle [29]. Therefore, the quarter-chord sweep angle is chosen to be zero.

The dihedral angle Γ_w is used to influence the dihedral effect, and in turn the spiral and Dutch roll stability. Reference data is used to estimate the dihedral angle, based on wing sweep and configuration. For an unswept, high wing configuration a dihedral angle between 0° and 2° should be selected [29]. However, these values are suggested for conventional aircraft configuration. The selected UAV configuration is not considered conventional however, and for stability reasons it is therefore decided to set the dihedral angle to $\Gamma_w = 3°$. This value will be review in the section on stability, Section 4.5.2.

To minimize the drag of the fuselage at cruise conditions, the wing is given an incidence angle i_w with respect to the fuselage. For general aviation an incidence angle of 2° usually introduced. This is also the angle of attack at which the design lift coefficient is achieved.

Table 4.9: Parameters for the preliminary wing planform design

Parameter	Symbol	Value	Unit
Taper ratio	λ	0.5	-
Quarter chord sweep angle	$\Lambda_{0.25c}$	0	°
Twist angle	ϵ_t	0	°
Dihedral angle	Γ_w	3	°
Wing incidence angle	i_w	2	°
Root chord	c_r	0.47	m
Tip chord	c_t	0.24	m
Mean aerodynamic chord	$\bar{c}$	0.37	m

C_D Calculation

It is of important to estimate the overall drag of the entire UAV. Drag consists of two parts, the zero-lift drag D_0 and induced drag D_i. The drag is directly related to the drag coefficient C_D, therefore,

$$C_D = C_{D_0} + C_{D_i} \tag{4.4}$$

In the plasma UAV, the contribution to the zero-lift drag comes from the fuselage, the wing and the tails, i.e.

$$C_{D_0} = C_{D_{0_f}} + C_{D_{0_w}} + C_{D_{0_{ht}}} + C_{D_{0_{vt}}} \tag{4.5}$$

The zero-lift drag coefficient of a fuselage is given by the following equation [30]:

$$C_{D_{0_f}} = C_f f_{LD} f_M \frac{S_{wet_f}}{S} \tag{4.6}$$

Where, with laminar flow,

$$C_f = \frac{1.327}{\sqrt{Re}} \tag{4.7}$$

$$f_{LD} = 1 + \frac{60}{(L/D)^3} + 0.0025(\frac{L}{D}) \tag{4.8}$$

$$f_M = 1 - 0.08M^{1.45} \tag{4.9}$$

The contribution from the wing and the tails can be determined in similar ways. More calculation details can be found in [30]. The total drag coefficient of the UAV during cruise is 0.07.

4.3.3 Aerodynamic Sensitivity Analysis

This subsection analyses the sensitivity of the aerodynamic design. In total three design variables can be distinguished for the aerodynamic design. The first is the design lift coefficient, which is the lift coefficient that is desired to be achieved and designed for. A change in the design lift coefficient leads to a change in airfoil selection. This is because the airfoil selection is mostly based on the amount of lift it can create.

The weight of the UAV is the second design variable. This variable has most influence on the wing planform. For an increase in weight, a larger wing surface is needed in order to keep the same wing loading (W/S).

The last design variable is the plasma actuator mechanism. It influences both airfoil and the wing planform. There are four circulation control mechanisms, and four separation control mechanisms. Plasma actuators for circulation control working along the stream work best at blunt trailing edge airfoils. It can be used on sharp trailing edge airfoils as well, though they only have an effect when used at 90° to the stream. Separation control works on both blunt and sharp airfoils, when functioning in the direction of the flow. The wing planform is influenced by the plasma actuators in the way that they have to be installed on the wing. Therefore, there should be enough space for them. Long wing spans provide longer areas along which the actuators can be placed. This results in longer moment arms which make the plasma actuators more effective.

4.3.4 Aerodynamic Verification

For the aerodynamic verification the following questions has to be answered: is the way to the final design solved in the right way and is the correct method used?

For the airfoil design JavaFoil was used. For the stability and control mainly XFoil and XFLR5 were used. All three programs give estimations for the aerodynamic analysis of a certain airfoil. This comes along with the fact that they are not precise at predicting separated flows. Also, JavaFoil does not account for separation bubbles. This concludes that it has to be kept in mind that all values that result from evaluations of these programs are estimations.

For the design of the UAV, it has been decided that loiter is the most fuel intensive stage of the flight. This resulted in a rather high lift coefficient of 0.9. The negative aspect of such a high lift coefficient is that it comes along with more drag as well. For the airfoil selection, one was found that suits this high lift coefficient. Fortunately, the maximum lift coefficient that belongs to that airfoil is only 1.3, which is considered an acceptable value.

In order to size for the wing planform, assumptions were made on the taper ratio, the twist angle, the sweep, dihedral and the wing incidence angle. The range in which these parameters normally lay were all found in Raymer [29], and were based on a large database of reference aircraft. However, this database was not specifically for UAVs; jet and propeller aircraft were included as well. This means that the chosen values for the wing planform parameters might coincide with values for reference aircraft, though not exactly for those of UAVs as the one that has to be designed.

4.4 Structural Design

This section describes the structural characteristics of the plasma controlled UAV. Firstly, the final structural design is presented in Section 4.4.1, followed by the approach and steps taken which led to this design. The first step in the structural design process is to determine the loads that the structure has to withstand in Section 4.4.2. Subsequently the stress analysis is covered for the structure in Section 4.4.3 and 4.4.4, after which a material evaluation and selection is performed in Section 4.4.5 and 4.4.6. This analysis will provide quantitative requirements on the structure of the UAV. This section is wrapped up with a sensitivity analysis and a verification and validation of the process in Section 4.4.8.

4.4.1 Final Structural Design

To give a proper insight into the structural design, the final design is briefly presented in this subsection. Note that the manufacturing of the UAV is described in the production plan, which is included in Section 5.2 and will also regard integration of cables and actuators.

Wing - Tail Assembly

The wing and tail assembly, Fig. 4.19, primarily consist of an airfoil geometry due to their function. They are designed to be produced with a 35 kg/m^3 polyurethane (PUR) foam core with a quasi-isotropically oriented TeXtreme 1027 carbon fibre skin for the lightest weight and relative production simplicity. The booms connecting the wing and tail are a hollow circular carbon fibre rod, which have been locally reinforced with TeXtreme 1027 carbon fibre where they are integrated in the wing and tail. The loads will be transferred to the skin of the wing and tail directly to protect the foam cores.

Figure 4.19: Structural design of the wing-tail assembly

Fuselage Assembly

The fuselage will be attached to the wing through an rubber lined interface fit in the fuselage, Fig. 4.20. The fuselage will be made of a 1 mm thick Airex foam core reinforced with a quasi-isotropically orientation of TeXtreme 1027 carbon fibre to withstand the impact of landing and keeping the weight of the fuselage low. The fuselage layout is discussed in Section 4.1.4 and the choice for a rectangular shaped cross section was made, because of both ease of manufacturing and subsystems layout.

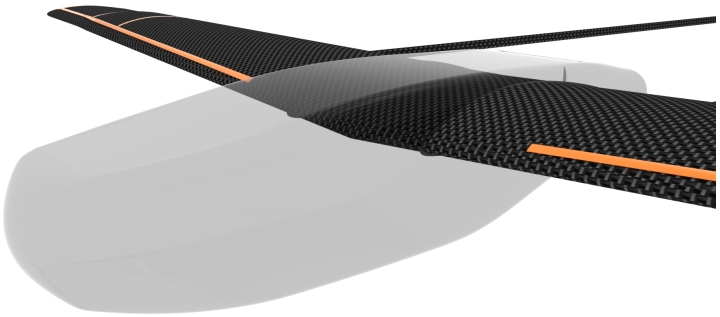

Figure 4.20: Structural design of the fuselage assembly

4.4.2 Load Analysis

When a structure is under a specific load, guiding the forces along the right paths will decrease the amount of material required in order to withstand the loads. It is therefore essential to know the types of loads that will be encountered. To determine the different loads, a qualitative breakdown of the structure was made. The UAV is mainly composed of a wing, fuselage and tail which are then bound together.

The structure of the UAV should be able to withstand the loads during its operation. The loads that appear during the operation are analysed and quantified in this section. The expected main forces and loads are shown in Fig. 4.21. The result from this analysis will be used as input for the internal stress analysis (described in Section 4.4.4) which determines whether the combination of the structure and a material is sufficient to withstand the loads.

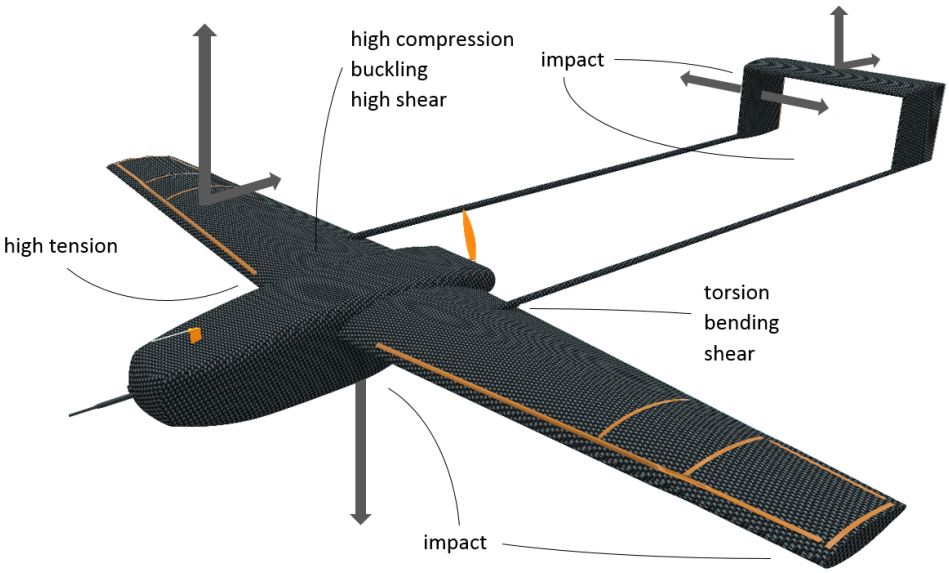

Figure 4.21: Overview of forces & anticipated loads

Reference Frames

In this section the UAV will be modelled and analysed. To do so, a set of reference frames has to be selected. For the structural analysis of the UAV two reference frames will be used; one global reference frame (Fig. 4.22a) to determine all the forces, moments and torques acting on the structure. Once all the loads have been determined, the structure is analysed locally. To do so, a local reference frame (Fig. 4.22b) is adopted to determine all the stresses acting in the structure and there-from evaluate the most optimal structural configuration with respect to material selection and structural geometry. The local reference frame will only be defined once for the wing structural group.

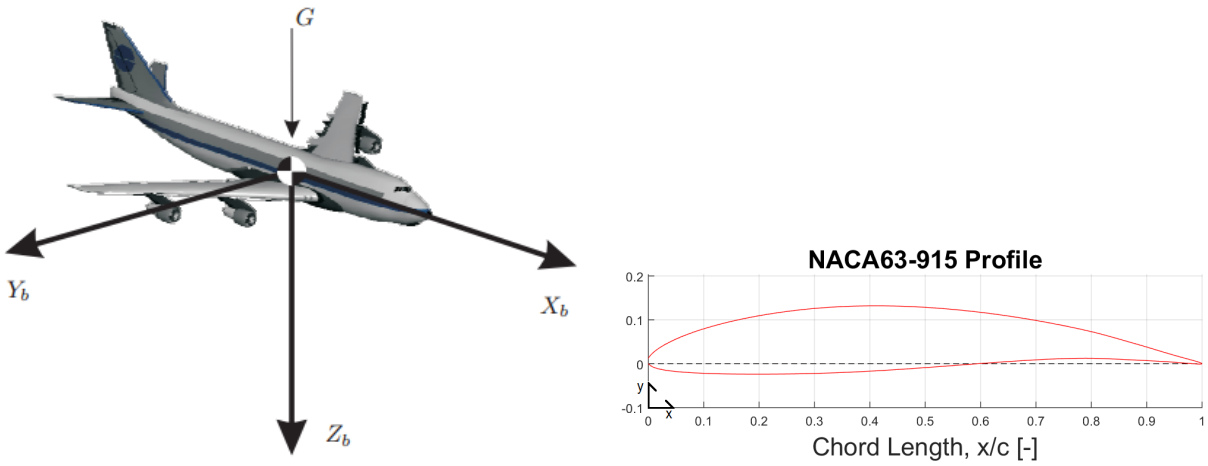

(a) Global reference frame [31]

(b) Local reference frame

Figure 4.22: Reference frames

Wing Group

The wing of the UAV can be seen as the centre of the structure. The fuselage is fitted to the wing while the tail will be attached to the wing symmetrically at two locations, as was established with the top level concept Fig. 4.21. The forces acting on the wing are due to lift, drag, fuselage weight and the forces and moments generated by the tail. These forces have been evaluated in Section 4.4.3, and will produce normal and shear stresses, along with torques due to shear forces acting away from the shear centre.

The wing group will mainly experience normal stresses due to the bending moments about the $x-$ and $z-$axes, due to the lift and drag forces respectively. There will also be a pitch-up/down moments (about the $y-$axis) acting on the wing due to the tail depending on the flight condition, and also some moments about the $z-$axis due to side wind gusts.

The shape of the wing is unsymmetrical, thus there will be an area moment of inertia I_{xy}. Due to the shape of the airfoil, I_{yy} (in the local reference frame) will be a lot larger than I_{xx}, and since the largest aerodynamic force is lift, the structural effects of the drag force are not critical and will be over-designed for that orientation. To make the wing as light as possible, the wing should have the minimum amount of material to withstand the lift forces multiplied by the determined load factor.

The shear forces in the wing will be smaller when compared to the order of magnitude of the normal stresses caused by the lift force. The most significant shear forces will come from the tail, since it spans almost two meters behind the wing. It is very important to make sure that the structure can withstand the combination of normal and shear stresses.

Tail Group

The tail will be attached to the wing through an optimized structure to transfer the loads. The shape will be determined at the end of the analysis since only then the most optimal geometry for the structure will be known. As determined by the top level concept Fig. 3.3, the tail will have two vertical surfaces and one horizontal surface which is to be located outside the prop-wash. The forces acting on the tail will be again mainly lift and drag forces, but will also be more sensitive to wind gusts coming from the side since the tail has a long arm over which the sidewards force acts. Since the tail experiences forces from all directions, all types of loads would be present in the structure connecting the tail to the wing. Therefore, using a hollow circular shape would be the most optimal way to take all loads into account, and have the structure with the lightest possible weight.

In the case that the tail hits the ground first during landing, the rods holding the tail must not break. Given that the UAV will weigh about 10 kg, the impact around 2.5 g, and a safety factor of 1.5, the total force expected on the tail is 368 N. The rods will be about 2 m long, which will result in a total moment of 735 Nm, thus 368 Nm per rod. The yield strength of carbon fibre is 600 MPa, and since the smaller the thickness of the rod, the lighter it is, a thickness of 1 mm is taken. From the bending equation and

the area moment of inertia of a rod, the diameter of the rod can be evaluated as follows:

$$d = \sqrt{\frac{M \times 4}{\sigma_{tensile} \times \pi \times t}} \times 1000 = 28mm \tag{4.10}$$

In order to make sure that the booms are strong enough, an inner thickness of 28 mm is taken, meaning that the outer diameter will be 30 mm[16] and will have a total weight of 510 grams per UAV.

Fuselage Group

In terms of load analysis, the fuselage is carrying all subsystems of the UAV. Structurally it should shelter the internal subsystems from the environment and transfer loads from the landing impact to the wing efficiently. The fuselage structure is dictated by the lay-out of subsystems (for the location of the centre of gravity), the stability of the aircraft (centre of gravity of the fuselage w.r.t. to the aerodynamic centre of the UAV) and the impact forces it has to cope with. The fuselage design process generally consists of the following steps: providing space for internal systems, choosing an aerodynamic shape, accounting for landing and launching forces, positioning of the interface fit of the wing and considering accessibility for operations and maintenance [32]. The first two are covered in Section 4.1.4.

During landing, the fuselage will impact the ground relatively smoothly in the case that the surface is straight and damped, such as a grass field. Due to the limited ability to size for impact within the scope of this project, a professional in structural analysis was contacted[17]. The impact on the belly is therefore sized as a 2.5 g acceleration with a UAV weight of 10 kg. A safety factor of 2 is included, which amounts to a force of about 500 N. If the initial impact is on a one square centimetre surface of the fuselage, the shear stress with which the belly has to cope is about 5 MPa. The stress in the fuselage is a lot smaller when compared to the ultimate strength of carbon fibre, which has an ultimate shear strength of 90 MPa[18]. As the stall speed is around 10 m/s and the weight of the UAV about 10 kg, the maximum energy to be dissipated is approximately 500 J. According to Yüksel this impact velocity can be regarded as a quasi-static response, which implies that after impact, strain rates will be low [33].

Another important aspect is the high-voltage environment of the plasma actuators which may interfere with fuselage subsystems. The fuselage should therefore act as Faraday's cage as well. The fuselage is to be designed as a monocoque, where the outside structure acts as internal frame at the same time. In this respect, the fuselage will have blunt corners while resembling a rectangular shape. The exact determination of the structural shape of the fuselage and the CFRP monocoque is considered too detailed for this report. The dimensions dictated by the fuselage lay-out are kept as dimension guidelines.

V-n Diagram

The $V - n$ diagram displayed in Fig. 4.23, shows the load factor during manoeuvring of the UAV. The maximum load factor, which is needed for the design, can be determined using the diagram. However, the diagram is constructed using certification regulations that apply to utility aircraft. As the plasma UAV does not need to comply with these regulations, the $V - n$ diagram is used as a reference. The load factor that results from the diagram is not directly constrained by the design.

[16] Carbon Tubes, accessed on June 22, 2015: `http://www.woolmer.co.uk/index.php?main_page=index&cPath=132_137`

[17] Personal communication with dr. ir. Christos Kassapoglou, June 10, 2015

[18] Carbon fibre properties, accessed on June 22, 2015: `http://www.performance-composites.com/carbonfibre/mechanicalproperties_2.asp`

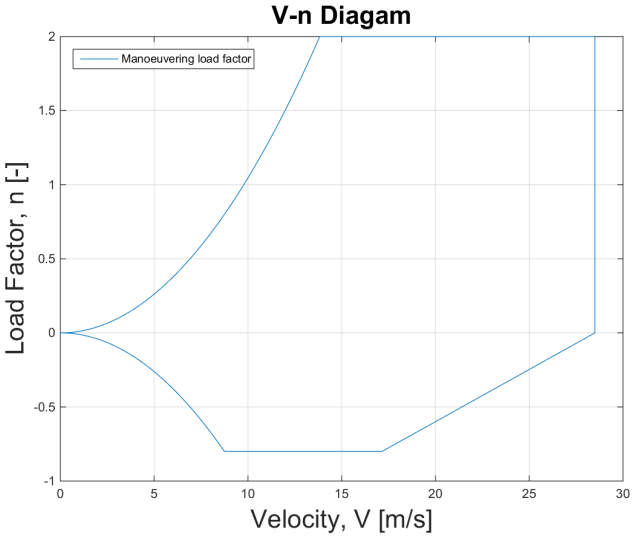

Figure 4.23: Graph of the load factor vs. velocity

4.4.3 Structural Modelling of the Wing

Modelling a structure is the ideal way to optimize a structure. By determining the maximum loads at each location, the minimum amount of material required at each section can be determined thus decreasing the mass of the structure. Since composites are used in the structure, and the bachelor study does not prepare students to deal with composite optimisation, a simple sandwich structure is analysed. The starting point of the analysis is making the right assumptions. Having the right assumptions is essential to determine the accuracy and validity of the model. The results of the tool will be explained, and finally the results of the tool are presented, concluding the section. The tail will be analysed first, since it will cause reaction forces and moments in the wing.

Primary Assumptions

PA1: Skin carries all loads.
PA2: Origin is on quarter chord line.
PA3: Deflection and twist of the wing and tail are neglected.
PA4: The amount of cuts is sufficient such that the cross-sections can be seen as un-tapered.
PA5: The wing is modelled as a cantilevered beam.
PA6: The contribution from the fuselage weight to the axial loads in the wing due to the 3° dihedral is neglected. A very small force component ($\sin 3°$) contributes to that axial load.

Secondary Assumptions

SA1: The mass of a subsystem will be defined by its average density
SA2: The quarter chord line is orthogonal to the $xz-$plane (plane of symmetry of the UAV).
SA3: The cuts made perpendicular to the quarter chord line.
SA4: The resultant lift acts on the quarter chord line.
SA5: The airfoil at the tip of the wing is assumed to be the same as the airfoil at the root.

Load Quantification - Tail

The tail can be modelled as if it were clamped in the wing through a 1.75 m rod (i.e. quarter chord of the wing to quarter chord of tail). From the aerodynamic specifications, the tail length, horizontal- and vertical-tail surfaces are known. The three reaction forces and moments that the tail causes on the wing are the maximum and most critical loads the tail can generate in flight conditions. In this model, there has been accounted for lift, drag, weight and a 10 m/s wind gust speed from the side. This resulted in the following reaction values at the wing-tail boom intersection, shown in Table 4.10.

Table 4.10: Wing-Tail boom intersection reaction forces

	x	y	z
Forces [N]	1.94	2.21	49.10
Moments [Nm]	18.61	-84.23	4.18

Load Quantification - Wing

By making a cut at every millimetre of the span of wing, a total a 1500 cuts will be made. As stated in the primary assumption 4, the amount of cuts should be large with the purpose of neglecting the taper in the wing structure. At every cut, the resultant forces will be evaluated in the global reference frame (Fig.4.24a, 4.24b, 4.24c), and secondly, the internal loads are determined at the same locations using the local reference frame. In the global reference frame, first the resultant forces are evaluated at all locations along the three axes, then, all the reaction moments.

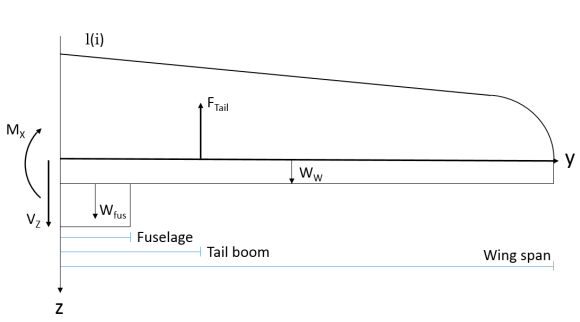

(a) FBD of forces in $z-$direction

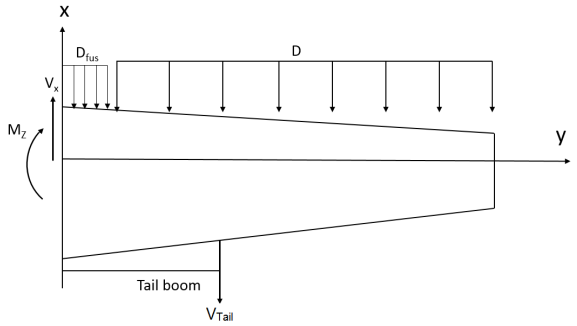

(b) FBD of forces in $x-$direction

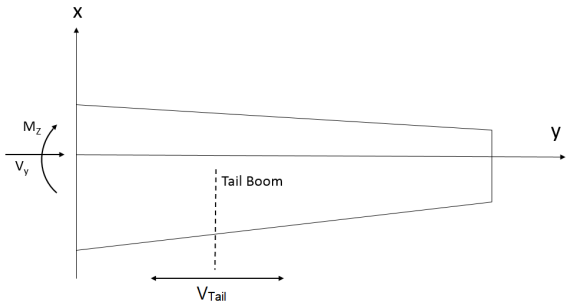

(c) FBD of reaction forces in $y-$direction

Figure 4.24: Free body diagrams of wing loads

Reaction Forces

To evaluate the reaction forces along the $z-$axis, a free body diagram showing the relevant forces was used (Fig. 4.24a). The largest force to take into account is the lift force and the contribution of the tail. The way the lift was modelled was by evaluating the average area of each section of the wing and evaluating the local lift force (Eq. 4.11). The reaction force at the cut location is the cumulative sum of all the local lift forces from the wing tip to the cut location.

$$L_{sec} = \frac{C_{L_{max}} \rho_{sea} V_{max}^2 S_{sec}}{2} \tag{4.11}$$

The contribution from the weight of the fuselage only affects the reaction forces where the fuselage is present. The fuselage was modelled as a distributed load of the total fuselage weight over the surface at which it is attached to the wing. The fuselage starts at 15 cm from the root of the wing. Similarly, the wing weight itself has been included by evaluating the average density of each wing section (Eq. 4.12). The average of the airfoil areas over a cut section is evaluated and multiplied by the density of the foam core. In the second part of the equation the average skin surface area of the cut section is evaluated, and

multiplied by the weight per square meter of the chosen carbon fibre plus its resin absorption mass; which is again multiplied by the amount of layers used. The total mass of the wing equals 2.376 kg.

$$W_{wing} = 2\left(\frac{A_{foil_{n+1}} + A_{foil_n}}{2} \cdot \rho_{foam} + \frac{Circ_{foil_{n+1}} + Circ_{foil_n}}{2} \cdot W_{carbon} \cdot n_{cloth}\right) y_{cut} \tag{4.12}$$

Finally, there is the contribution of the tail. At the location where the tail is attached to the wing through a circular rod, there will a transfer of forces and moments affecting the loads on the wing. The loads on the tail have been previously evaluated in Table 4.10. By adding all the forces and multiplying them by the load factor of 2, the total reaction force can be evaluated (Fig. 4.25).

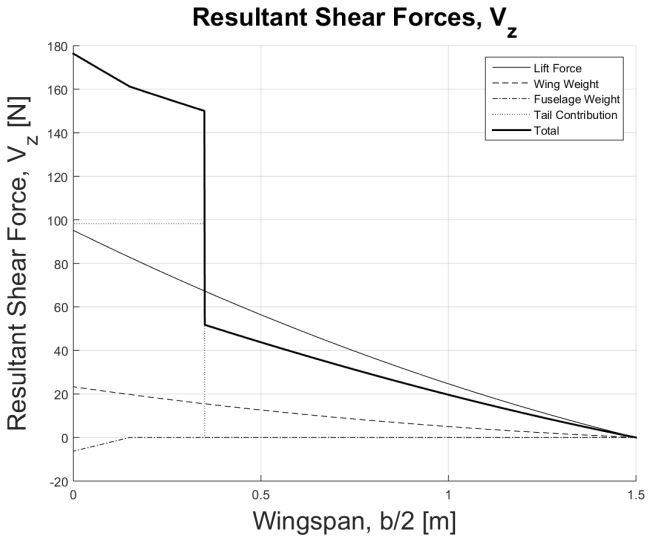

Figure 4.25: Reaction forces along the $z-$axis

When adding up the forces along the $x-$axis, only the drag forces acting on the wing, fuselage and tail are considered (Fig. 4.24b). The drag force has been evaluated similarly to the lift (Eq. 4.11) however this time lift coefficient is replaced with the maximum drag coefficient of the airfoil (Eq. 4.13). The resultant reaction forces can be seen in Fig. 4.26.

$$D_{sec} = \frac{C_{D_{max}} \rho_{sea} V_{max}^2 S_{sec}}{2} \tag{4.13}$$

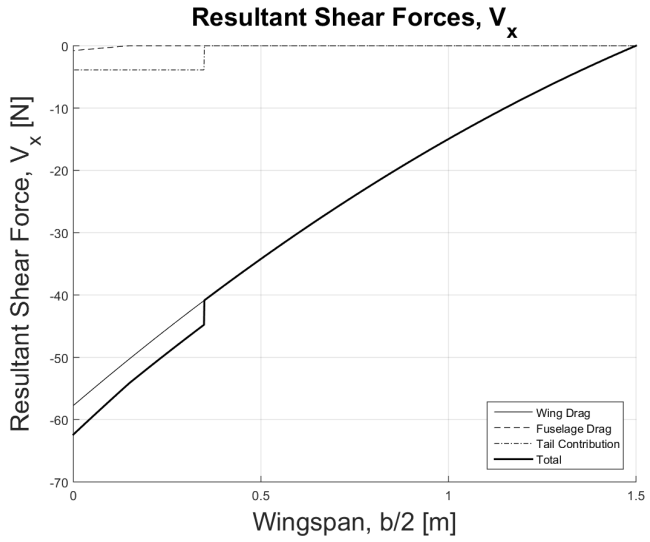

Figure 4.26: Reaction forces along the $x-$axis

Having evaluated all forces along the $z-$ and $x-$axis, and established the reaction forces present in the wing at each location, the same needs to be done with respect to the $y-$axis. Since there are no axial loads other than the ones resulting from bending and the tail contribution, the reaction forces parallel to the $y-$axis can be seen in Fig. 4.27. Due to assumption primary assumption 6 the $y-$components from the fuselage weight due to the dihedral in the wing are neglected. The only axial loads present in the wing are therefore those due to the tail contributions when they are struck by a gust of wind in either direction (Fig. 4.24c). The ultimate reaction forces will therefore be of opposite signs depending on the direction the wind is coming from (Fig. 4.27).

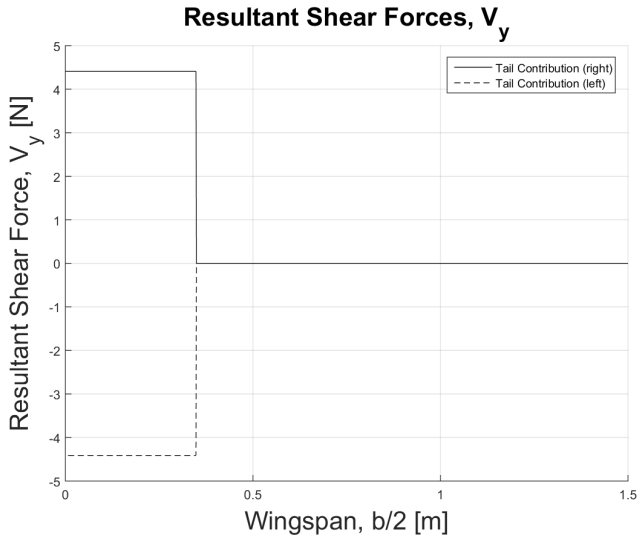

Figure 4.27: Reaction forces along the $y-$axis

Reaction Moments

The resulting reaction moment around the $z-$axis is displayed in Fig. 4.28. The graph shows that the major contribution to M_z comes from the tail. Horizontal wind gusts on the vertical tail surfaces are the cause of this moment. The other contribution comes from the drag on the wing.

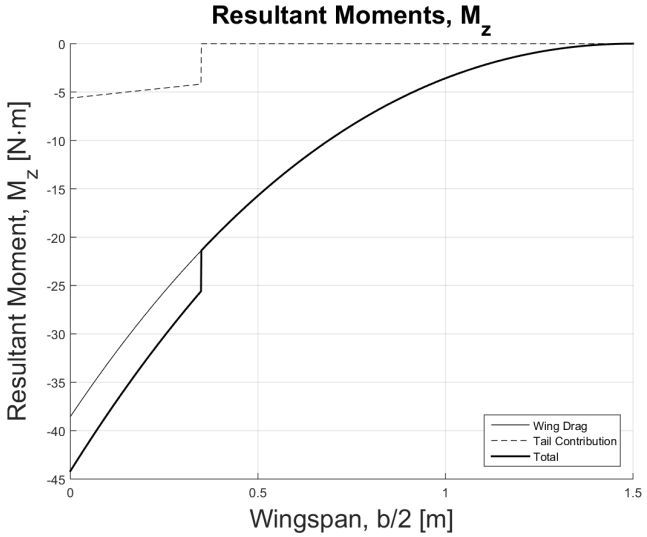

Figure 4.28: Reaction moment along the $z-$axis

In Fig. 4.29 the reaction moment around the $x-$axis is displayed. A major contribution comes from the moment created by the lift force. The tail also has a large contribution to the moment around the $x-$axis, that is because the calculation accounted for a gust wind on the vertical tail surface.

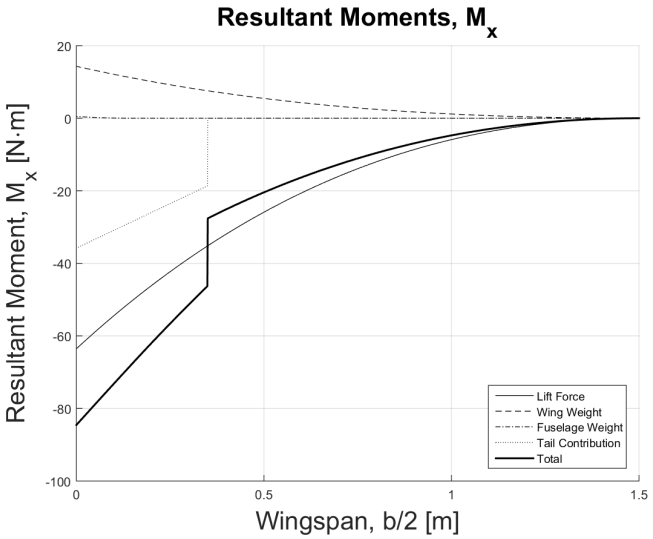

Figure 4.29: Reaction moment along the $x-$axis

The torsion on the wing box is the resultant moment around the $y-$axis. It is shown in Fig. 4.30. As it is assumed that the lift acts on the quarter chord line (secondary assumption 4) and the moments are calculated around the quarter chord. The lift does not contribute to the torsion on the wing and the major contribution comes from the tail. The lift force from the horizontal tail surface introduces a torsion moment in the wing.

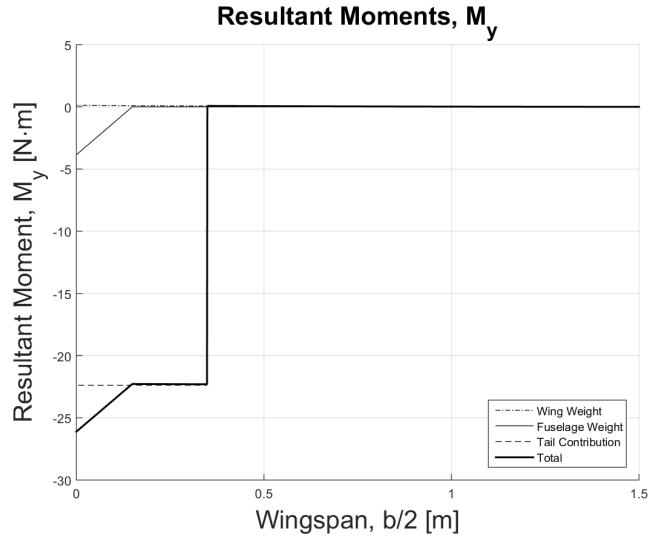

Figure 4.30: Reaction moment along the $y-$axis

4.4.4 Internal Stress Analysis of the Wing

In the previous section, the static loads on the UAV structure were determined. This section discusses the internal stress analysis, which will prove that the wing of the plasma UAV is strong enough. Firstly, a suitable modelling method has to be chosen. Subsequently, the results of the stress analysis of the wing are presented.

Modelling Methods

A UAV is a complicated shape to work with. It is therefore necessary model it in a way that computations are simplified in such a way that the results are not compromised. There are two ways to model a structure: one through shape approximation and the other by using booms to model the skin of, for instance, an airfoil.

Approximating a shape can be done through the use of polygons and circular shapes. It is possible to validate the area moment of inertia with the value generated by either XFLR5 or CAD software. It is then possible to analyse the shape according to the relevant loads.

Using the booms method consists in simulating the shape with a grid of point masses connected by panels. In this approach the normal stresses are carried by the booms, whereas the shear stresses are carried by the skins. The location of the booms can be easily determined by using (for instance) an airfoil coordinate system provided by XFLR5 or JavaFoil and the respective moment of inertia. In this model however, only the skin is considered in the evaluation of stresses, which might be the best case in case of a composite layup since the core is not supposed to be carrying any large loads.

As previously mentioned, the structure will experience a large variety of loads which are analysed in the following paragraphs. The parameters that need to be evaluated are normal and shear stresses, the shear centre and shear flow and finally the von Mises criteria to take stresses in all directions into account. First the approach for shape approximation is presented, which is then followed by the boom method.

General Equations - Shape Approximation Method

When considering the shape approximation method, the centroid and the area moment of inertia of the section have to be as close as possible to the values presented by validating software. Once they have been determined, it is then possible to continue with the analysis by evaluating the internal loads that the structure is subjected too.

Normal stresses occur due to pure bending. Stresses are largest at the maximum distance from the neutral line, which signifies the location where neither compression or tension occurs. In the case of unsymmetrical bending (Eq. 4.14, [34]) the normal stresses about an axis can be evaluated by adding the moments acting onto the orthogonal plane.

$$\sigma_z = M_x \left(\frac{I_{yy}y - I_{xy}x}{I_{xx}I_{yy} - I_{xy}^2} \right) + M_y \left(\frac{I_{xx}x - I_{xy}y}{I_{xx}I_{yy} - I_{xy}^2} \right) \tag{4.14}$$

Once the normal stresses are accounted for, the shear stresses (Eq. 4.15, [34]) need to be evaluated. The starting point is determining the shear flow (Eq. 4.16, [34]) through the structure. Since the section is closed, the shear flow is composed of both basic shear flow (Eq. 4.17, [34]) and an unknown value $q_{s,0}$ at a location s on the cross-section [34]. The basic shear flow, also known as the open section shear flow, is computed by first making a 'cut' in a convenient location. The shear flow at the cut location is zero as it would be in a open section.

$$\tau = \frac{q_s}{t} \tag{4.15}$$

$$q_s = q_b + q_{s,0} \tag{4.16}$$

$$q_b = -\left(\frac{S_x I_{xx} - S_z I_{xz}}{I_{xx}I_{zz} - I_{xz}^2} \right) \int_0^s txds - \left(\frac{S_z I_{zz} - S_x I_{xz}}{I_{xx}I_{zz} - I_{xz}^2} \right) \int_0^s tzds \tag{4.17}$$

The unknown shear flow value $q_{s,0}$ is evaluated by equating the applied and internal moments taken about a convenient moment centre and solving the equation (Eq. 4.18, [34]). Finally, when the shear flows have been added (Eq. 4.16, [34]) the shear stress (Eq. 4.15, [34]) can be evaluated.

$$S_x\eta_0 - S_z\xi_0 = \oint pq_b ds + 2Aq_{s,0} \tag{4.18}$$

General Equations - Booms Method

When considering the booms method, the centroid and the area moment of inertia of the section have to be as close as possible to the values presented by validating software. The centre of mass and the moment of inertia are dependant on the areas of the booms, but since there are no actual stringers in the structure it would be most correct to give all the booms an equal area. The area is based on the amount of mesh points and the thickness of the carbon, and to verify the total area it was compared to the circumference of the airfoil multiplied by the thickness of the carbon sheets. The normal stress can be evaluated with Eq. 4.14. Once all the boom areas have been evaluated, the area moment of inertia can be evaluated by summing the product between the boom areas and the squared distance from the neutral axis (Eq. 4.19, 4.20, 4.21). If the required inertia is higher than the obtained inertia, the boom areas can be increased until the inertial condition is met.

$$I_{xx} = \sum_{n=1}^{r} B_n z^2 \qquad (4.19) \qquad I_{zz} = \sum_{n=1}^{r} B_n x^2 \qquad (4.20) \qquad I_{xz} = \sum_{n=1}^{r} B_n xz \qquad (4.21)$$

Once the normal stresses are accounted for, the shear stresses (Eq. 4.15, [34]) need to be evaluated. Again, the shear flows (Eq. 4.16, [34]) in the cross section have to be determined, and since the shear forces will most likely act away from the shear centre, a equivalent torque has to be accounted for. The procedure is the same as in the previously explained method, however the basic shear flow (Eq. 4.22, [34]) is evaluated differently due to the presence of booms. The unknown shear flow value $q_{s,0}$ is evaluated by equating the applied and internal moments taken about a convenient moment centre and solving the equation (Eq. 4.18, [34]). When the shear flows have been added (Eq. 4.16, [34]) the shear stress (Eq. 4.15, [34]) can be evaluated.

$$q_s = -\left(\frac{S_x I_{xx} - S_z I_{xz}}{I_{xx} I_{zz} + I_{xz}^2}\right)\left(\int_0^s t_D x ds + \sum_{n=1}^{r} B_n x_n\right) - \left(\frac{S_z I_{zz} - S_x I_{xz}}{I_{xx} I_{zz} + I_{xz}^2}\right)\left(\int_0^s t_D z ds + \sum_{n=1}^{r} B_n x_n\right) + q_{s,0} \qquad (4.22)$$

Due the complexity of the code, it was decided to use a simplified model to evaluate the shear stress. Instead of Eq. 4.22, which calculates the shear flow at multiple locations through the cross section of the wing, a constant shear flow was assumed. As the carbon skin of the wing has a constant thickness, the shear stress in the wing was calculated using Eq. 4.23. This equation uses the shear force at the cross section (V) and the area of material with area parallel to the applied force vector (A). The area A is estimated by multiplying the maximum thickness of the wing with the thickness of the carbon skin.

$$\tau = \frac{V}{A} \qquad (4.23)$$

In addition to the shear stress due to the shear forces, a shear stress due to torsion has to be taken into account. The shear stress due to torsion can be evaluated using Eq. 4.24 [34]. In order to evaluate for the worst case scenario, the sum of the absolute values of the shear stresses was used for the yield criteria.

$$\tau = \frac{T}{2tA} \qquad (4.24)$$

The last step is to check if the material fails under the calculated stresses. This evaluation is performed using a formula that depends on the material. In the case of metals, the Von Mises yield criteria is used (Eq. 4.25, [35]). In the case of composite materials, a different equation is used to check for failure (Eq. 4.26, [36]). If Eq. 4.26 is lower than 1, the stresses in the structure do not result in a material failure. However, if the equation results in a number greater or equal to 1, the stresses will result in a failure of the material.

$$\sigma_{VM} = \sqrt{\frac{1}{2}\left[(\sigma_{xx} - \sigma_{yy})^2 + (\sigma_{yy} - \sigma_{zz})^2 + (\sigma_{zz} - \sigma_{xx})^2\right] + 3(\tau_{xy}^2 + \tau_{yz}^2 + \tau_{zx}^2)} \qquad (4.25)$$

$$\left(\frac{\sigma}{{F_1}^{tu}}\right)^2 + \left(\frac{\tau}{{F_{12}}^{tu}}\right)^2 = 1 \qquad (4.26)$$

Results of the Internal Stress Analysis

For the internal stress analysis the boom method was chosen to analyse the wing. This method is easy to use in a numerical model. The results of the analysis are presented in Fig. 4.31.

Fig. 4.31a displays the calculated bending stresses in the wing. It shows the wing in maximum loading conditions during flight. In the plot can be seen that there is an abrupt increase of the magnitude of the stresses at a span-wise location of 0.35 m. This jump can be explained by the loads from the tail, which are introduced at this location. The upper surface of the wing is in compression and the lower surface is in tension. A peak in tensile stress is located at the leading edge at the root of the wing. The peak at the leading edge is caused by the moment around the $z-$ axis which comes from the tail and the wing drag.

The shear stresses in the wing are displayed in Fig. 4.31b. The introduction of the tail loads is again clearly visible. It can be seen that the shear stress increases gradually from tip to root. Using Eq. 4.26 the graph shown in Fig. 4.31c was created. The calculated values are below 1, which means that the wing will not show tensile failure or shear failure when the maximum in-flight load case is encountered.

Landing on the tail is not allowed, as the moments caused by the impact will cause the wings to break off. More about the landing procedure can be found in Section 5.4.2.

It should be noted that the analysis did not include a calculation on buckling failure, due to compressive stress. A buckling analysis should be carried out in order to be sure that the wing does not fail during its operation, however due to the complexity of composite buckling analysis in a tapered airfoil-shaped wing it was not considered.

In conclusion, the wing does not fail under the specified loads. It is even able to withstand higher loads. It could be argued that the wing is over-designed. However, the current configuration is a very lightweight solution and will work for the plasma UAV. Future work could focus on an optimisation of the structural design, by for instance utilising the minimum amount of carbon and foam at each section.

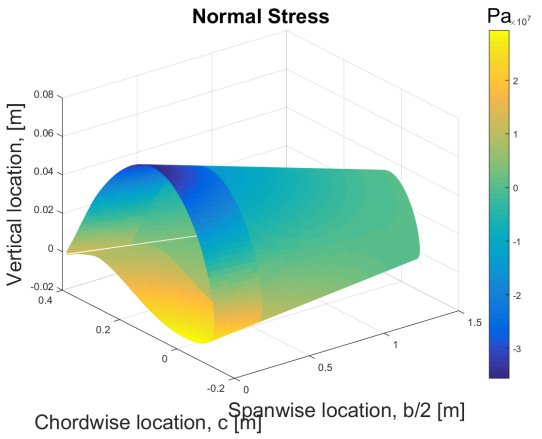

(a) Normal stresses due to bending

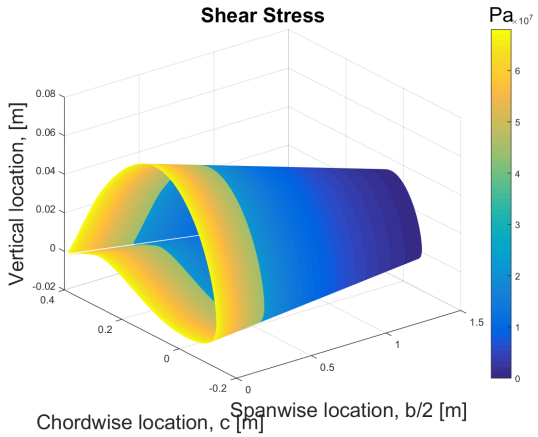

(b) Shear stresses in the wing due to torque and shear forces

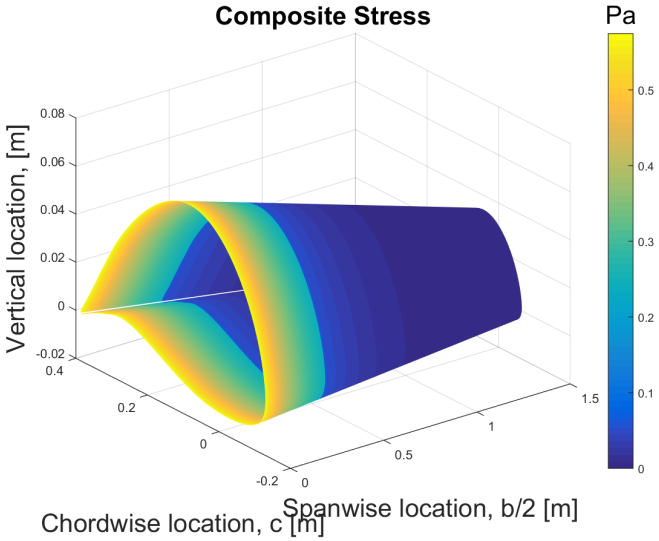

(c) Check for failure in the composite material of the wing

Figure 4.31: Results of the internal stress analysis

4.4.5 Material Characteristics

This section explains the design approach with respect to materials. Firstly, materials which are used in aerospace design are evaluated. Subsequently, the criteria on materials are discussed. Finally, it will be clear which type of materials are suitable for application in the structural design of the plasma UAV.

Evaluation of Materials

When comparing a UAV to a conventional aircraft, the nature of the forces is the same, however the order of magnitude is a lot smaller. This results in different requirements on the material properties and therefore a larger range of materials can be used for UAV design. Currently, the majority of UAVs in the Mini UAV category are built using plastics and composite materials [20]. The only parts that are required to carry higher loads (e.g. the landing gear) include metals. However, due to the development of composite materials, the use of metals is decreasing [37]. In the next paragraphs, the materials which are applicable to the UAV are discussed. A selected group of materials is displayed in Fig. 4.32. This figure is constructed using the CES EduPack 2014 software[19] and it gives an overview of the strength and density properties of various materials, which are of major importance in the material selection.

Plastics - A large number of polymers can be classified as plastics. Plastics have a wide variety of material properties, both very stiff and very elastic plastics exist. Plastics are heavier than wood, but much lighter than aluminium alloys. Applications of plastics are for example in lightly stressed parts and energy absorbing shields [34]. A plastic which is interesting in particular is ABS because it has outstanding strength and toughness properties [38]. Therefore, only ABS plastic has been included in Fig. 4.32.

Fibre-Reinforced Composites - This group of materials is designed to have excellent specific strength and specific modulus parameters. These advantages make composites a perfect material for the application in UAVs. The material consists of two phases, a fibre phase and a matrix phase. The fibres can be made out of different materials, for example glass-polyester or carbon. The matrix phase of the composite is usually made of a metal or a polymer. However, in UAV design composites with a polymer matrix are most common. An important property of composite materials is the anisotropic behaviour. This property should be taken into account when it is used in the design of the plasma UAV [34].

Structural Composites- Materials that combine multiple layers of composite and homogeneous materials are structural composites. Two concepts of structural composites are sandwich panels and laminar composites. Laminar composites are materials that consist of stacked up layers of (anisotropic) materials. This results in a material that has favourable mechanical properties in more than one direction. Sandwich panels are structures that consist of two strong sheets which are separated by a core material, which increases the composites moment of inertia. Therefore, these structures can achieve a high strength and stiffness at relatively low densities [38]. A core material which is often applied in UAV design is foam due to its light weight. Therefore, foams have been included in Fig. 4.32.

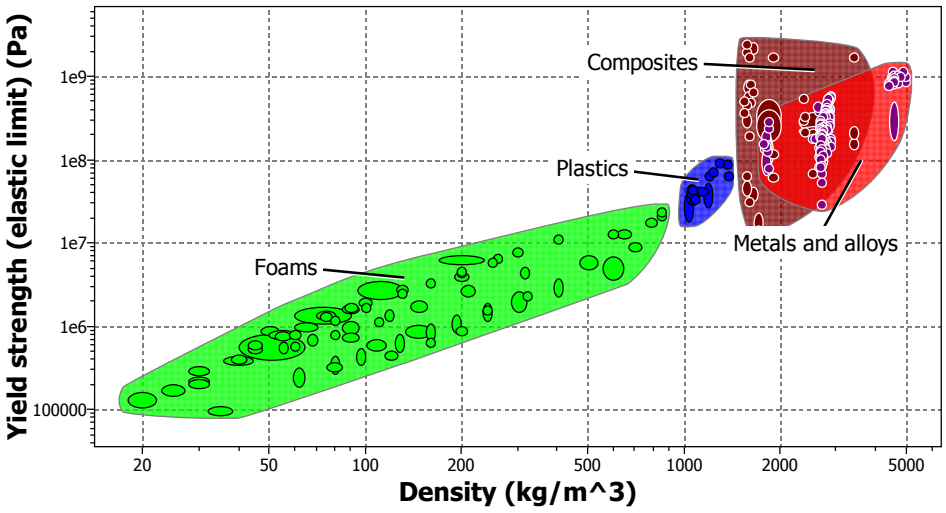

Figure 4.32: Yield strength vs. density

[19]The CES EduPack 2014 Software uses data from Granta Design.

Material Properties

The selection of materials for aerospace application is usually done with a thorough inspection of important material properties. The driving material properties in the selection procedure consists of costs, weight and stiffness. To clarify the subsequent process of material evaluation an overview of generally important material properties for the UAV design is presented in Table 4.11. Brittleness and fracture strength are important to withstand impact, which is also of major importance to the design. Next to that, electrical conductivity is a parameter that should not be neglected as the UAV houses high voltage electrical systems throughout the structure. Finally, the manufacturability of the structure should be taken into account during design and will be elaborated on in the Section 5.2.

Table 4.11: Considered material properties

Class	Property	Expressed in	Symbol	Unit
General	Cost	Euros	€	[€]
	Weight	Density	ρ	[kg/m^3]
Mechanical	Stiffness	Young's Module	E	[GPa]
	Strength	Elastic limit	σ_y	[MPa]
	Fracture Strength	Tensile Strength	σ_{ts}	[MPa]
	Brittleness	Fracture Toughness	K_{ic}	[Pa/$\sqrt{\text{m}}$]

4.4.6 Materials Selection

As mentioned in Section 4.4.2, the structural design can be divided in three groups: the wing group, the tail group and the fuselage group. Each group has a specific load case and therefore different material properties play a role in the material selection. The most important function of the wings is to sustain the lift and drag loads from the wings themselves and from the tail. Therefore stiffness is an important material property. The fuselage needs to protect the systems inside the UAV and should withstand landing impact loads. The material of the fuselage needs to have a high fracture toughness.

The wing of the UAV is a composite structure. It will consist of a foam core and a carbon skin. Using this structure, a stiff and lightweight wing can be designed. From the criteria in Table 4.11, weight and stiffness were chosen to be the most important criteria on the materials. Thus, the foam and carbon[20] should be as light as possible. Using the CES EduPack software, the Ashby plot in Fig. 4.33 were made. Using the plots a first material has been chosen to apply in the design. The material for the foam core is either PVC, PUR[21] or EPS low-density foam. The chosen carbon skin material is a light-weight woven fabric carbon in combination with epoxy resin. Similarly, the tail of the UAV will use the same structure as the wing. The structural composite that uses a foam core and a carbon skin, is also applicable to the tail structure. To obtain the lightest weight, TeXtreme® carbon fibre is considered. TeXtreme® is known to produce among the lightest fibres, however, the costs are much higher when compared to standard carbon fibre. Due to the weight savings of using TeXtreme®, the extra expense is made.

An important issue is the conductivity of carbon. Since the UAV will use plasma actuated control, high voltage electrodes will be present at the wing surface. The conducting wing should be insulated from the electrodes. Insulation could be achieved by applying an insulating coating on the carbon or by implementing an insulating material between the electrode and the wing such as Kapton® tape.

As described in section 4.4.2, the fuselage consists of a box that should protect the systems and the payload of the mission. Fracture toughness is important for the fuselage, because it will have to deal with impact loads during the belly landing. It is important to keep the structure as light as possible. Therefore the density of the material is an important selection criteria.

In Fig. 4.33 can be seen that plastics are a good material for the skin, as they have lower densities than composites and metals. Using foam as material for the fuselage, could be an even lighter solution, but in that case, the fuselage would be very sensitive for impact and easy to break. Composites are heavier, but as they are stronger, less material is needed to make a robust structure.

[20] Carbon fibre properties, accessed June 19, 2015: `http://www.performance-composites.com/carbonfibre/mechanicalproperties_2.asp`

[21] PUR foam properties, accessed June 19, 2015: `http://www.poliuretanos.com/pdf/planchas-bloques/ES/Planchas-de-poliuretano-D35--Poliuretanos.pdf`

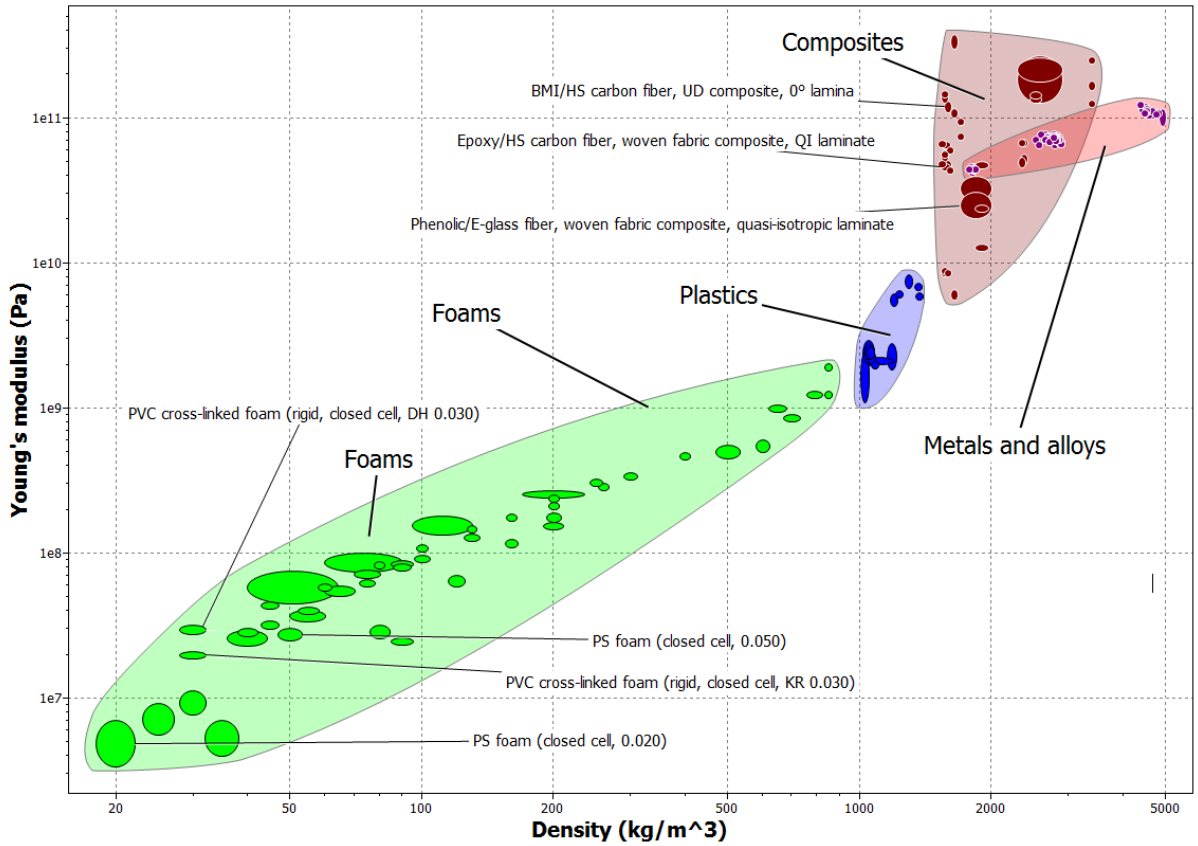

Figure 4.33: Ashby plot [created using Granta's CES Edupack]

Table 4.12: Overview of applied materials

UAV Part	Material	Density	Failure Strength [MPa]
Wing - skin	Carbon fibre - epoxy composite	160 g/m^2	Tensile 600, Shear 90
Wing - core	PUR foam	35 kg/m^3	Tensile 0.180, Shear 0.100
Tail - skin	Carbon fibre - epoxy composite	160 g/m^2	Tensile 600, Shear 90
Tail - core	PUR foam	35 kg/m^3	Tensile 0.180, Shear 0.100
Wing - Tail connection	Carbon rod	50.5 g/m	Tensile 600, Shear 90
Fuselage - skin	Carbon fibre - epoxy composite	160 g/m^2	Tensile 600, Shear 90

4.4.7 Structural Sensitivity Analysis

The sensitivity analysis for the structural design provides insight into the effect of altering parameters on the design and performance. By knowing the effect of a parameter, a prediction may be made on how it will alter the simulation.

Four types of design variables can be distinguished [39]. The first are material property design variables. In structural design, material properties are used as a design parameter. Such a parameter (e.g the Young's Modulus), tends to be the same throughout the design due to the chosen material. However, changing for example an alloy can impose a change on material properties. The second parameter is sizing design variables, which are related to the geometry of the structure. By reducing the plate thickness in a design to reduce weight will alter the performance, however it does not affect the global geometry of the structure. The sizing design variable and material property design variable are similar in the sense that they both change the parameters of the structural problem. Thirdly there are shape design variables. This is directly related to the structure's geometry. Note that the shape of a structure does not explicitly appear as a design parameter in a formulation. This typically results from other design criteria (e.g. the aerodynamic shape of an airfoil). Finally, the configuration design variable has to be considered.

The above mentioned design variables are to be assessed for the structural design in this chapter. The change of material in the aforementioned structures can have an impact on the parameters in Table 4.11. If the CFRP would prove unsuitable for the structure and a metal was chosen, the weight would dramatically increase for equal performance compromising the lightweight design requirement.

The sizing design variables are of major importance for the structural sensitivity analysis, mainly because of the use of a carbon fibre skin around a foam core in the wing and tail. The skin carries most of the shear, tension and compression loads which are dominant in the wing. Reducing the amount of layers of fibre significantly reduces the structural performance. The same holds for the tail. The carbon rods vary their performance depending on the moment of inertia of the tube, hence, the larger the diameter the lower the weight of the rod. The structural code shows the effect of changing skin thickness and foam core thickness. It has to be noted that the skin thickness is a multiple of the individual fibre layer thickness. One layer of woven carbon fibre has unidirectional properties at a 90 degree orientation. It is therefore necessary to have at least 2 layers of fibre in a 0-90 and 45-135 degree orientation to obtain quasi-omnidirectional performance. Failing to do so will drastically deteriorate structural properties and will violate the engineering bending theory used in the sizing process. This constraints the minimum thickness and has to be accounted for at all times. The closed cell foam core offers structural rigidity and buckling resistance. Removing excessive foam volume will significantly decrease the weight of the structure but is above the scope of the project to compute and simulate. Decreasing the volume of foam is definitely an improvement on the current design and suggested for future iterations of the structure.

The shape design variable in structural analysis is predominantly depending on the aerodynamic design and stability considerations. If the design does not meet the set requirements (e.g. maximum lift coefficient), the airfoil geometry and structural design have to be altered. The structural code is build on the airfoil geometry to evaluate all relative stresses in the skin. Ultimately, an altered airfoil with slight changes in thickness over chord will not have major consequences for the structural design. However, note that for a significantly more slender airfoil the distance between the upper and lower skins will lower, thus decreasing the area moment of inertia and consequentially the bending stiffness of the wing.

Finally, the configuration design variables are considered. An alteration in the chosen UAV configuration (a high wing, twin-boom H-tail, rear fuselage pusher propeller) can lead to a change in structural performance. As an example, if the tail is positioned more aft, the moments in the wing resulting from the tail will increase causing the resulting bending moments at the wing root to proportionally increase and possibly cause for yielding.

4.4.8 Structural Verification & Validation

The wing structure of the plasma UAV is analysed using a MATLAB script. Firstly, the script computes the global forces and moments acting on the wing structure. The global load analysis is needed for the local internal stress analysis, which will show the capability of the wing to withstands the loads. The verification and validation of the structural analysis is of major importance for the obtained results.

The script has been verified by comparing the numerical solutions with and analytic solution. The programme calculates loads and stresses for a large number of locations on the wing, therefore not all points can be verified using analytic calculations. However, by picking and analysing a number of representative locations (such as the root of the wing), the quality of the calculations can be assessed.

Th Validation of the structural analysis can be achieved by comparing the results of the programme with the results of an actual stress test. The wing could be the actual wing of the UAV or a similar wing. At this moment in the design process, the validation has not been carried out as it would require an ultimate loading test. The validation has to be part of the future work if the project is continued.

4.5 Stability and Control

This chapter will focus on the control and stability characteristics of the UAV, which are of primary importance to an operator. First the design of the tail, which provides a major force in stability and control design, is treated, which is followed by a stability analysis. This analysis is then conducted several times, in order to determine the centre of gravity limits.

4.5.1 Tail Design

In this section the details of the tail design are presented. The properties of the tail, especially the geometry and the mass, are required to conduct a proper stability analysis, which is why the tail characteristics are treated first.

Tail Surfaces

In the Mid Term Report [12], a preliminary horizontal tail area of 0.1462 m^2 and a vertical tail area of 0.1847 m^2 were found. These values were calculated using the tail coefficient method. This method estimates the tail size from statistical data.

The design has been worked out in more detail since the mid term report, and this has given some additional constraints for the tail dimensions. The most influence is exerted by the propeller size and location. In the design, the propeller is placed at the back of the fuselage, and it is positioned in between the tail booms. This means that the horizontal tail surface should be at least as wide as the propeller, to prevent it from hitting the booms. In Section 4.1.1, a propeller with a 13-inch diameter was selected. This means that the span of the horizontal tail should be at least 33 cm, including a margin around the edges. Using a span of 50 cm, a chord of 30 cm is obtained, which is used as the initial starting point in the design process.

In addition, it is desired to move the horizontal tail surface outside the propeller wake, to make it more effective. If it is assumed that the propeller shaft will be installed at the same height as the main wing, the horizontal tail should be placed at least 6.5 inch (or 16.5 cm) above the main wing. It is decided to place the horizontal tail 30 cm above the main wake, to have a small margin. To ensure smooth horizontal-vertical tail integration, the chord of the vertical tail is also taken to be 30 cm.

Using these constraints, a preliminary tail configuration can be made, and it can then be assessed whether the configuration is stable using XFLR5. Should the proposed configuration not be stable, the tail design can be altered and an iterative design process is started. In altering the design, it is desired to increase span over chord, to keep the Reynolds number as low as possible, and hence the plasma actuators as effective as possible.

Tail Booms

The sizing of the tail of course also depends on the length of the tail arm. A larger arm gives the tail a larger moment hence smaller tail surfaces and control forces are required. The tail also should not be too long however, keeping in mind the structural weight of the tail and the rear centre of gravity limit for stability.

In the Mid Term Report [12], a tail arm of 1 m was taken, so this is used for the initial design configuration. This value can be changed however, to increase the controllability of the aircraft.

4.5.2 Stability and Control Analysis

This section describes the approaches taken to assess the stability and control characteristics of the UAV. First the software used is explained, followed by the presentation of results.

If an aircraft is capable of returning to its initial flight conditions when perturbed, it is said to have stability. There are often two aspects of stability, static stability and dynamic stability. Static stability is an aircraft's instantaneous response characteristic, whereas dynamic stability is the aircraft response over time. Controllability is the easy by which an aircraft can be controlled.

In order to address the stability of the UAV, the stability derivatives need to be calculated. This is done using XFLR5. XFLR5 is an analysis tool for airfoils, wings and planes operating at low Reynolds Numbers[22]. The software was used to determine the stability derivatives of the UAV based on the geometry, and these were used to simulate the aircraft response to control input to assess the design controllability. The detailed approach is elaborated on below.

Analysis in XFLR5

First a 2D airfoil analysis is carried out on both of the airfoils used in the wing, as explained in Section 4.3.1. The analysis covers Reynolds Number from 10,000 to 10,500,000, C_l from -0.3 to 2.5 and angle of

[22] XFLR5, accessed on Jun 5, 2015: `http://www.xflr5.com/xflr5.htm`

attack from -10 to 30. This is essential since the interpolation of 3D plane analysis requires a fine mesh of parameters. In addition to aerodynamic analysis, XFLR5 also allows stability analysis. To proceed, the entire UAV model is built and moment of inertia is estimated by XFLR5 using user-provided component mass values. To model the fuselage, it was taken as a point mass and this point mass was placed at the expected fuselage centre of gravity location. In this way, the most accurate estimate of the stability characteristics is made. A summary of all variables is presented below in Table 4.13, and the XLFR5 representation of the UAV is given in Fig. 4.34. As can be seen in the table, the plasma actuator width is given. This is of importance, since the part of the wing used for roll control will have a blunt TE airfoil, leading to different UAV stability characteristics. The length given in the table is the length per wing. The centre of gravity of the fuselage is at a negative x-coordinate because it is located in front of the wing.

Table 4.13: Initial configuration for stability analysis

Component	Parameter	Symbol	Value	Unit
Main Wing, Mass = 3 kg	Root Chord	c_r	0.47	m
	Tip Chord	c_t	0.24	m
	Span	b	3	m
	Sweep	Λ	0	$^\circ$
	Dihedral	Γ	1	$^\circ$
	Plasma Actuator Length	l_{plasma}	0.25	m
Horizontal Tail, Mass = 1 kg	Chord	c_h	0.3	m
	Span	b_h	0.5	m
	Tail Arm	l_h	1	m
	Tail Height	y_h	0.3	m
Vertical Tail, Mass = 1 kg	Chord	c_v	0.3	m
	Span	b_v	0.3	m
	Tail Arm	l_v	1	m
Fuselage, Mass = 4 kg	Fuselage COG Position	$x_{cg,fuselage}$	-0.3	m

After implementing this aircraft geometry, a stability analysis can be performed to assess whether the initial design configuration is stable. With these stability characteristics, the controllability of the UAV can also be assessed.

Static Stability

To asses the aircraft's static stability, three stability parameters are considered: C_{m_α} for longitudinal stability and C_{l_β} C_{n_β} for lateral stability. The first two variables should have a negative value for stability, whereas the last variable should be positive [31].

Dynamic Stability

Next to the static stability, the aircraft dynamic stability is of importance. To determine the dynamic stability properties of the aircraft the eigenvalues of the configuration are examined. XFLR5 generates the state-space system in the form shown in Eq. 4.28. From theory, it is known that the aircraft is stable if the real part of an eigenvalue is negative [31]. The UAV has five eigenmotions, 2 for longitudinal and 3 for lateral motion, and hence it has five eigenvalues that have to have a negative real part.

$$\dot{\bar{x}} = A\bar{x} + B\bar{u} \tag{4.27}$$

$$\bar{y} = C\bar{x} + D\bar{u} \tag{4.28}$$

Control

It is very important to know and quantify the control characteristics of the UAV, since the main purpose of the project is to assess whether plasma actuators are a viable control mechanism. Fortunately, this quantification is possible using XFLR5, as is explained here.

From dynamics, it is known that the angular acceleration of an object is related to the applied moment and the object's moment of inertia, Eq. 4.29

$$M = I_m\ddot{\theta} \tag{4.29}$$

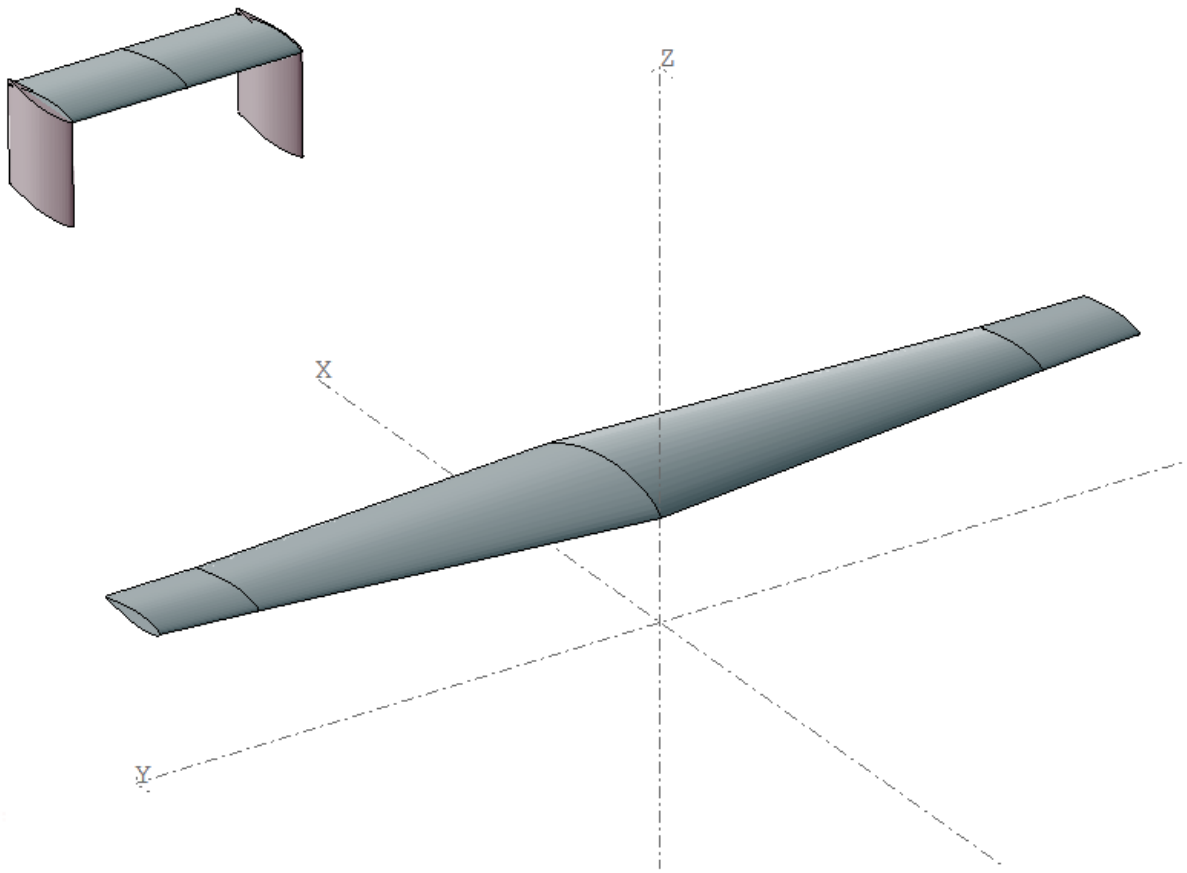

Figure 4.34: Initial UAV configuration in XFLR5

If I_m and M are known, the angular acceleration can be integrated from 0 to 1 to obtain the several control rates in radians per second. From the wind tunnel tests, Section 4.2.2, the maximum change in lift coefficient per control mechanism is known, and by combining this with the known aircraft geometry the moments applied by each control surface can be obtained. From XFLR5 the 4 mass moments of inertia of the aircraft are known, so using a simple calculation the control rates about the three axes can be calculated. The obtainable changes in lift coefficient per control rate can be found in Table 4.16.

Results

Taking into account all of the above, the initial design configuration presented in Table 4.13 is iterated several times to obtain a sufficiently stable and controllable aircraft. This led to a proposed aircraft configuration presented in Table 4.14 with the stability properties presented in Table 4.15. The control properties of the aircraft can be found in Table 4.16.

Table 4.14: Final configuration for stability analysis

Component	Parameter	Symbol	Value	Unit
Main Wing, Mass = 2.5 kg	Root Chord	c_r	0.515	m
	Tip Chord	c_t	0.257	m
	Span	b	3	m
	Sweep at quarter chord	$\Lambda_{0.25c}$	0	$^\circ$
	Dihedral	Γ	3	$^\circ$
	Plasma Actuator Length	l_{plasma}	0.25	m
Horizontal Tail, Mass = 0.344 kg	Chord	c_h	0.3	m
	Span	b_h	0.7	m
	Tail Arm	l_h	2.2	m
	Tail Height	y_h	0.3	m
Vertical Tail, Mass = 0.295 kg	Chord	c_v	0.3	m
	Span	b_v	0.3	m
	Tail Arm	l_v	2.2	m
Fuselage, Mass = 6.3 kg	Fuselage COG Position	$x_{cg,fuselage}$	0.17	m

Table 4.15: Stability characteristics

Type	Property	Value	Unit
Longitudinal Static Stability	C_{m_α}	-1.73	[-]
Lateral Static Stability	C_{l_β}	-0.04	[-]
	C_{n_β}	0.21	[-]
Dynamic Stability	Phugoid	$-30.6 \pm 21.95i$	[-]
	Short period	$-0.0065 \pm 0.222i$	[-]
	Aperiodic roll	-81.83	[-]
	Dutch roll	$-7.178 \pm 18.94i$	[-]
	Spiral	-0.01626	[-]

Table 4.16: Control characteristics

Type	Property	Value	Unit
Control Forces	$\Delta C_{L,roll}$	0.10	[-]
	$\Delta C_{L,pitchup}$	0.11	[-]
	$\Delta C_{L,pitchdown}$	0.10	[-]
	$\Delta C_{L,yaw}$	0.10	[-]
Control Rates	p	47	[deg/s]
	q_{up}	18	[deg/s]
	q_{down}	55	[deg/s]
	r	36	[deg/s]

As can be seen from the table, the aircraft is always statically and dynamically stable. The second

eigenmode, the phugoid, is only marginally stable, however it is still stable and the most commonly occurring form of this motion, the short period, is very stable. There will therefore be no large issues during flight.

As for the control rates, no reference values are readily available. This is first of all due to the fact that UAV's have many different missions and optimal control rates differ for every mission. In addition, specific numbers for control rates are considered sensitive information, so corporations are not very forthcoming regarding these parameters. Footages of other similar UAVs during flight are available online and can be used to estimate the control rates of other UAVs. Common sense can also be used to assess whether the control rates are sufficient. For example, the roll rate of the UAV is 47 degrees per second, it takes approximately less than 2 seconds to turn 90 degrees. Based on the time required to turn 90 degrees, it is decided that the obtained control rates are sufficient enough for normal UAV operations. Especially search and rescue or reconnaissance missions can be flown easily. The difference in pitch up and down rate is due to the fact that the elevator is used to pitch down and the wing is used to pitch up, and these control forces have different moment arms.

4.5.3 Centre of Gravity Limits

In this section, the centre of gravity limit of the UAV will be explored. This is performed using the model built in XFLR5. Since the weight of the wing and tail are fixed, the centre of gravity can only be moved by varying weight and location of the fuselage.

The position of the fuselage is varied to obtain the centre of gravity limit, with different payload weight. The results are presented in Table 4.17 and Table 4.18.

Table 4.17: Centre of gravity range. Payload = 0 kg

x_{cg} limit	Fuselage position [m]	x_{cg} [m]	Pitch-up arm
Most forward	-0.17	0.2346	0.10585
Most aft	-0.08	0.2825	0.15375

Table 4.18: Centre of gravity range. Payload = 1 kg

x_{cg} limit	Fuselage position [m]	x_{cg} [m]	Pitch-up arm
Most forward	-0.1	0.2351	0.10635
Most aft	-0.01	0.2872	0.15845

Note that the fuselage position is defined in the coordinate system depicted in Fig. 4.34, while the x_{cg} position is expressed with respect to the leading edge of the wing root chord, and pitch-up arm is calculated with the assumption that the lift is generated on the quarter chord line.

Since the stability improves with x_{cg} moving forward, strictly speaking there is no limit in the forward x_{cg} position regarding stability. Note that in order to achieve pitch-up motion, the aerodynamic centre of the wing is required to lie in front of the centre of gravity. From the pitch rate requirement, it is required to have a minimal moment arm of 0.1 m. This together with the fuselage design restrict the most forward position of the centre of gravity.

The most aft position of the centre of gravity is constrained by the aircraft stability. When the fuselage is located more afterwards, the tail is no longer capable to trim the aircraft. With these requirements, the centre of gravity position ranges of the fuselage can be determined and are shown below. Please note that these ranges are relative to the leading edge at the rood chord and negative values are ahead of the leading edge.

Table 4.19: Longitudinal centre of gravity range of fuselage, relative to root chord leading edge

Payload mass [kg]	$x_{c.g.}$ [m]
0	[-0.08 , -0.17]
1	[-0.01 , -0.10]

The actual centre of gravity position of the fuselage is dependent on the position of all the components in the fuselage. The fuselage length was taken as an initial guess to be 1 m, with the root of the wing positioned at the rear of the fuselage. As the root chord is 0.51 m, its leading edge is positioned at 0.49 m from the nose of the fuselage.

As discussed before, the centre of gravity of the fuselage and all its components has to be between 0.01 m and 0.10 m ahead of the root chord leading edge with a payload present of 1 kg and between 0.08 m and 0.17 m when no payload is present in the aircraft. The centre of gravity of the fuselage is calculated, using an estimated longitudinal position of the position of the components in the fuselage to determine whether it is within these ranges.

Some positions of components are fixed, for example the motor and propeller on the rear of the fuselage and the flight controller near the c.g. of the aircraft. The parachute is mounted just ahead of the wing, as it cannot deploy through the wing. If the centre of gravity should shift to the rear when payload is loaded, it should be positioned in the rear of the fuselage. The electronic power components, such as the batteries, the bridge board, the ignition coils and the electronic speed controller are positioned in logical order: The batteries are mounted in the nose, that lead power to the bridge board and in turn to the ignition coils. The electronic speed controller is between the flight controller and the motor. After some iterations in position of the components, the calculated centre of gravity was within the required ranges. These results are summarized in Table 4.20.

Table 4.20: Centre of gravity of fuselage and positioning of components

		Mass [kg]	x_{front} [mm]	x_{LE} [mm]
Structural	Fuselage	0.630	509	19
Propulsion	Electrical motor	0.066	1040	550
	Propeller	0.016	1060	570
	ESC	0.014	920	430
UAV Systems	Flight controller	0.038	720	230
	GPS module	0.017	290	-200
	Pitot tube	0.050	110	-380
	Parachute	0.417	430	-60
	RF Module	0.006	20	-470
	Antenna	0.045	-55	-545
	RC Receiver	0.017	0	-490
	Wiring	0.850	800	310
Power	Battery	1.764	150	-340
	Full-bridge board	0.300	250	-240
	Ignition coils	1.225	350	-140
Payload		1.000	530	40
Total without payload		5.45	381	-591
Total with payload		6.45	405	-551

The components were positioned in the fuselage using a CAD model to check whether they fit. The resulting model can be seen in Fig. 4.35.

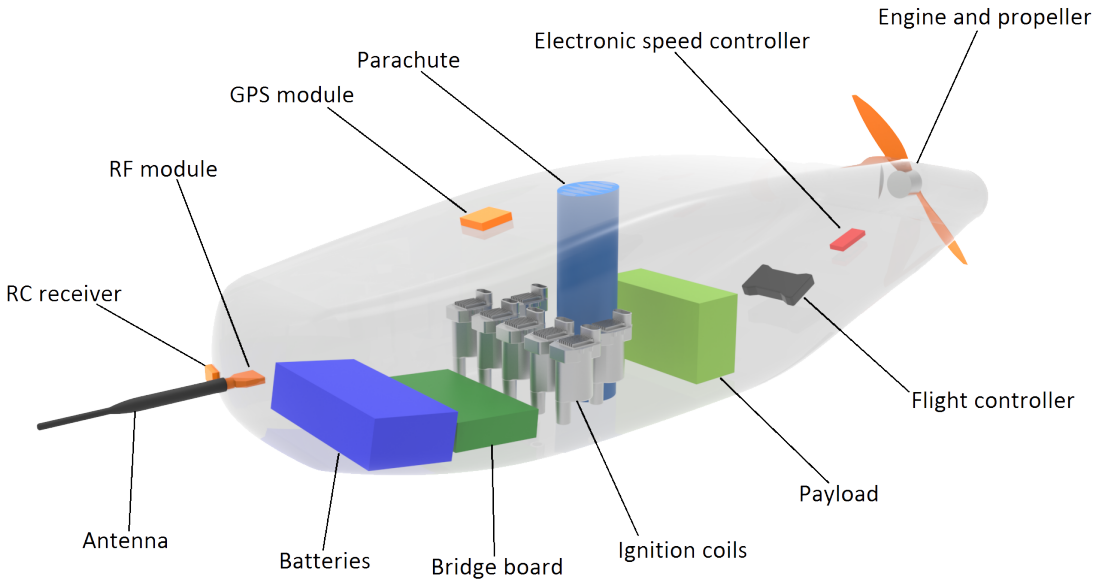

Figure 4.35: Overview of systems in the fuselage

4.5.4 Stability and Control Sensitivity Analysis

The UAV is a complicated system and the performance and stability characteristics depend on several subsystems. Therefore it is important to address the sensitivity of the design to a change in the design parameters. For stability, the most important aspects are the centre of gravity location and the tail design. Other parameters such as dihedral and sweep angle also influence the overall stability.

Centre of Gravity Location

As explained in Section 4.5.3, the x_{cg} is constraint by the static stability and the pitch-up rate. From the analysis of XFLR5, the design is relatively sensitive to the change in centre of gravity. x_{cg} influences the moment of inertia and the moment arm, thus furthermore changes all the stability derivatives. Moving the x_{cg} back improves the pitch-up performance while decreasing the stability. Therefore it is a trade-off between the stability and pitch-up rate.

Tail Design

Tail is essential to stability and control. The horizontal tail needs to generate sufficient lift to compensate the lift generated by the wing. Since the airfoil used for the elevator is symmetric, the elevator area and tail length have to be large enough. However, increasing the elevator area or tail length shifts the center of gravity backwards, which makes the UAV more unstable. From the material selection, the weight of the elevator and fins are relatively small, therefore the design is less sensitive to a change in tail parameters.

Other Parameters

Other parameters taken into account are the dihedral, sweep angle and wing design. Dihedral improves the lateral stability, so does the sweep angle. The wing comprises two different airfoils, one cambered and one symmetric. The spanwise width of the symmetric airfoil is an important variable. Increasing this width essentially increases the effective area of plasma actuators, which is improves the rolling performance. However, since the airfoil to which the plasma actuator strips are attached is symmetric, less lift is generated in this part of the wing, which makes the UAV more difficult to pitch up. This design parameter has minor impact on the stability derivatives but larger influence on the roll and pitch up performance.

4.5.5 Stability and Control Verification

In the following, a qualitative description is given of the verification and validation process of the method used in the assessment of the stability and control characteristics of the aircraft. This will mainly focus on the software used, since software was used almost exclusively in the process, however some other aspects will also be considered.

First of all, within the scope and time span of the project it is quite hard to verify the software used with an analytical solution. For this reason, the manual in [40] is used to verify the approach taken here. In this manual, the results from XFLR5 are compared with the outcome of another 3D software, AVL. The results from these two tools match very well, and when comparing the results to the outcome of a flight experiment it is found that the tools model reality quite well. Hence, at this stage of the design process the model can be considered verified. In a later design phase, analytical solutions could be found and the model results could be checked against those.

4.6 Validation of Technical Design

Now that the technical details of the UAV have been discussed, the methods and models used in the design have to be verified an validated. Verification was already discussed in the applicable section, while validation of the aircraft system design, the plasma actuator design, the aerodynamic design, the structural design and the stability and control design is outlined below.

4.6.1 Aircraft System Design

Regarding the validation of the aircraft systems, most of the validating cannot be done until a full scale model has actually been produced. This is due to the fact that isolated component performance is known, but that integrated component performance, which is the part that is to be validated, is very difficult to determine beforehand.

The specification sheet of the propulsive system for example shows values of the propeller under optimal conditions. However, since the propeller is placed behind the fuselage, there could be a slight loss in the air intake of the propeller. This has to be tested in the real configuration.

The parachute is more difficult to validate as it is very difficult to recreate the flight and drop condition. It can, however, be tested if the structural components can withstand the loading during the deployment. The parachute can also be deployed during a wind tunnel test, to get an estimate of its performance. This, however, only reassembles the horizontal velocity component of the aircraft and not the vertical.

The flight controller should give the right input to the actuators when they are activated and the autopilot should be capable of flying its programmed path. This is to be tested and validated quite easily, by operating the flight controller in a test set-up. The same thing goes for the telemetry, remote control and sensors, whether or not the range and data range matches with the specified values. The data values can be quite hard to validate, but no full scale model is needed for this. Finally, it should be tested if electromagnetic interference occurs between the high-voltages and the sensors and equipment. This last test can only really be performed with a complete model, since this is sensitive to component locations.

4.6.2 Aerodynamic Design and Plasma Actuators

The aerodynamic validation can mostly be done with a new wind tunnel test. The main design steps that need validation are plasma actuator and wing plan form performance. In the new wind tunnel test, the entire wing planform configuration will have to be tested: A full span wing with 2 different airfoils and the full plasma actuator configuration. The test data used in the plasma actuator design for this project were obtained for an airfoil different from the one that is actually used, plus the data was obtained in conditions representing 2D configuration.

The purpose of the test will therefore be to validate the translation of the test results from a 2D to a 3D configuration. In addition, an accurate drag and lift measurement of the total wing can be made; since the wing is composed of two airfoils normal panel methods do no give an accurate representation of the planform lift and drag.

As for the plasma actuators, the virtual wing-tip mechanism can be quantified in the wind tunnel using the 3D configuration. A very rough estimation was made during the plasma actuator design, but for more optimal control more accurate quantification is needed. Finally, experimental research could be performed on mechanism 8 from Section 2.1.2, to determine whether it would be beneficial to include this mechanism in future designs.

4.6.3 Structural Design

Verification and validation of the structural design is of utmost importance as it ensures structural integrity during the nominal lifetime of the UAV. The first was done in Section 4.4.8, the latter is discussed here. This is done in threefold, namely for wing and empennage structure, fuselage structure and the aircraft in total.

The wing and empennage are wound up as one single part. Therefore it is proposed to validate this structure as a whole in terms of load bearing. It is common for aircraft structure to undergo a full loading test in a test-rig. A mechanical system that simulates the aerodynamic lift and drag can be devised for this relatively small UAV system [41]. Such a load test can validate the wing, tail-boom and tail structural load bearing capacity. Note that fatigue characteristics could be validated as well with such a set-up by applying a number of load cycles, but is considered out of the scope of this project as a total flight time of 20 hours is anticipated. A widely validated FEM analysis could be applied to the final production CAD design to validate the load bearing capacities. This could be especially interesting for structurally complex parts in the structure, such as the joint between wing and tail-boom.

The validation of the fuselage structure is of grave importance as it shields the UAV subsystems during flight, take-off and landing. The first is validated with the aforementioned test set-up. Loading the fuselage with a certain weight in the rig can validate the structural load bearing capacities of nominal flight manoeuvres. Parachute deployment can be modelled by dropping the fuselage while suspended with a chord attached to the parachute anchor point. The validation of the capability to withstand landing impact is also of major importance. Impact validation with a FEM analysis is generally used for low velocity impact [42]. Low velocity impact of the UAV implies that the whole structure reacts due to dynamic deformation. To fully validate the adequacy of the structure to cope with this event such an analysis is paramount.

Finally, to fully validate the structure of the assembled UAV with all subsystems on-board, an in flight test is used as final validation. This encompasses the ability of the structure to keep all systems in place during take-off, landing and parachute deployment. Also the capability to shield subsystems from the electromagnetic field generated by the high voltage environment is to be validated. This can be done by measurement of the electromagnetic field generated when turning on the plasma actuators and by testing the other subsystems in such a field.

4.6.4 Stability and Control

For stability and control, the software used to perform the stability analysis is the part that needs validation. The best way to validate this software is to conduct one or more flight tests. In these flight tests, the different eigenmotions can be induced to see if their response follows the response modelled by XLFR5. In addition, the longitudinal and lateral static stability characteristics can be assessed in a flight test. This requires the production of a full scale model of the design, just as the validation of the system design.

The most critical properties to be validated for control are the control rates. In the scope of the overall design it is very important that validation of these rates occurs, since it is the heart of the innovative concept of the design. A test is the only way to validate the control rates, because here is no other way to validate calculations regarding the control properties of plasma actuators; it is quite hard to model the 3D response of the overall aircraft to the plasma actuators. From the measured control rates the control forces can be derived, so the theoretical plasma induced change in lift coefficient can also be validated using a flight test. This will also help in the validation of the plasma actuator design.

4.6.5 Requirements Compliance

As a part of the overall project validation, a requirement compliance matrix is set-up. In this matrix, which can be found in Table 4.21, an overview of the top requirements from Section 2.2.1 is presented,

and it is noted whether this requirement was fulfilled or not. For some of the requirements, such as the noise and avionics, data from the next chapter was used. As can be seen in the matrix, the proposed UAV design meets all top level requirements. The requirements for the control rates were not quantified at the start of the design phase, since it proved to be very difficult to do this. Therefore, the quality of the obtained control rates is assessed using common sense and prior knowledge, leading to the check-marks in the 'Met' column for the control rates.

Table 4.21: Overview of top level requirements

Requirement	Desired value	Actual value	Met?
Pitch rate	similar to conventional UAVs	34 °/s	✓
Roll rate	similar to conventional UAVs	47 °/s	✓
Yaw rate	similar to conventional UAVs	30 °/s	✓
Range	≥10 km	10 km	✓
Endurance	≥ 2.0 h	2.0 h	✓
Wing span	≤ 3.0 m	3.0 m	✓
Payload	≥ 1.0 kg	1 kg	✓
Cost	≤ € 10,000	€ 9,355.09	✓
Noise	≤ 105 dB	91 dB	✓
Moving control surfaces	0	0	✓
Autopilot	yes	yes	✓
Two-way telemetry	yes	yes	✓

Chapter 5 - Operational Details

The previous chapter explained the technical details of the plasma UAV and focussed on the design of the propulsive, aerodynamic and structural subsystems. This chapter continues with the analysis of the operational aspects of the UAV. The operations and logistic concept are first defined in more detail in Section 5.1. This also includes the sustainable development and reliability, availability, maintainability and safety characteristics. Section 5.2 contains a detailed description of the UAV production process. After this, the communications subsystem design is explained in Section 5.3. Finally, Section 5.4 presents an overview of the final UAV performance.

5.1 Operations and Logistic Concept Description

To illustrate the use and support of the UAV, the concept description of the operations and logistics is given. This encompasses all activities needed before, during and after flight to ensure the fulfilment of the mission objective. In a time-wise order this consists of: mission planning, mission preparation, mission execution, landing, storage and overall maintenance.

Mission Planning and Preparation

The mission planning consists of translating customer needs into mission objectives and checking all necessary regulations of all parties involved. The second part of mission planning is allocating resources in terms of facilities, human resources and systems. For example, take-off and landing facilities, communication systems and operators are to be accounted for. In terms of systems, the UAV, ground communication, launch and landing systems and spare parts have to be allocated. This shall all be fitted into a feasible time frame and will be checked with a risk assessment.

Mission preparation involves the execution of the mission planning, ensuring all resources are prepared for the actual mission. This involves bringing all necessary equipment to the right location. Next to that, specific mission coordinates are set and fulfilment of regulatory requirements is to be checked again.

Launch to Landing

The pre-flight logistics consist of a weather update to ensure proper flight conditions and pre-flight inspections of all subsystems. This includes all moving parts, the payload, communications, engine, battery and propeller. The launcher system is set up and checked as well.

During mission execution, the UAV is airborne and puts the payload to work. The amount of autonomy dictates the logistics in this part of the mission. Semi-autonomous or controlled flight asks for operators to control the UAV, including the initialization and operation of the payload. Gathered data is stored or sent to the ground station autonomously.

This part of the mission also depends on the landing location. In case of a predefined landing grid, the landing system is put in place pre-flight. If the landing grid is chosen during the mission, possible landing gear and operators have to be brought to the location during mission execution. After the landing manoeuvre and final stand-still, the UAV system is visually checked and prepared for storage. This includes the detaching or recharging of batteries and data retrieval if stored on-board. All used systems during landing will be prepared for storage as well. A more elaborate description of the take-off and landing procedures can be found in Section 5.4.2.

Storage and Maintenance

The storage of all UAV systems, that is the vehicle, launch and land systems, communication, control and transport systems and extra parts such as batteries, is an important logistic part of the mission. This is very dependent on the mission profile and the means of take-off and landing, Section 5.4.2.

The maintenance of the UAV system is an important aspect when considering continued operation. Maintenance can be in field for small maintenance or in a designated workplace for larger maintenance. Spare systems and parts have to be available during operation. Again, for a precise determination of spare parts and a logistic plan for maintenance, a more advanced design of the UAV is needed.

5.1.1 Sustainable Development

This section quantifies the environmental impact of the plasma controlled UAV. The analysis is limited to four fields: noise production, emissions, disposal of replaceable parts and a life cycle analysis. The requirements on these sustainability aspects were stated in Section 2.2.1.

As stated in Subsection 5.4.3, the noise production is thought not to exceed 94 dB. That is with combined maximum engine noise and plasma actuator noise, which is significantly less than comparable UAV's equipped with a combustion engine. In terms of emission special attention is paid to the effect of plasma actuators. The discharge produces ozone, which in turn is diluted by the airflow. The ozone concentrations will stay well below the thresholds and do not pose a risk for the environment as discussed in Subsection 5.4.3.

The final requirement that is considered is that the UAV shall be able to test flight for 30 hours in total. Although it will probably exceed this minimum amount of flight hours, eventually some parts of the UAV have to be disposed and replaced at their end of life. The two major replaceable are the battery and the plasma actuators. The lithium-ion polymer batteries have low environmental impact compared to the more toxic nickel-cadmium ones. Moreover, the fact that the batteries can be recharged also diminishes their impact. Furthermore, the Kapton® tape requires no special disposal.

To improve the sustainability of the UAV, a Life Cycle Analysis (LCA) can be performed on the iteration of the UAV design. This procedure is know as Eco-design process. Eco-design consists in improving the product's life cycle by focusing on its unique functional unit (i.e. embodied and required energy per flown kilometre). The improvement of the products life cycle can be done by performing a life cycle analysis on the product, which can be done with tools provided by the faculty of Industrial Design [43] [1][2]. The LCA consists of four important parts: production, transport, customer-use and disposal. In order to perform a successful design through the Eco-design approach, decreasing the amount of points scored in the analysis by the product in each of the four life stages is necessary. The Eco-design method is especially effective in the field of redesigning an existing product, making it most applicable for the iteration of the prototype.

5.1.2 Reliability, Availability, Maintainability and Safety

This subsection elaborates on the Reliability, Availability, Maintainability and Safety (RAMS) characteristics of the system. The respective terms can be defined as follows. Reliability is the probability that the system will perform in a satisfactory manner for a given period of time, when used under specific operating conditions. Availability is the degree to which a system will be available when required for use. Maintainability is the ease, accuracy, safety, and economy in the performance of maintenance actions, while safety is a measure of the hazards to human and equipment [44].

Reliability and maintainability are inherent characteristics of a design. Availability is a result of the degree of reliability and maintainability in the system design. The desired degree of safety will drive the amount of reliability that has to be built into the design, but the safety of the system again depends on the maintainability characteristics of the system. Therefore, it is valid to say that the four RAMS characteristics are interdependent. A graphical representation of the relation between these properties is shown in Fig. 5.1.

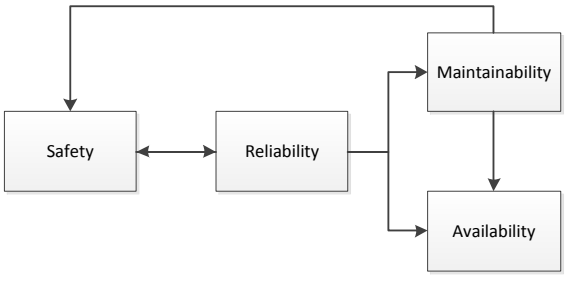

Figure 5.1: Relation between reliability, availability, maintainability and safety [44]

[1]Material Database, accessed on April 23, 2015: http://www.matbase.com/material-categories/
[2]Eco-Design LCA tool, accessed on April 23, 2015: http://www.ecocostsvalue.com/EVR/model/theory/5-data.html

Now, a brief description of each characteristic is given, along with its implications on the design under consideration.

Reliability

Systems can fail due to a variety of causes. Think of fatigue, overload, wear, oxidation etc. The reliability of a system is defined as 'the probability that a system will perform in a satisfactory manner for a given period of time when used under specified operating conditions' [44]. From a systems engineering perspective, there are several tools to consider in the design of a system that fulfils the specified reliability requirements.

The FMECA (Failure Mode, Effect and Criticality Analysis) method, is used to evaluate reliability and safety aspects of a system design. It considers failure modes of each component, determines the effect of failure on system operation and is performed with a functional approach in the early design phase (top-down) and with a hardware approach later-on (bottom-up, actual hardware failure). To construct a model, a system has to be defined, with functional block diagrams that define all possible functional failure modes, where-after causes and effects of each failure mode and severity of failure modes have to be determined. For every failure mode a corrective action has to be denoted.

The Fault Tree Analysis (FTA) is a tool to evaluate reliability and safety effects. It is a top-down approach to identify and rank failure modes and hazardous conditions. To construct a model, top events (e.g. In Flight Shut-Down) will be identified. Lower level events which can cause such events shall be determined and mapped into the tree. After that the minimum cut sets will be defined, which are combinations of events that lead to a top event. The unacceptable minimum cut sets have to be eliminated by design measures.

For the design under consideration, the required reliability is relatively low since the UAV to be designed is a prototype. In section it was stated that 30 hours of test flight are expected from one prototype. This should therefore be used as a guideline in the reliability design. It is of course desired to have a higher degree of reliability, but since novel technology is being used in this case what is feasible has to be found out.

Availability

Due to the fact that the preliminary design of the plasma UAV has not been determined yet, it is difficult to state the availability of the system, since it depends on some design choices still to be made. In general, the availability of the plasma controlled UAV is high. According to requirement TOP-PRF 3 in Section 2.2.1, the maximum wing span is 3.0 m, meaning the UAV can be easily handled and that it can be taken along and flown immediately. For convenience in transit, the design could be made to have the wings come off to make it more mobile. It would then have to be reassembled again before launch, however. The launch and landing method is a factor that can either increase or decrease the availability up to a great extend. If the UAV is hand launched, it can be deployed almost immediately, in contrast to a catapult or even a runway.

UAVs are known for their simple design, implying that repairs will generally not take a lot of time. This aids in its availability, since any down time due to maintenance will be short. The next paragraph will elaborate on this.

Maintainability

Maintainability describes the ease by which a system can be maintained. It also includes the accuracy, safety and economy of the performed maintenance activities. A major benefit of controlling the UAV by means of plasma actuators is that it replaces the moving control surfaces. Moving parts are more prone to wear than static parts, and tend to be more complex. Therefore, the removal of moving control surfaces greatly reduces maintenance cost, effort and down time.

Safety

During the design of the UAV it is important to assess and consider the design's safety. The safety often sets a key requirement for the design, and will drive the degree of reliability that is built into the system.

As for all aircraft, the UAV should be safe to fly. This means that it has back-up systems for vital components, such as the wiring for the plasma actuators, and that its design in general is fail safe. The

degree of safety for the UAV can be a little less than for manned aircraft however, since no people are on board of the UAV and hence no humans might get killed in a crash. The only way this could happen is in case the UAV hits civilians or civil buildings upon impact. It could therefore be made a requirement that the UAV is able to safely land on its own, even when the main control system fails.

The plasma actuators introduce some additional safety concerns to the design. First of all, the plasma is created by an exposed electrode. However, the actuators will only be activated when control is needed, so during for example launch there is no safety issue. The safety issue introduced by the exposed electrode should still be solved, so some form of insulation or protection could be looked at.

Finally, since the UAV will not have people on board, good situational awareness is needed. The operator should know properly where the UAV is, to avoid the UAV crashing into its surroundings. This could for example be achieved by carrying a camera on-board the UAV or combining a detailed area map with GPS coordinate navigation.

5.2 Production Plan

Designing for manufacturing, assembly and integration is essential to efficiency of the final design. Failing to take this into consideration may result in the tardy realisation that an optimized part may be too expensive or even impossible to manufacture. An overview of the process from raw material to final product is shown in Fig 5.2. Firstly, raw material is imported to process. The manufacturing techniques to create parts are largely dependent on the preferred material. Therefore only some examples are given in the overview. Generally, they can be divided into mechanical working and laminating. Secondly each subsystem (wing, fuselage, tail and plasma actuator) is assembled separately. All these sub-assemblies are then integrated with the systems such as the electronics, batteries and communications hardware have to be installed. Some of these systems can already be implemented in the sub-assembly. Finally, the integration leads to the final product, providing the possibility of testing the system. This structured way of build-up from small parts to larger structures is customary for production of complex systems.

Not every component is produced from raw materials as it can be more cost effective to buy them 'off-the-shelf'. Furthermore, after each production phase, a quality check is to be performed to assure the overall quality and progress of the process. Note that it is important to include the most expensive parts (e.g. engines) last, for this reduces risk on financial issues.

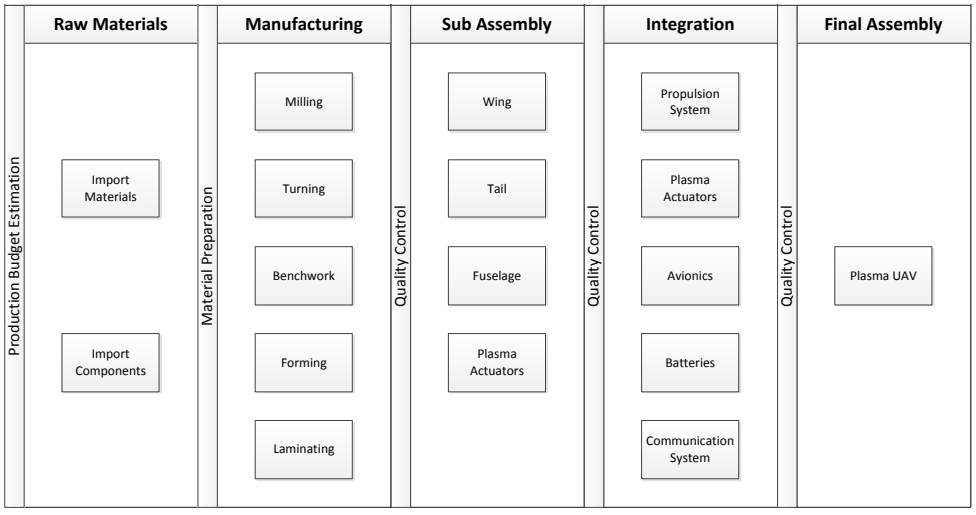

Figure 5.2: An overview of the process from the raw materials to the assembled UAV.

This section will treat the production methods used to make wing, tail and fuselage of the UAV. The components of the UAV are made using hand lamination. Firstly, the apparatus and raw materials for the individual processes are selected and a cost estimation for the process is made. Secondly, the production steps are presented and the section is concluded with the assembly of the components.

5.2.1 Lamination Process

Most of the components that require manufacturing are hand laminated. Hand lamination is a cost effective way to work with composites. It is ideal for a small scale production, and since two UAVs have to be produced, hand lamination is the best production method. The production can be easily carried out by a team of four students, especially if some of them have prior experience with the process. Gaining access to a foam/metal milling machine and a carbon-working location is possible with the collaboration of various TU Delft faculties or by outsourcing the production of the foam products. The faculties of interest are industrial design, mechanical engineering, aerospace engineering or the dream hall (two team members are also Dream-Team members), whereas the Multi-Form[3] is capable of making complex foam shapes. The use of the facilities can drastically reduce the production costs. If that is not the case, the milling has to be outsourced which may become costly.

Estimating the budget for purchase of all the raw materials and required apparatus in the process is the starting point of the production line. Defining the budget will determine whether the process is feasible. In Table 5.1 the quantity and price of each material required for the production of two wings and tails are listed. Some items, like safety equipment and the vacuum pump, only need to be purchased once since they will still be usable in future hand-lamination sessions. If facilities are made available by the university, some items (denoted with an asterisk (*) in the table) on the list can be removed decreasing the production costs by € 647.16.

Table 5.1: Hand lamination process

Required Materials	Quantity and dimensions	Cost €
Breather	40 m × 1.25 m	82.80
Peel Ply	40 m × 1 m	120.00
Epoxy Resin	4 units	77.92
Vacuum Bag	40 m × 1 m	122.70
Vacuum Pump*	1 unit	399.42
Vacuum Tubing	5 m	7.65
Vacuum Tape	2 × 30 m rolls	36.00
Dremel Tool*	1 unit	55.00
Safety Goggles*	4 units	47.16
Safety Gloves*	2 boxes	4.58
Safety Mask*	3 units	141.00
Plastic Beakers	10 units	64.08
Painting Rollers	6 units	35.94
Adhesive Spray	3 units	30.87
Rubber Strip	2 units, 1200 mm × 10 mm × 2 mm	180.00
TeXtreme® 1027 Fibre	32 m × 1 m	2,816.00
Carbon Tube	2 units, ∅30/28mm × 1.75 m	234.05
Airex C51	2 units, 1 m × 0.9 m × 1 mm	50.00
Foam Wings	4 units	1,258.00
Foam Tails	4 units, 1.3 m × 0.3 m × 23 mm	100.00
Total Estimation		5,863.17

Preparation and Safety

Before starting the hand lamination process, allocating resources and assuring the safety of the students performing the process is of utmost importance. Starting with safety, everyone should wear a long sleeved lab coat or old clothing to protect the skin from the resin. Latex gloves[4], safety goggles[5] and a mask[6] are mandatory for the lamination process and carbon preparation as carbon particles easily become airborne and should not be inhaled.

[3] Multi-Form was contacted for the milling of the cambered airfoil wing, and they were so kind to make a price estimation, which is included in Table 5.1: `http://www.multi-form.eu/`

[4] Latex gloves, accessed on June 12, 2015: `https://www.gamma.nl/assortiment/gamma-latex-handschoen-10-stuks/p/B427961`

[5] Safety goggles, accessed on June 12, 2015: `http://tinyurl.com/od3wn3s`

[6] Safety mask, accessed on June 12, 2015: `http://tinyurl.com/nfkxdg7`

Preparing the fibre is done by cutting the TeXtreme® 1027[7][8] into sheets of the right dimensions wasting as little material as possible by finding the optimum nesting combination. The fibre has a 0-90 orientation, but if transposed 45 degrees the 45-135 directions are covered as well. 24 square meters are enough to laminate two sets of wings and tails, however the actual nesting of the cloth has not been worked out in the report.

Regarding the foam cores, the wing foam core can be manufactured by Multi-Form[9] for about €600 a piece, and will be delivered in four halves allowing the inside of the airfoil to be carved with a dremel tool[10] to fit the cables and the booms that connect to the tail before the upper and lower halves are glued[11] together in preparation for lamination. If necessary, the foam can be sandpapered with a 400 kernel to smooth out imperfections.

The tail on the other hand, being a symmetric airfoil, can be made by the students if permission to use a milling machine is given by the TU Delft. It will be made in halves (upper and lower surface) as well, to carve and place the required cabling and booms. The horizontal and vertical surfaces have no taper and an equal chord length, meaning that all surfaces can be made simultaneously. When a 1.6 m wing has been made, it is cut in the correct spans (0.7 m for the horizontal surface, and two times 0.3 m for the vertical surfaces). The foam finally has to be sandpapered with a 400 kernel to smooth out imperfections.

Finally, the vacuum apparatus needs to be prepared. A vacuum bag needs to be prepared by using the vacuum foil[12] and vacuum tape[13], being very careful to leave one side open to insert the laminate. The bag is connected to a vacuum pump[14] through a tube[15]. Peel-ply and Breather need to be cut such that they can be wound around the laminate. The peel-ply[16] prevents the resin from attaching the vacuum bag and breather, whereas the breather[17] makes sure that vacuum can be achieved over the entire surface and removing excess resin.

Wing and the Tail Production

The wing and the tail has a similar lamination process since they are both made from an airfoil shaped foam core, which is to be laminated with TeXtreme® 1027[18] carbon fibre. This section describes the production process of their two components, starting from the prepared foam-cores and cut fibre.

Once the the rods and wires have been inserted, the wing is glued into one piece and the lamination process can start. It is very important to finish the process within the setting time of the resin[19], which is 15 minutes. Applying the resin on the foam and carbon with a painting brush or a roller[20] is a quick way to impregnate the foam and fibres for most optimal adhesion. Once the two layers have been applied in the right orientation, the wing is wound in peel-ply and breather carefully not to alter the layout of the carbon layers.

When everything is securely wrapped, it is placed inside the vacuum bag which is then sealed with vacuum tape and connected to a vacuum pump through a tube. The pump is turned on and if vacuum is achieved, it can be left to cure at room temperature for at least 24 h. If there is a leak in the seal it can be found by listening for a leak and closing it until near-vacuum is achieved. In the case that the laminate still is not completely dry after the curing time, it can be left to cure outside the vacuum since

[7] TeXtreme® 1027, accessed on June 12, 2015: http://compositeenvisions.com/textreme-1027-hm-high-modulus-60gsm-1-77oz-spread-tow-carbon-fiber-1121.html

[8] TeXtreme® for 88€/m^2, Information obtained from Andreas Martsman: Andreas.Martsman@textreme.com

[9] Information obtained from Remko Pelders: remko@multi-form.eu

[10] Dremel, accessed on June 12, 2015: http://www.carbonwinkel.nl/nl/vacuum-techniek/55444894-vacuum-folie.html

[11] Adhesive Spray, accessed on June 12, 2015: https://www.gamma.nl/assortiment/bison-lijmspray-200-ml/p/B677186

[12] Vacuum foil, accessed on June 12, 2015: http://www.carbonwinkel.nl/nl/vacuum-techniek/55444894-vacuum-folie.html

[13] Vacuum tape, accessed on June 12, 2015: https://www.acpsales.com/Vacuum-Bagging-Supplies.html

[14] Vacuum pump, accessed on June 12, 2015: http://www.carbonwinkel.nl/nl/vacuum-techniek/549-vacuum-pomp.html

[15] Vacuum tube, accessed on June 12, 2015: http://www.carbonwinkel.nl/nl/vacuum-techniek/556-vacuum-slang.html

[16] Peel ply, accessed on June 12, 2015: http://www.carbonwinkel.nl/nl/scheurweefsel-peelply/232-peel-ply-95-g-m-75-cm-breed-plain-geweven.html

[17] Breather, accessed June 12, 2015: http://www.easycomposites.co.uk/products/vacuum-bagging/breather-fabric.aspx

[18] TeXtreme® 1027, accessed on June 12, 2015: http://compositeenvisions.com/textreme-1027-hm-high-modulus-60gsm-1-77oz-spread-tow-carbon-fiber-1121.html

[19] Epoxy resin, accessed on June 12, 2015: http://www.carbonwinkel.nl/nl/epoxyhars/55444453-epoxyhars-l-verharder-s-set-van-2-componenten.html

[20] Muurverfroller, accessed on June 12, 2015: http://tinyurl.com/p8c2yug

a 3 m wing is too big to fit in an oven. When the resin is dry, the wing is finished and ready for the integration of the plasma actuators.

The tail is made in the same way, and is also laminated to the carbon rods. Together they make the wing-tail assembly. The cabling required in the tail is led through those hollow carbon rods and come through the airfoil surface at the required locations, much like in the wing. The vertical and horizontal stabilizers are permanently glued together. As a final reinforcement, an additional layer of fibre is laminated on the joint between the boom and the skin of the wing and tail. This ensures that the loads are transferred from the boom to the skin instead of transferring it from the boom to the foam core.

Fuselage Production

The fuselage is hand-laminated as well. As opposed to the wings and tail, the fuselage needs to withstand much smaller loads and can therefore be made of normal carbon fibre[21], which is a lot less costly. The foam core will consist of Airex C51 foam[22], which is ideal for curved surfaces and has a high fracture toughness making it perfect for a fuselage subject to impact. The fuselage will be made in two parts: the main part consists of the floor, side wall, nose and the back, which carries all the inner components whereas the second part consists of just a side wall. The two halves are joined when the wing is inserted on either side, and locked in place with fasteners and a small aluminium plate glued to the main fuselage part, joining the two parts (Fig. 5.3).

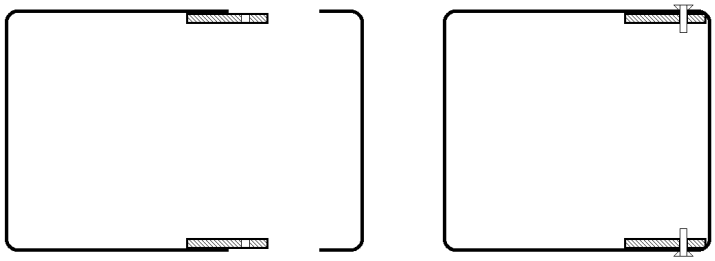

Figure 5.3: Joining method of fuselage halves

The fuselage requires a destructive mould in order to be made. The mould is made out of a foam block, which is hollowed out with a milling machine to match the negative of the fuselage. The mould is then lined with a layer of wax to make the releasing process easier. Once the wax is dried, the two layers of carbon fibre are individually impregnated and laid down in 0-90 and 45-135 orientation. The 1 mm thick foam sheet is then added (Airex C51 is ideal for curved surfaces since it can be easily laid into the shape) and impregnated with resin as well, to be covered symmetrically with carbon fibre. The mould is covered with peel-ply and breather and enclosed in a vacuum bag attached to a vacuum pump. After 24 hours, the resin has cured and the mould can be broken to release the fuselage. Finally, with the aid of full scale technical drawings, the airfoil cross-section can be carved out of the fuselage's side walls and lined with rubber[23] to increase grip and remove high loading regions between the components.

5.2.2 Integration

When the structural elements of the UAV have been produced, all the hardware needs to be integrated in the system. The hardest thing to integrate in the UAV are the plasma actuators. Since the skin of the wing is made of carbon fibre, it is conductive. This means that the copper strips have to be insulated. This can be done by applying an extra layer of Kapton® underneath the copper electrodes. If the insulation proves not to be sufficient more layers can be added during service.

The cabling was integrated in the lamination process, and at this point, there are cables at the root of the wing and at the locations of the copper electrodes on the wing and tail. When the main fuselage component is placed on the wing, the cables are connected to the ignition coils, which are then connected to the bridge board. All the components inside the fuselage (Fig. 4.35) are locked into place with fasteners

[21] Carbon fibre, accessed June 12, 2015: http://www.carbonwinkel.nl/nl/carbon-weefsel/55444610-carbon-weefsel-160-g-m-100-cm-breed-keper-geweven.html

[22] Airex C51, accessed June 19, 2015: http://www.3accorematerials.com/en/products/airex/airexreg-c51.html

[23] Rubber strip, accessed on June 19, 2015: http://www.rubbermagazijn.nl/collectie/pakkingmateriaal/plaatrubber-sbr/2811_zwart_plaatrubber-sbr-10x2mm-120cm.html

so that they can be removed from the fuselage easily if necessary, with the exception of the batteries, which are kept in place with Velcro. When everything is in the correct location and the centre of gravity has been confirmed to be where it was designed, the remaining fuselage wall can be fastened to the UAV closing the fuselage and protecting the hardware.

Finally, the parachute has to be positioned ahead of the wing to avoid creating holes in the wing. The centre of gravity, however, lies on the wing. The parachute needs to be tethered on or behind the centre of gravity to avoid having the aircraft hanging with the tail down during an emergency landing. The fuselage is strong enough to take the landing impact, whereas the tail is more fragile.

5.3 Avionics

Avionics include all the electrical systems that are used on board of the UAV, with the purpose of providing power to the engine, controlling the UAV using plasma actuators, communication to a ground station and navigation.

The UAV control system consists of the following components:

- Flight controller
- Plasma control system
- Electronic Speed Controller (ESC)
- Full bridge board
- Low voltage switches
- Ignition coils
- Remote control system
- Telemetry
- Sensors

The general layout of the control system is depicted in Fig. 5.4. First, the plasma control system is explained in detail in this section and the requirements that plasma control poses on the flight controller are discussed. These requirements are then used to choose a flight controller. Subsequently, an ECS is selected for engine control and the high-voltage generation system is discussed. Then, after treating the remote control system of the UAV the telemetry components and sensors in the fuselage are discussed.

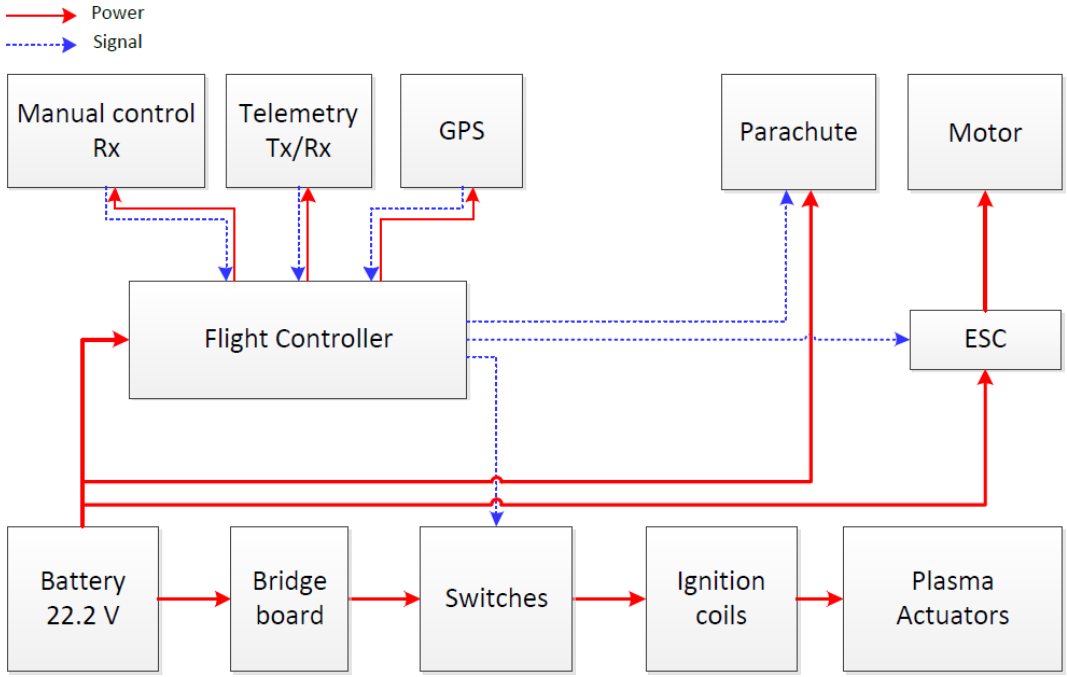

Figure 5.4: Layout of UAV control system

5.3.1 Plasma Control System

In Section 4.2.3 the plasma actuator integration methods to achieve pitch, roll and yaw control were discussed. The layout of the plasma actuators on the wing and tail surfaces that came out of this discussion is depicted in Fig. 5.5.

In this figure, it can be seen that the plasma actuators have been given an annotation and some of the plasma actuators have been grouped. This has been done to distinguish the control motion they induce roll, pitch or yaw. Attention has to be paid to the plasma actuators on the vertical tail-planes. Both the vertical tail-planes contain a plasma actuator on the left side (denoted with L) and one on the right side (denoted with R).

Electronically, plasma actuator control works as follows: a DC battery signal is converted to an AC signal. This is then fed to a number of switches that pass the AC signal to automotive ignition coils, if the switches receive the right signal from the flight controller. The automotive ignition coils transform the low voltage AC to high voltage AC, which is then fed to the plasma actuators.

The system to convert the DC battery signal to high voltage AC is discussed in Section 5.3.4. Below, it is explained which switch and control output are connected to what plasma actuator to achieve a certain aircraft motion.

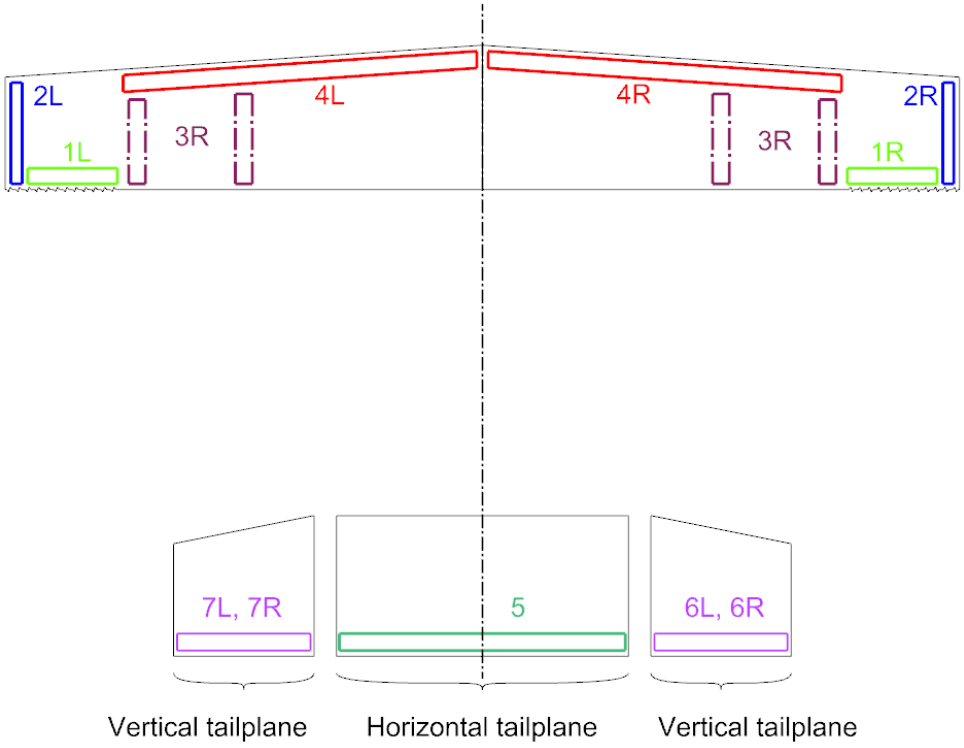

Figure 5.5: Plasma actuator layout on wing and tail surfaces

Each switch is connected to a control output of the flight controller. Roll control is achieved by activating either plasma actuator 1L or 1R. Positive rolling moment(right wing moving down) is achieved by activating actuator 1L and Control 1 is assigned to this. Control 2 is connected to actuator 1R for producing negative rolling moments.

To achieve pitch control plasma actuators 2L, 2R, 3L and 3R are activated to pitch up, and actuator 5 for pitch down motion. Plasma actuator 5 is operated with Control 3 and actuators 2L, 2R, 3L and 3R are operated with Control 4.

Yaw control is accomplished by operating the plasma actuators on the vertical tail surfaces. Activating plasma actuators 6R and 7R creates a positive yawing moment(left wing forward) and this is connected to Control output 5. Actuators 6L and 7L are operated with Control 6 for negative yawing.

Actuators 4L and 4R are used as high lift devices and require only one control output of the flight controller, assigned to Control 7.

Table 5.2 summarizes the designation of the control outputs to the plasma actuators and Fig. 5.6 schematically shows the wiring of the flight controller outputs, the high voltage switches and the plasma actuators.

Table 5.2: Designation of control outputs to plasma actuators

	Control	Plasma actuator
Positive roll	1	1L
Negative roll	2	1R
Pitch down	3	5
Pitch up	4	2L, 2R, 3L, 3R
Positive yaw	5	6R, 7R
Negative yaw	6	6L, 7L
High lift devices	7	4L, 4R

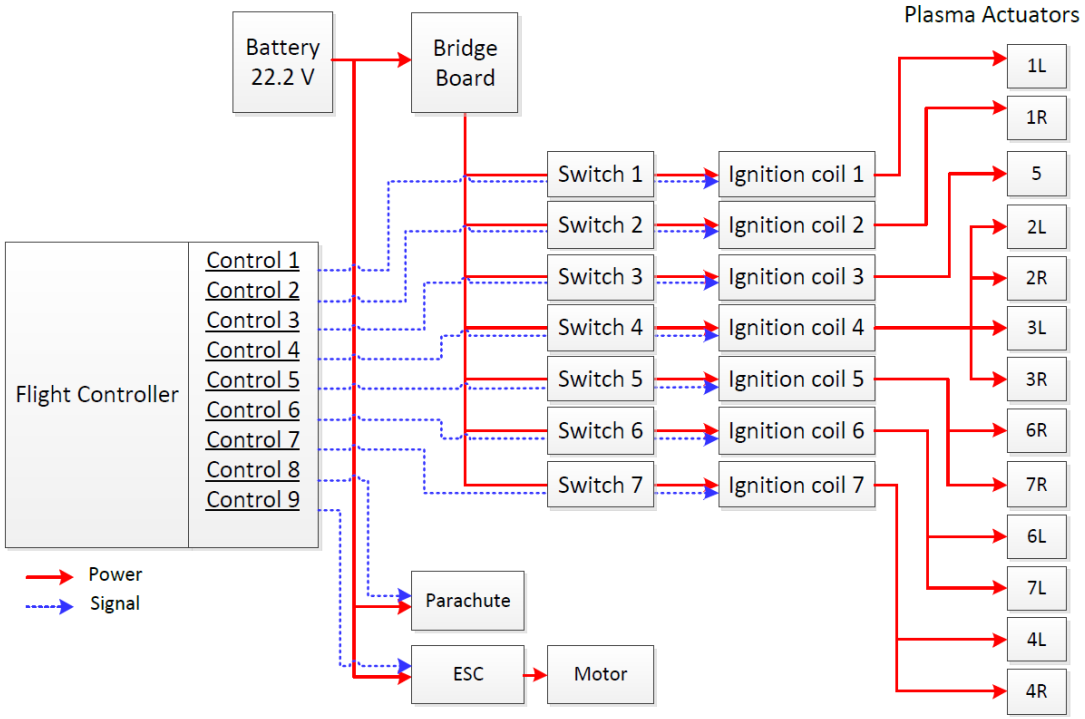

Figure 5.6: Control outputs of the flight controller

5.3.2 Flight Controller

The flight controller is the main component of the UAV control system. It translates manual control inputs to an engine power output signal, control signals for plasma actuation and activates parachute deployment. The flight controller includes an autopilot system, that can autonomously fly way points and perform take off and landing, using GPS as navigation. A module for two way telemetry can be connected to the flight controller to send flight data to a ground station and send commands to the UAV.

First in this subsection, it is discussed what has to be done to adjust the flight controller in order to use it for plasma control. Secondly, a flight controller is selected.

Adaptations

The flight controller algorithm has to be rewritten in order to be used for plasma control, because it is designed for moving control surfaces, actuated by servos. Usually, the outputs of the controller are

proportional to deflection angles for a servo that is connected to a moving control surface. While the value of a control surface deflection angle can vary, a plasma actuator can only be on or off.

A plasma control mechanism can resemble a control surface with variable deflection angle by pulsing the output signal. This means turning the plasma actuator back off again for a certain time before turning back on, to achieve a variable ΔC_L. For this, it is assumed that plasma establishes and breaks down very fast[45], and the transition time between flow conditions is small compared to the time of discharge. Pulsing of the output signal has to be done with a certain control pulsing frequency f_c. The frequency of pulsing has to be sufficiently high to approximate a quasi linear relation between the pulsing of the output signal and the ΔC_L of the plasma actuator.

Two frequencies are already used in the plasma actuation. These are the AC frequency at 2000 Hz and the pulsing frequency for separation control at 160 Hz. The control pulsing frequency has to be sufficiently smaller to avoid interfering the aerodynamic effects. Therefore, the control pulsing frequency is set one order of magnitude smaller than the separation control frequency, at 16 Hz.

To pulse the signal to the plasma actuator the parameter pulsing duty cycle D is introduced, which is the fraction of one periodic cycle in which the signal is active, with $D = 1$ being continuously on and $DC = 0$ continuously off. The duty cycle is graphically described in Fig. 5.7[24].

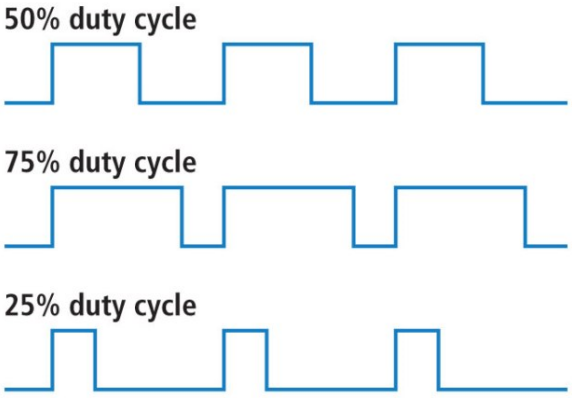

Figure 5.7: Duty cycle parameter

Since plasma establishes very fast upon actuation, it is assumed that the amount of ΔC_L that the plasma actuation mechanism produces is proportional to the duty cycle. In an aircraft with regular control surfaces, the ΔC_L of these control surfaces are usually proportional to their deflection angle. So instead of having the ΔC_L of a regular control surface proportional to its deflection angle, the ΔC_L of a plasma actuator is proportional to the corresponding duty cycle. This means that the duty cycle can also get a negative value, while this is not possible due to the definition of the duty cycle itself. Later in this subsection it is discussed what needs to be done in the event that the duty cycle is negative.

The state space system for plasma control was derived in Section 4.5 and is in the form of:

$$\dot{\bar{x}} = A\bar{x} + B\bar{u} \tag{5.1}$$

$$\bar{y} = C\bar{x} + D\bar{u} \tag{5.2}$$

The input vector of the state space system can then be rewritten in terms of the duty cycle, using a constant k, such that $-1 < D < 1$. For the symmetric motion:

$$\delta_e = k_{\delta_e} D_{\delta_e} \tag{5.3}$$

For the asymmetric motion:

$$\begin{bmatrix} \delta_a \\ \delta_r \end{bmatrix} = \begin{bmatrix} k_{\delta_a} D_{\delta_a} \\ k_{\delta_r} D_{\delta_r} \end{bmatrix} \tag{5.4}$$

[24]Duty cycle parameter image, accessed on June 16th, 2015: https://learn.sparkfun.com/tutorials/pulse-width-modulation/duty-cycle

The $B \cdot \bar{u}$ and the $D \cdot \bar{u}$ terms have to be rewritten, for the symmetric motion in the form:

$$\begin{bmatrix} B_1 \\ B_2 \\ B_3 \\ B_4 \end{bmatrix} k_{\delta_e} D_{\delta_e} = \begin{bmatrix} k_{\delta_e} B_1 \\ k_{\delta_e} B_2 \\ k_{\delta_e} B_3 \\ k_{\delta_e} B_4 \end{bmatrix} D_{\delta_e} \tag{5.5}$$

And for the asymmetric case:

$$\begin{bmatrix} B_{11} & B_{12} \\ B_{21} & B_{22} \\ B_{31} & B_{32} \\ B_{41} & B_{42} \end{bmatrix} \begin{bmatrix} k_{\delta_a} D_{\delta_a} \\ k_{\delta_r} D_{\delta_r} \end{bmatrix} = \begin{bmatrix} k_{\delta_a} B_{11} & k_{\delta_r} B_{12} \\ k_{\delta_a} B_{21} & k_{\delta_r} B_{22} \\ k_{\delta_a} B_{31} & k_{\delta_r} B_{32} \\ k_{\delta_a} B_{41} & k_{\delta_r} B_{42} \end{bmatrix} \begin{bmatrix} D_{\delta_a} \\ D_{\delta_r} \end{bmatrix} \tag{5.6}$$

In an analogous way, this can be done for the D matrices.

The state space system is implemented in the control system in Fig. 5.8. A desired state $\bar{x}_{ref}$ is compared to the actual state vector $\bar{x}$, yielding the state error $\Delta\bar{x}$. This is then fed through a controller that gives the rewritten state space input vector $\bar{u}_D$, containing the duty cycles.

A closed loop with PID controller is used, consisting of a proportional, an integral and a derivative term. The proportional term gives the input vector of the state space system $\bar{u}_D$, that is proportional to the state error vector $\Delta\bar{x}$. This means that a large state error yields a large control input. The integral term is used to eliminate the steady state error. To ensure stability and improve the settling time of the system, the derivative term is used. The state space system then calculates the new state $\bar{y}$, which is then fed back through a sensor measurement to the desired state $\bar{x}_{ref}$.

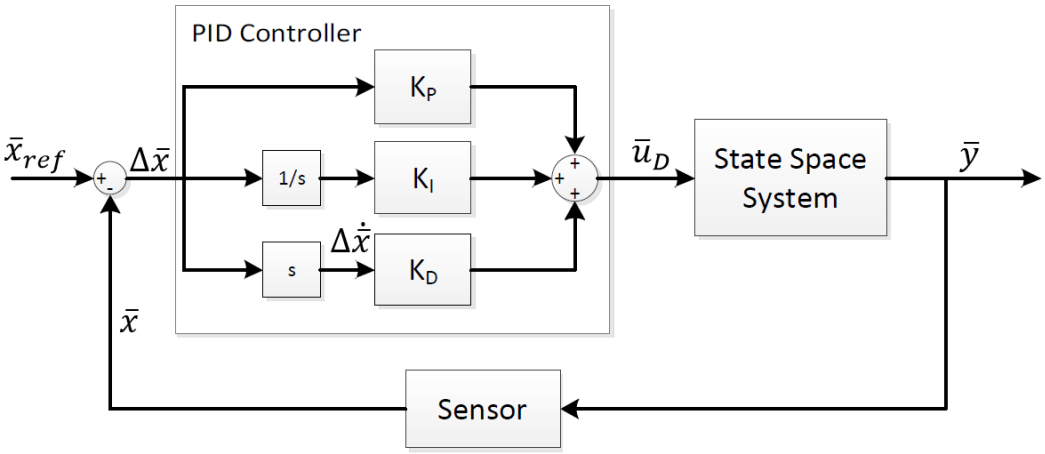

Figure 5.8: Flight controller control block diagram

Negative control surface deflection angles yield negative duty cycle values for the plasma UAV. For example, when a pitch down motion is desired, the elevator deflection angle is positive and the pitching duty cycle D_{δ_e} is also positive. A signal with the duty cycle D_{δ_e} is then given to plasma actuators corresponding to pitching down (No. 5 in Fig. 5.5). When a pitch up motion is required, the pitching duty cycle D_{δ_e} is negative. In this event, a signal with the absolute value of the negative duty cycle D_{δ_e} has to be given to the plasma actuators corresponding to pitching up (No. 2L and 2R or 3L and 3R). The signals that the flight controller has to give to plasma actuators for positive or negative duty cycles D_{δ_e}, D_{δ_a} and D_{δ_r} are listed in Table 5.3.

Table 5.3: Flight controller actions, for positive and negative values of duty cycle, DC

	Action	
	$D > 0$	$D < 0$
Pitching duty cycle D_{δ_e}	Signal with D_{δ_e} to P.A. 5	Signal with $\lvert D_{\delta_e} \rvert$ to P.A. 2L, 2R, 3L and 3R
Rolling duty cycle D_{δ_a}	Signal with D_{δ_a} to P.A. 1R	Signal with $\lvert D_{\delta_a} \rvert$ to P.A. 1L
Yawing duty cycle D_{δ_r}	Signal with D_{δ_r} to P.A. 6L and 7L	Signal with $\lvert D_{\delta_r} \rvert$ to P.A. 6R and 7R

Flight Controller Selection

As explained in Section 5.3.1, for the plasma control, the propulsion and the parachute a total of 9 control outputs are needed. Potentially, other outputs could be used to, for example, control a camera as payload. This would be done by controlling two axes of rotation. A flight controller should therefore be chosen that has at least 11 control outputs.

Since the flight controller requires adaptations in the software, it is important that it features open source software. In addition, the computing performance of the flight controller has to be sufficient to be able to compute all control outputs. Since no estimation has been done for the computing power required, a safe choice, i.e. relatively high performance has to be chosen.

The flight controller that is chosen for this is the 3DR Pixhawk[25]. Being specifically designed for autonomous flying, it encompasses autopilot functions, but can also be controlled manually. The Pixhawk includes 14 control outputs, using pulse width modulation (PWM) and features an advanced 32 bit ARM Cortex® M4 high performance processor. In also contains a sufficient amount of connectivity options for radio-control receiver, telemetry or a GPS module. The controller is priced at $199.

5.3.3 Electronic Speed Controller

The propulsion system consists of an electric engine which is connected to an ESC. This ESC is connected to the battery and the flight controller and regulates the amount of power that goes to the engine, to adjust the engine speed. ESCs are rated in the amount of current that they can continuously deliver to the engine.

In the power budget in Section 4.1.2 the peak power that is drawn from the battery is estimated at approximately 405 W, yielding a peak current of 18.2 A using the 22.2 V from Section 4.1.2. Therefore, the T-MOTOR AIR 20 A is chosen, as it is capable of delivering up to 20 A[26]. It is made by the same manufacturer of the chosen engine, which might contribute to efficiency.

5.3.4 High Voltage Pulse System

To convert the DC battery signal to high voltage AC, initially a solution was found using the Minipuls 2.1 from GBS Elektronik[27]. This product converts a DC supply with a voltage between 15 and 40 V to an AC signal with a maximum peak-to-peak voltage of 20 kV and a frequency between 5 and 20 kHz. The high voltage frequency generator weighs a total of 1.1 kg, however to generate the voltage required for plasma actuators two of these Minipuls 2.1 units are required.

This leads to quite a heavy system, therefore the complete design is much more complicated and needs to be modified to comply with the weight constraint. Instead of the transformer circuit in the Minipuls 2.1, automotive ignition coils are used. They are normally used to transform a car battery voltage to a higher voltage level needed to create an electric spark[28].

Previously, it was decided to use a combination of Minipuls 2.1 and one high voltage switch for every plasma actuator on the UAV, resulting in a total number of 8 high-voltage switches. However, the high voltage switches are found to be heavy and expensive, and an ignition coil is chosen to replace such a

[25] 3DRobotics Pixhawk, accessed on June 6, 2015: `https://store.3drobotics.com/products/3dr-pixhawk`
[26] T-motor ESC, accessed on June 4, 2015: `http://www.rctigermotor.com/html/2014/esc_1223/284.html`
[27] GBS Elektronik, accessed on June 5, 2015: `http://www.gbs-elektronik.de`
[28] Ignition coil, accessed on June 15, 2015: `https://en.wikipedia.org/wiki/Ignition_coil`

configuration. Since the ignition coil is relatively light-weight, each of them can be used to generate a high voltage signal for one plasma actuator with one low voltage switch in between the full bridge board and the transformer, see Fig. 5.4. These low voltage switches greatly reduce the weight since their weight is in magnitude of less than 1 gram.

Several components are needed for this configuration, including the Minipuls 2.1 full-bridge converter and 7 ignition coils. The Delphi Pencil Coil Multi-Port Fuel Injection[29] is capable of transforming the voltage to 34 kV, which is more than sufficient. The weights of the system components are presented in Table 5.4.

Table 5.4: Weight distribution of the high voltage pulse generator

	Quantity	Mass [g]	Total Mass [g]
Full-bridge board	1	300	300
Delphi ignition coil	7	175	1225
Total			1525

5.3.5 Remote Control

When the UAV is in sight, it is possible to manually control the UAV. This is extremely useful for the launch and during landing, in order to have quick response and be able to account for the terrain, which the autopilot is not fully capable of. The remote control to be used is the Frsky TARANIS 2.4 GHz R/C system. This remote control is "very highly recommended"[30] for all RC uses and is compatible with the Pixhawk autopilot. The remote control already comes with a receiver that can be directly plugged into the autopilot. The operating range of the remote control and receiver equals 1.5 km and the dimension of the receiver are 46.5×27×14.4 mm with a weight of 16.8 gram[31]. Favourable features of the remote control include RSSI signal strength feedback so loss of signal will not occur easily, three programmable fail-safe modes and a very low latency of just 9 ms[32].

According to the Dutch Ministry of Infrastructure and Environment, no additional permit has to be applied for at the Telecom Agency of the Ministry of Economic Affairs if the so called "free frequencies" are used, i.e. 2.4 and 5.8 GHz [17].

5.3.6 Telemetry

For the telecommunications subsystem two specific components are used aboard the UAV: a transmitter to encode and send the signal and an antenna to transmit the data to the ground station. Both of these are connected to the flight controller.

The radio frequency (RF) module that will be used as transmitter is the XBee-PRO® 900HP [46][33], produced by Digi International Inc. Its range of up to 22 km will prove to be very useful as the flying range of the UAV is set to 10 km. This range is, however, in the most optimal case, where the UAV has to be in the line of sight and no noise is interfering. The transmitter has an operating frequency of 900 MHz, an interface data rate of 230.4 kbps, a transmit power of up to 24 dBm and a receiver sensitivity of -101 dBm. The RF data rate is 125 kbps. Both RPSMA and MMCX connectors are can be connected to the transmitter, which uses FSK modulation. A frequency of 900 MHz is used to avoid interference with the remote control, which already uses 2.4 GHz. The RF module will be connected to the flight controller, which relays the data that needs to be sent to the ground station as can be read in Section 5.3.8.

Due to certain factors the range may vary though. Compared with general or average specifications, these so called range enhancers are better receiver sensitivity, higher transmitter power, shorter antenna cable,

[29] Delphi Ignition Coils, accessed on June 15, 2015: `http://www.delphi.com/manufacturers/auto/powertrain/gas/ignsys/igncoils`

[30] ArduPilot, accessed on June 9, 2015: `http://copter.ardupilot.com/wiki/common-pixhawk-and-px4-compatible-rc-transmitter-and-receiver-systems/`

[31] Range Video, accessed on June 9, 2015: `http://www.rangevideo.com/receivers/99-frsky-x8r-16ch-receiver-sbus-smart-port-pcb-antenna.html`

[32] Range Video, accessed on June 9, 2015: `http://www.rangevideo.com/radios-and-receivers/96-frsky-taranis-24ghz-rc-system.html#/mode-2_throttle_stick_left/combos-x8r_receiver_included`

[33] Digi International Inc., accessed on June 9, 2015: `http://www.digi.com/products/wireless-wired-embedded-solutions/rf-modules/xbee-rf-modules/xbee-proprietary-rf-modules/xbee-pro-900hp`

no physical obstruction between transmitter and receiver, interference-free environment, lower data rate and lower frequency[34]. Since the range of the XBee PRO is up to 22 km, there is some contingency. However, optimizing these parameters will maximise the operating range. In the case that the range turns out to be insufficient, the parameters mentioned above can therefore be optimised. Halving the data range can for example increase the range by 26%. Finally, not having a long antenna cable should also not be too difficult to achieve[34].

The antenna that will be used is the 800-900 MHz 1dBi Omni antenna by Titan Wireless [35]. As the name implies, the antenna is able to transmit at 900 MHz. This antenna transmits omni-directionally with a beam of 360° horizontally and 180° vertically, which corresponds to half a sphere underneath the UAV. For obvious reasons it is unnecessary to send data upwards, since the ground station will not be stationed at a higher altitude than the UAV, when operating in the Netherlands. In the case that the UAV is to be used during an operation where the ground station is higher located than the UAV, such as in a canyon or in a mountainous environment, the antenna can be replaced with MicroTik's omnidirectional antenna. This antenna has comparable specifications, and radiates energy in the entire spherical direction, in order to have full coverage[36]. The advantage of the chosen antenna (i.e. transmitting only downwards), implies that no power will be lost in transmitting in directions that will not be used anyway. Furthermore, no complex and expensive system is needed for a mechanism that directs the antenna towards the ground station.

Practical details of both components consist of the following. The transmitter consumes up to 0.44 W. The size of the transceiver equals 33×25×10 mm. The size of the antenna is a cylinder of height 0.1575 m and diameter 0.0127 m. In terms of weight, the antenna and transceiver weigh 0.0454 and 0.0064 kg respectively, adding op to 0.0518 kg. The ground station needs exactly the same two components which are connected to a computer via USB in order to be able to read the data, as depicted in Fig. 5.9.

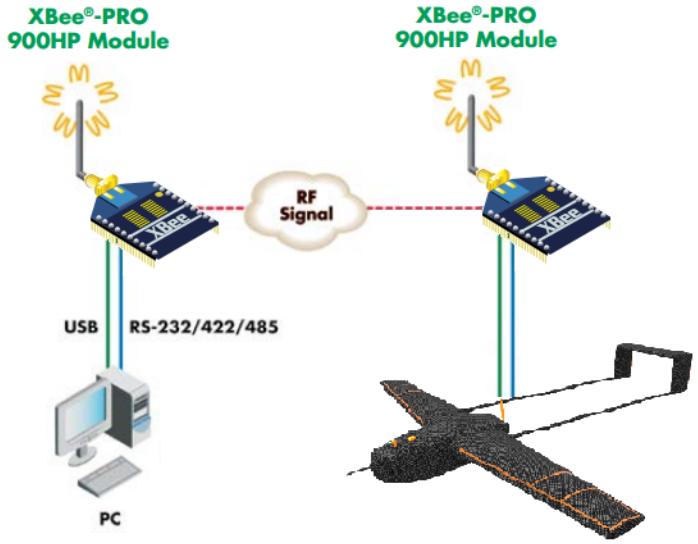

Figure 5.9: Schematic depiction of communication system [46], [47]

5.3.7 Sensors

The chosen autopilot, the Pixhawk, already has four sensors in its module. These four consist of the following: ST Micro L3GD20 3-axis 16-bit gyroscope, ST Micro LSM303D 3-axis 14-bit accelerometer/magnetometer, Invensense MPU 6000 3-axis accelerometer/gyroscope and MEAS MS5611 barometer. To this module, a GPS module and airspeed sensor are added.

[34] Digi International Inc., accessed on June 1, 2015: `http://www.digi.com/technology/rfmodems/rangereducers`

[35] Titan Wireless LLC, accessed on May 19, 2015: `http://www.titanwirelessonline.com/800-900MHz-1dBi-Omni-p/at-1sbx-900.htm`

[36] Titan Wireless LLC., accessed on June 1, 2015: `http://www.titanwirelessonline.com/MikroTik-Omni-MMCX-Pigtail-Kit-p/at-rbin-m.htm`

The ST Micro L3GD20 3-axis 16-bit gyroscope measures both angular rates and temperature. It features three selectable full scales of ±250/±500/±2000°/sec and 8-bit temperature resolution[37].

The ST Micro LSM303D 3-axis 14-bit accelerometer/magnetometer measures 3 magnetic field channels and 3 acceleration channels. It features a full-scale magnetic scale of ±2, ±4, ±8 and ±12 Gauss (10^{-4} T) and a gyro range of ±2 g, ±4 g, ±8 g, and ±16 g with 16-bit output data[38].

The Invensense MPU 6000 3-axis accelerometer/gyroscope acts as six-axis motion tracking device, including a 3-axis gyroscope and a 3-axis accelerometer. The part features a user-programmable gyroscope full-scale range of ±250, ±500, ±1000, and ±2000°/sec and a user-programmable accelerometer full-scale range of ±2 g, ±4 g, ±8 g, and ±16 g[39].

The MEAS MS5611 barometer is an extremely accurate barometer with an accuracy of about 0.0024 mbar pressure and 0.01°C temperature. Its output is both the (static) pressure and temperature in 24-bits, yields an altitude resolution of 0.10 m[40].

Even-though several of the sensor functions are present in double, it has been done for reliability, redundancy and frequency analysis. The values can now be taken from several sensors, which makes the data more reliable. The redundancy benefit is very clear: if one sensor fails, another one can still do the job. Considering frequency analysis, if a sensor samples at a certain rate and an external frequency is applied with the same frequency, the data is not reliable anymore, because these two interfere with each other. If two different sensors sample at a different frequency, this problem will not occur.

In addition to these sensors, a GPS module is needed to acquire the UAV's position. The module that is used is the 3DR uBlox GPS with Compass Kit[41], with 5 Hz update rate. Dimensions and mass are 38×38×8.5 mm and 16.8 gram[42] respectively.

With these five instruments; the angular accelerations, heading, altitude and temperature can be determined. To evaluate the airspeed, the dynamic pressure needs to be evaluated since the GPS can only be used to determine the UAVs speed with respect to the ground. Therefore a pitot tube is needed to measure the dynamic pressure. The component that will be used for this is the Pixhawk Airspeed Sensor. It features a Measurement Specialties 4525DO sensor, with a measurement range of up to 100 m/s (360 km/h), with a resolution of 0.84 Pa. It measures both the static and the dynamic pressure. An advantage is that it also measures the air temperature with which it can calculate the true airspeed from the indicated airspeed using the MS5611 static pressure sensor on the Pixhawk autopilot[43], which costs $54.99[44]. The sensor is estimated to be 10 cm long and is to be placed parallel to the fuselage separated at least 4 cm in order to be in clean air. To achieve this, a mount can be downloaded, free of charge, and 3D printed[45].

Electromagnetic Interference

The plasma actuators used to control the UAV require a high-voltage AC signal, which is essentially an oscillating electric field. This in turn produces a magnetic field, which could give rise to electromagnetic interference (EMI) with sensors [48]–[50], communication [51], GPS signals [52] and data storage and analysis tools [53].

Although the DBD plasma actuator generates significantly lower levels of EMI than, for example, the pulsed-arc discharge [51], it is still a parameter to be taken into account. The level of interference was assessed, but as the reaction of the specific instruments used for measurement and storage on the presence of oscillating fields couldn't be predicted, the assessment was inconclusive. The most straightforward way

[37] ST Micro L3GD20 Datasheet, accessed on June 8, 2015: `http://www.st.com/web/en/resource/technical/document/datasheet/DM00036465.pdf`

[38] ST Micro LSM303D Datasheet, accessed on June 8, 2015: `http://www.st.com/web/en/resource/technical/document/datasheet/DM00057547.pdf`

[39] MPU-6000 and MPU-6050 Product Specification Revision 3.4, accessed on June 8, 2015: `http://store.invensense.com/datasheets/invensense/MPU-6050_DataSheet_V3%204.pdf`

[40] MEAS MS5611-01BA03 Datasheet, accessed on June 8, 2015: `http://www.meas-spec.com/downloads/MS5611-01BA03.pdf`

[41] 3D Robotics, accessed on June 9, 2015: `https://store.3drobotics.com/products/3dr-gps-ublox-with-compass`

[42] B & H Foto & Electronics Corp., accessed on June 9, 2015: `http://www.bhphotovideo.com/c/product/1098161-REG/3d_robotics_gps_kit_0003_gps_module_for_pixhawk_apm.html`

[43] Pixhawk Airspeed Sensor, accessed on June 9, 2015: `https://pixhawk.org/peripherals/sensors/px4airspeed`

[44] 3D Robotics, accessed on Jun 9, 2015: `https://store.3drobotics.com/products/pixhawk-airspeed-sensor-kit`

[45] Mniac 3DR Pitot Tube Mount v1.5, accessed on June 9, 2015: `http://www.thingiverse.com/thing:169317`

of knowing the EMI is by performing a test or theoretical treatment [54], [55], but both are outside the scope of this project.

In case the test shows levels of EMI created by plasma actuators that are not acceptable, there are several ways to solve the issue. It can be eliminated by the grounding and shielding of the electrical equipment [48]. An optical insulation circuit could also be used, as shown in Fig. 5.10 [53]. The electronic circuitry that is located too close to the EMI source can be insulated [55], [56]. Regarding the high voltage cabling, insulation or grounded conductive coatings could be installed, as instructed by the 'Quantum Transport group TU Delft[46]. The pulsing frequency and its higher harmonics can be filtered out of the collected data in case of contamination [51]. The contamination can also be filtered out of the data, by comparing the signals for plasma actuator switched off and on [50].

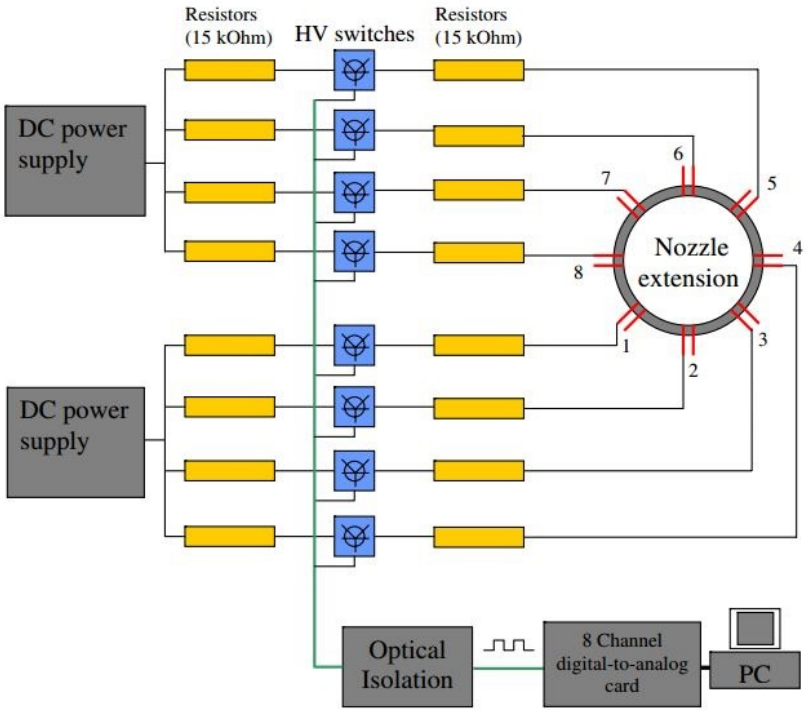

Figure 5.10: An optical insulator

Until further research and tests on EMI are performed, the high voltage wiring are insulated, to keep the design as safe as possible. When two wires with opposite current are placed close to each other, the electromagnetic fields might cancel each other out, eliminating the EMI. Coaxial cables or twisted pairs will be used to transport the high voltage to the plasma actuators. However, the insulation will still be required to shield the high-voltage in the wires.

5.3.8 Block Diagrams

This section will contain several block diagrams related to communications and data handling. In addition, an electrical block diagram is presented to give an overview of the UAV electrical system that was treated in the previous subsections.

Communication Flow Diagram

In this section, the basic structure of the communication subsystem is elaborated. This is presented in the communication flow diagram below.

[46] Quantum Transport of the Kavli Institute of Nanoscience at Delft University of Technology. QT designed instrumentation, accessed on June 19, 2015: `http://qtwork.tudelft.nl/~schouten/linkload/index-linkload.htm`

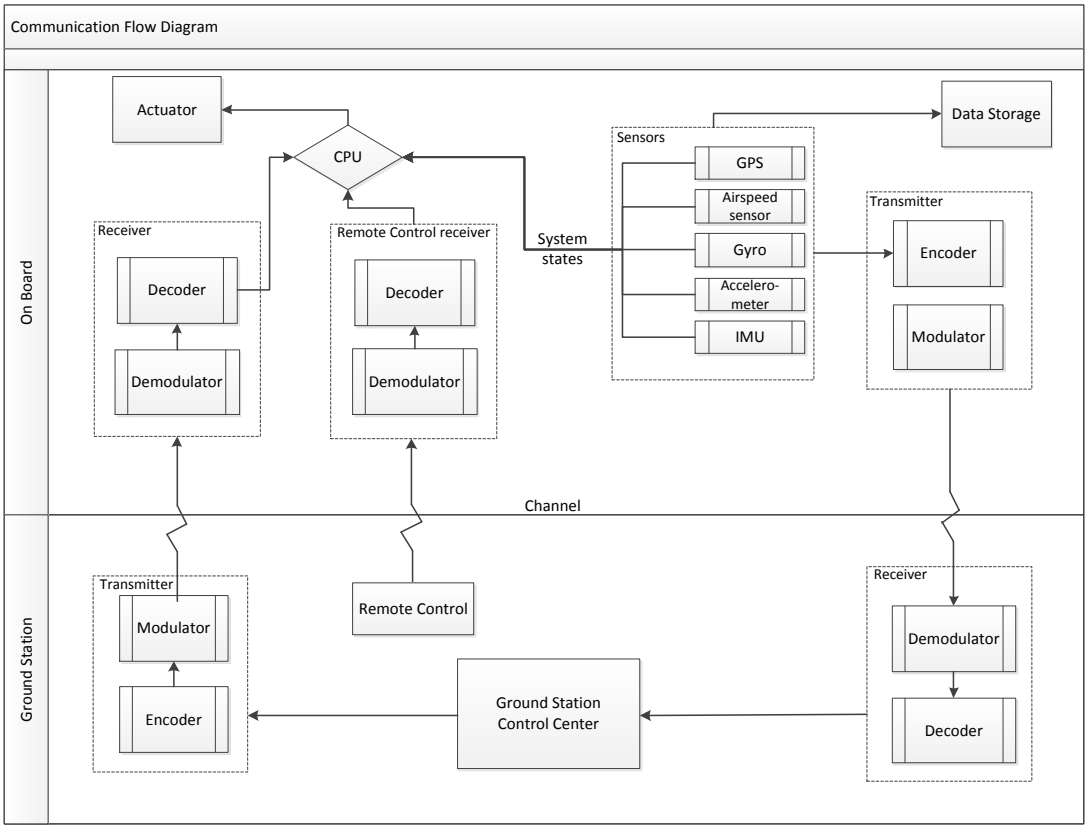

Figure 5.11: Schematic depiction of the communication flow

As can be seen in Fig. 5.11, both the ground station and on board system have a transmitter and a receiver. The transmitter comprises an encoder, which converts a signal or data into code, and a modulator which maps a baseband signal into another signal (carrier signal) that can be physically transmitted. Analogously, the receiver consists of a demodulator and a decoder.

There are multiple sensors on board, as explained in Subsection 5.3.7, through which the system states can be obtained. The information is then fed into the CPU for calculations, followed by the actuation of the voltage input to the plasma actuators to alter the attitude of the UAV. Some sensor information is also stored on the on-board MicroSD Card for further data analysis on the ground.

The aforementioned process illustrates the flow of data through the system and to and from its environment. If the UAV is controlled manually, the sensor information has to be transmitted to the ground station to involve the remote control. This is described by the data link through the ground station shown in Fig. 5.11.

Data Handling Block Diagram

The avionics of the UAV need to handle the entire data flow of all systems. In the data handling flow diagram, the different components of the data handling system of the UAV are shown, including the kind of information that is sent through. Wherever possible, specific characteristics of the hardware or connection such as memory size, computing power, data rates, etc. have been added.

Such as the diagram in Fig. 5.12 depicts, the flight controller is the central element for the data handling. All data is processed by the flight controlling element of the 3DR Pixhawk[47], as described in 5.3.2. Its 32-bit STM32F427 Cortex M4 core and 32-bit STM32F103 fail-safe co-processor process all the information.

There are two different data flows: incoming and outgoing. The telemetry is both incoming and outgoing due to its two-way nature. The incoming data flow consists of the remote control, the battery, the

[47] 3DR, accessed on June 5, 2015: `https://store.3drobotics.com/products/3dr-pixhawk`

GPS sensor, which send in the flight commands, battery status, and GPS coordinates respectively. The outgoing data flow consists of the deployment command to the parachute launcher unit, the data to be saved to the memory card, the required current to the ECS and the signal to the plasma actuator switches to enable the different plasma actuators. The data to be saved is the entire flight data, which otherwise would be sent to the ground station, but is also saved on board to avoid an eventual loss of data in telemetry.

Finally, the telemetry is both incoming and outgoing. The input from the ground station are GPS coordinates or paths, the UAV has to fly to and the command to enter a certain flight mode. The outgoing side of this connection are mostly data about the state of the UAV: GPS coordinates, airspeed, altitude, attitude angles and rates, given power of the electrical engine and battery status.

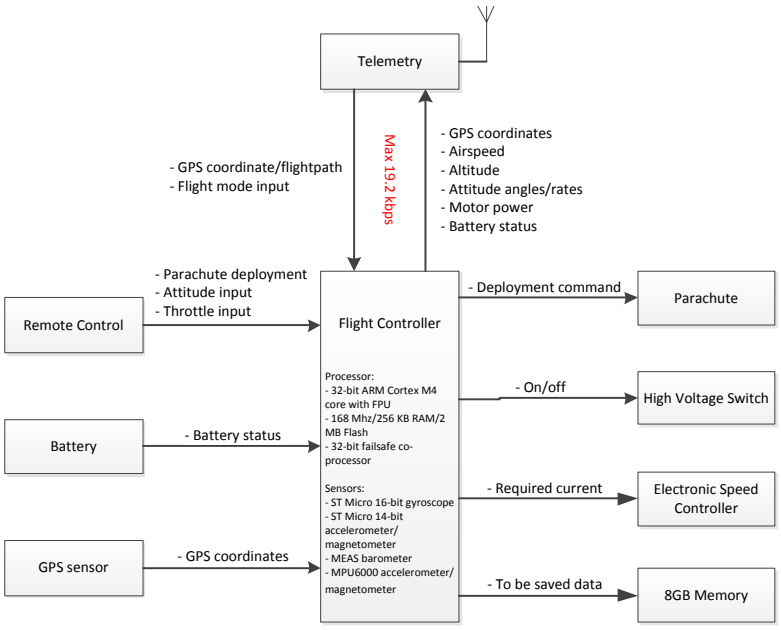

Figure 5.12: Schematic representation of the data handling

5.4 Performance Analysis

This section focuses on the analysis of the performance of the UAV. First the flight profile diagram will be discussed. Then in Section 5.4.2 the performance in different flight modes will be analysed. These are cruise, climb, turns, take-off and landing. The noise and emissions that come along with the UAV during flight will be elaborated on in Subsection 5.4.3. At last, the weight, cost and power budget will be given.

5.4.1 Flight Profile Diagram

Considering the range of 10 km, endurance of 2.0 hours, and payload mass of minimally 1.0 kg, the final product can be used for many applications. Specific applications require different mission profiles in terms of requirements for i.e. agility, loiter time and endurance. Considering this wide range of applications, the UAV has to be adapted for every single application to meet specific requirements such as being able to continuously transmit live video footage. Therefore, a collaboration could be set up in the future with an external company that can implement the mission specific payloads.

The following mission profile has been determined. As depicted in Fig. 5.13, the UAV will take-off and climb to its optimal cruise altitude. Once the UAV has reached its position of interest, it descends to the optimal altitude to perform its mission. This could be to account for the resolution of a camera, dropping its payload, being within range of a specific object, etc. After this it will climb again to an optimal cruise altitude, fly back and finally descend and land. The UAV could also climb/descend to its optimal loiter altitude, but as said, it is expected that this altitude is lower than the cruise altitude.

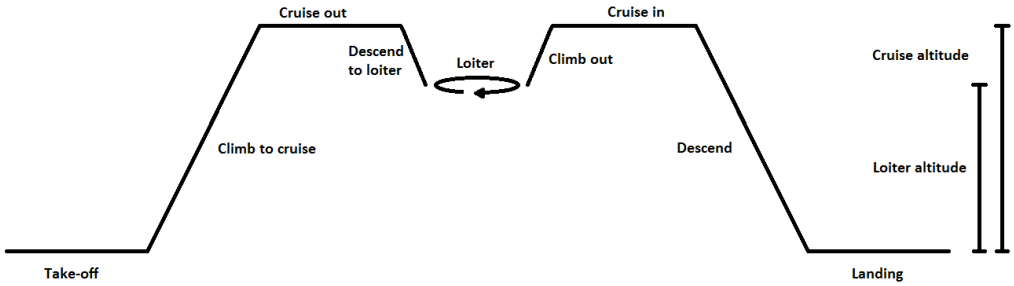

Figure 5.13: Mission profile of the plasma actuator controlled UAV

5.4.2 Flight Mechanics

For the flight mechanics, a closer look has to be taken to the different motions in flight. These are cruise, climb, turning, take-off and landing performance. The analysis will be done with help of certain diagrams, that give a schematic overview of the performance of the UAV. At the end of this section, in Table 5.5 all flight performance parameters are given for five different flight phases: stall, loiter, cruise, range and maximum speed. In addition, a summary of the required C_L and angle of attack is given.

Cruise and Climb Performance

For the climb performance of the UAV it may be assumed that it performs a steady climb. This is because the UAV will not reach very high altitudes, so the atmospheric parameters such as the density remain constant. Eq. 5.7, shows that when the density remains constant, the equivalent airspeed V_E equals the true airspeed V [57]. This means that at a constant power setting, the airspeed will remain constant as well and a constant rate of climb can be achieved.

$$V = V_E \sqrt{\frac{\rho_0}{\rho}} \tag{5.7}$$

The performance diagram as can be seen in Fig. 5.14a shows the required power curve and the available power curve. The required power P_r is the power needed to overcome the drag during flight. The available power P_a is the power that can be achieved with the thrust from the electrical motor. For the motor that is installed on the UAV, there is an available power of 180 W. As can be seen in the Fig. 5.14a, the required power is lowest when loitering. This happens at an airspeed of 12 m/s, which is the optimum speed for endurance. When decreasing or increasing this speed, the required power will have a higher value.

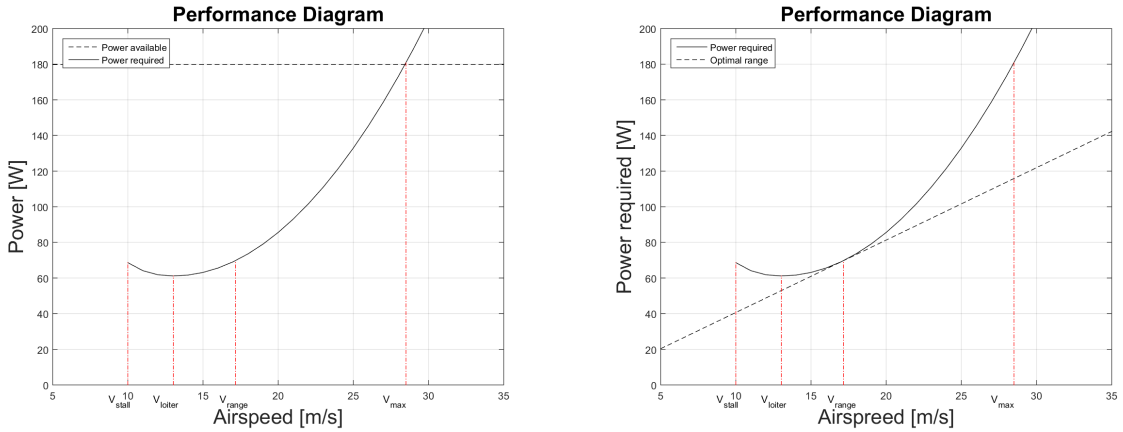

(a) Power required

(b) Optimal Range

Figure 5.14: Performance diagrams

Fig. 5.14b shows the performance diagram again. A line can be drawn from the intercept of the origin to the graph. In order to take the lowest slope, only one intersection point will be found. This is the point

where drag is minimum and where the lift over drag ratio is maximum. In other words, this is the speed at which maximum range can be achieved. This is however not the most battery efficient speed to fly at.

From this performance diagram, a climb rate diagram can be deduced. This is shown in Fig. 5.15. It shows at which airspeed the maximum rate of climb can be achieved for a steady climb performance, i.e. the minimum amount of time to perform a certain climb. According to both figures, the highest climb rate which can be achieved is 1.25 m/s. This can be achieved at loiter speed, which is 13 m/s. The climb will only be optimal when the selected airspeed for the maximum steady rate of climb is kept constant. The steady rate of climb can be calculated with Eq. 5.8.

$$RC_{steady} = \frac{P_a - P_r}{W} \tag{5.8}$$

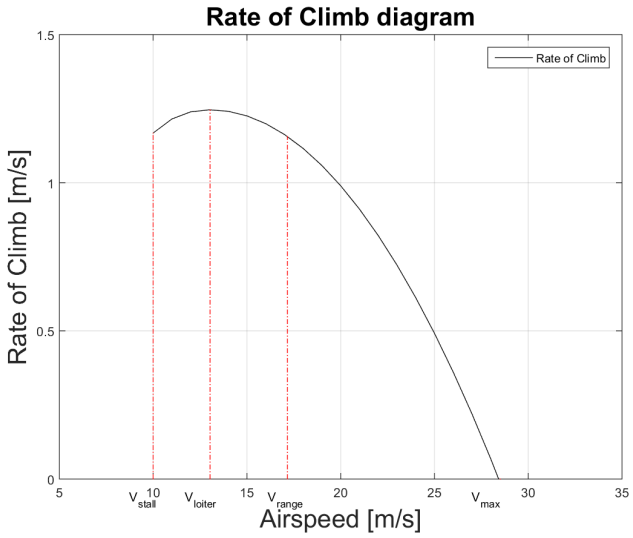

Figure 5.15: Rate of climb diagram

For each flight, a decision can be made whether to fly as long as possible (endurance) or as far as possible (range). When choosing for endurance, the optimum cruise speed is the loiter speed of 13 m/s. When the furthest range is preferred, one has to fly at the range speed, which amounts 17.2 m/s. When only a short flight will be made, in both time and distance, it is best to choose a cruise speed which lays between these two values.

Turning Performance

To determine the turning performance, one can calculate the minimum turn radius, minimum time to turn, or maximum load factor. In other words; the tightest possible turn, fastest possible turn or steepest possible turn. From Ruijgrok, the equilibrium equations for a horizontal sustained turn are as follows [57]:

$$L\sin\phi = \frac{W}{g}\frac{V^2}{R} \tag{5.9}$$

$$W = L\cos(\phi) \tag{5.10}$$

$$n = \frac{L}{W} = \frac{1}{cos\phi} \tag{5.11}$$

Since the UAV does not have to comply for the comfort of passengers or cargo, it has no restriction on the bank angle. However, a restriction is set on the bank angle to $\phi = 60°$. From this a load factor of $n = \frac{1}{\cos\phi} = 2$ follows. The previous equations can be used to determine the radius of a turn, which is described by Eq. 5.12, where n is the load factor. Using this fact and the previous equations, the minimum radius to turn can be determined using Eq. 5.16. The time to complete a turnaround, or in other words a 180° turn, can be determined using Eq. 5.13 [57].

$$R = \frac{V^2}{g\sqrt{n^2-1}} \tag{5.12}$$

$$T_{180°} = \frac{\pi R}{V} \tag{5.13}$$

The results of these two parameters are depicted in Fig. 5.16 and Fig. 5.17. For completeness the values for a bank angle of $\phi = 30°$ and $\phi = 45°$ are included. It can be seen that the graphs are quasi-linear and that, obviously, a smaller bank angle results in a larger radius and longer time to turn. Full specifications of the flight performance can be consulted in Table 5.5.

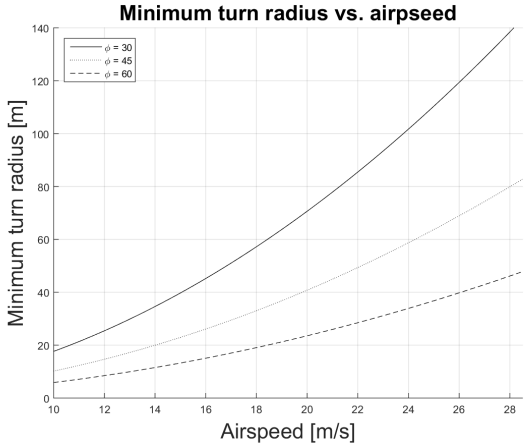

Figure 5.16: Graph of minimum turn radius

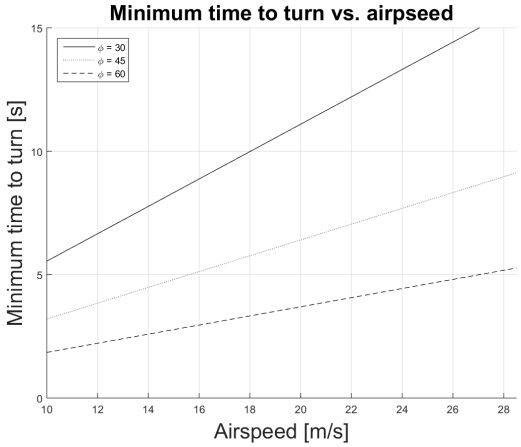

Figure 5.17: Minimum time to turn

Take-off and Landing Performance

Three different take-off methods can be distinguished. A self propelled (runway) take-off and assisted take-off, which can be differentiated into mechanically launched and hand launched. The latter can already be rejected, as the projected take-off weight of 10 kg together with a minimum take-off (stall) speed of 10 m/s ask for an increase in kinetic energy that the human body cannot put in by throwing. A self-propelled runway take-off was discarded during the initial design phase [12] as such endeavours ask for too much extra logistic effort, e.g. availability of the runway, transport to the locations and limited range due to restricted take-off locations. This leaves the assisted take-off as preferred take-off method. The requirements for a launch system are as follows:

- The launch system shall accelerate 10 kg to 20 m/s.
- The launch system shall fit in a $1 \times 1 \times 0.5$ m^3 box
- The launch system shall cost less than € 1000.
- The launch system shall be deployable within 30 minutes.

The available launch systems that provide a minimum kinetic energy increase of 2000 J, to provide for the first requirement, make use of pneumatic systems or bungees with winches. However, they prove to be rather expensive in the price range of € 10.000, which is out of range for this project[48][49]. The hobby UAV community offers some examples of homebuilt launch systems at the fraction of the price and with comparable performance. For this project, due to cost restrictions, a homebuilt system is chosen with the guidelines from a technical report [58]. This system consists of a sled on a 2 m rod under a 15° angle. The sled is attached to the fuselage body as this structure is able to transfer the maximum force endured during this acceleration of about 1000 N for the fulfilment of the first requirement. Another possibility is to put a sled-attached V-shaped peg around the wing which pushes the trailing edge during take-off. Such a peg would ensure and maintain the proper pitch attitude during take-off.

The options for landing are a parachute landing, field landing or runway landing. The parachute landing is rather cumbersome for repeated use for landing, although a parachute is on-board for emergency procedures. The runway landing implies the aforementioned logistic constraints and so the field-landing on the belly of the UAV remains as the best option. During the landing procedure, the UAV will come close to the ground, several meters above it, slow down to stall speed and pitch up using the wing tip mechanism. When an angle of attack of 14° is reached, the HLD's are activated, since they perform best at that angle of attack. This enables the UAV to slow down, to decrease the impact speed at landing. Because the high lift devices are located on the main wing, activating them will make the UAV pitch up,

[48] UAVFactory, accessed on June 11, 2015: `http://www.uavfactory.com/product/21`
[49] Eli, accessed on June 11, 2015 `http://eli.ee/products/7/uav-pneumatic-catapult`

past the optimum angle. In addition, the UAV will become uncontrollable at extreme angles of attack and therefore the HLD will have to be pulsed. In this manner, the optimum angle of attack will be maintained while also keeping control of the UAV. The front part of the fuselage, primarily designed for initial impact, will hit the ground first. This will render the tail and propeller impact free. Although the tail is able to sustain possible impact, the fuselage is preferred as it roughly houses the centre of mass, thereby lessening possible rotation on impact. Due to the ground contact the nose will pitch down and will make impact as well, after which the UAV slides to a halt. This procedure is commonly used for reference UAVs in the comparable lay-out and weight range[50]. Note that the velocity is mostly parallel to the ground surface, thereby minimizing the normal perpendicular impact force. The energy is mostly dissipated by ground friction and the fuselage belly is designed to withstand the impact.

Table 5.5: Overview of flight performance parameters

Flight phase	Stall	Loiter	Cruise	Range	Max	Unit
Airspeed	10	12	13	15	20	[m/s]
Power required	68.63	61.17	61.17	69.72	180.83	[W]
Rate of climb	1.17	1.25	1.25	1.16	0	[m/s]
Minimum radius to turn	5.89	9.99	9.95	17.13	47.80	[m]
Minimum time to turn	1.85	3.79	2.40	3.17	5.27	[s]

From the values in Table 5.5 and the overall aircraft geometry, the required lift coefficient for every flight phase can be determined. In addition, using the airfoil polars in Section 4.3.1, the required UAV angle of attack can be found. These two values are summarized for all flight phases in Table 5.6. In this table, the angle of attack values for landing and take-off are also added for completeness.

Table 5.6: Operating angle of attack for different flight phases

Flight Phase	C_L	Angle of Attack
Take-Off (Launcher)	[-]	15°
Stall	1.37	9°
Loiter	0.86	2°
Cruise	0.9	2°
Range	0.47	-2°
Maximum	0.17	-7°
Landing	[-]	14°

5.4.3 Noise and Emissions

In this section the noise emissions of the propeller of the UAV are quantified. For the noise, the sound pressure level (SPL) of both the propeller and the plasma actuators are taken in to account. Hereafter, the emission of ozone due to the plasma actuator will be discussed as well.

Noise of Propeller

The noise the UAV will produce consists of two main components: the propeller and the plasma actuators. The induced noise due to the airflow and turbulence is considered to be negligible because of the low airspeed.

Propeller noise is a subject that is still difficult to account for due to the large amount of uncertainties[51]. According to Lothar Bertsch, PhD. of the Deutsches Zentrum für Luft- und Raumfahrt (DLR), it is not really possible to make a guesstimate of the noise of our UAV. The models in his knowledge would not work for our configuration and specifications. This is mostly due to the fact that the velocity and thrust force values do not come near the range of these empirical models. Furthermore, he mentioned that these models cannot be scaled or extrapolated to our values[52].

[50] MiniFalcon Tactical UAV Landing, accessed on June 11, 2015 `http://www.innoconltd.com/?CategoryID=180&ArticleID=105`

[51] Personal communication with Mirjam Snellen, PhD. Associate professor aircraft acoustics, TU Delft, June 4, 2015

[52] Personal communication via e-mail with Lothar Bertsch, Research engineer at DLR, June 8, 2015

One of these models is the following empirical model. According to Ruijgrok, the noise a propeller makes can be calculated with the empirical formula in Eq. 5.15, in which N_{blades} is the number of blades per propeller, N_{prop} is the number of used propellers and r the distance from the sound source. M_t is the Rotational Tip Mach number which is defined in Eq. 5.14 [59].

$$M_t = \frac{\pi D_{prop} \omega}{60 \cdot a} \tag{5.14}$$

$$SPL = 83.4 + 15.3 \log P_{br} - 20 \log D_{prop} + 38.5 M_t - 3(N_{blades} - 2) + 10 \log N_{prop} - 20 \log r \tag{5.15}$$

The formula yields a noise level of 91.80 dB at maximum power and 75.32 dB at loiter configuration. These are feasible sound values, but slightly high for a small UAV and small propeller. These two values come across to a heavy truck/bulldozer at 15 m and a regular car at 15 m respectively[53].

It has to be mentioned that this formula has been determined, and published in the year 1977, by the Society of Automotive Engineers [60]. At this time UAVs did not exist and it can be stated that this specific formula cannot account for small (carbon) propellers rotating at high rpm. This train of thought makes sense according to Michael Arntzen, R&D engineer at the DLR and assistant professor at the ANCE group of the TU Delft. Due to the size, altitude and weight of the UAV and the atmospheric absorption, the noise should not be of any problem[54]. Bertsch agrees with this: for such a small vehicle and its specifications, the noise of the propeller should not be considered as a problem at all. Especially if the UAV would be operated in urban areas, because there are too many other sources that produce significant more noise which would therefore 'mask' the noise of the UAV. Bertsch therefore expects that the UAV is able to be operated more or less unnoticed by third parties[52].

If not, some alterations could be made to decrease the propeller noise. Bertsch advises to select another rotor design such as a low-noise design, sweep the blade edges, use no blunt trailing edges or select a larger propulsion system than required but operate it with lower rpm. Shielding effects of the propeller, however, can be neglected to reduce the produced noise, because the engine is placed at the back of the fuselage [61]. Finally, a pusher engine produces more noise in general because of the turbulent and disturbed inflowing air. The boundary layer of the fuselage, the wake of the wing and the wake of high-lift elements might all directly or indirectly impinge on the propeller. This generates interaction noise[52]. The interaction of the fuselage and wing on the propeller cannot be evaded, but considering all this, the noise of the propeller is expected to not to have a significant contribution on the acoustic footprint the UAV leaves.

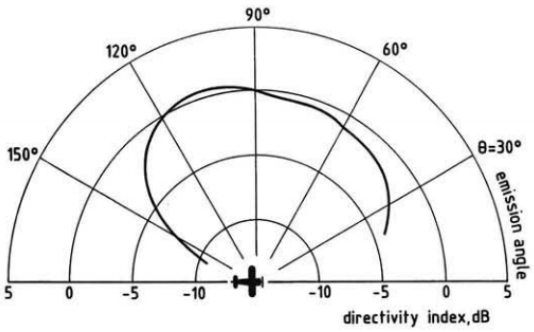

Figure 5.18: Directivity index of propeller produced noise [59]

The maximum noise that the propeller will produce occurs at an estimated emission angle of about $\theta = 105°$. This maximum SPL is slightly higher than its average. This method assumes though that the directivity pattern is independent of the type of aircraft and flight and engine condition [59].

Noise of Plasma

The plasma actuators also produce a fairly significant amount of noise, compared to other UAV components. During the wind-tunnel test that was performed during the project, no noise measurements were

[53] Media Power Pro, Licht - Beeld - Geluid, accessed on June 15, 2015: `http://lichtbeeldgeluid.nl/geluid/akoestiek/hoe-hard-klinkt-een-decibel/`

[54] Personal communication with Michael Arntzen, R&D engineer at NLR and Assistant professor ANCE, June 10, 2015

made. The plasma actuators were still heard though, and using a reference chart[55] the plasma actuator noise production is estimated to be round 85 dB at a distance of around 2 m. When combined with the maximum engine noise, the maximum total UAV noise is estimated to be around 94 dB. The UAVs similar to the plasma UAV produce around 105 dB at about 2 m [62]. From this, it can be concluded that the proposed UAV design does not produce more noise than similar UAVs.

Emissions

Another requirement is that the emissions shall be equal or lower than similar UAVs. The fact that the plasma UAV uses batteries instead of fuel as energy source means that no carbon dioxide is produced directly. Indirectly, the electrical energy production might have used fossil fuels. A more important pollutant to consider is the ozone that is produced at the dielectric barrier discharge surface. Ground level ozone is hazardous because it is strongly oxidizing, very toxic and corrosive. Therefore, the European directive [63] set the information threshold at 180 $\mu g/m^3$ ozone in ambient air. Hong et al. studied the ozone production rate of a plasma actuator under experimental conditions similar to that of the mission profile [64]. The production rate was 21 g/kWh, which is less than produced by an industrial ionizer, but not negligible.

If the plasma actuators need 100 W for 1 h, 2.1 g of ozone is produced. To avoid exceeding the threshold, this should be diluted in 12×10^3 m^3 air. Also, 590 μg is emitted per second, in which the UAV travels 10 m, considering the stall speed. The lifetime of ozone is about 20 days, so flying in unventilated areas is not advised.

5.4.4 Mass, Cost and Power Budget

In the following section the budget breakdown of the mass, power and costs are depicted in the respective tables.

Mass Budget

Table 5.7[56] shows the general budget allocation of the masses. During the preliminary design phase, an estimation had been made for the mass budget. In this preliminary estimation, the following was guesstimated: a payload weight of 1 kg, a battery weight of 1 kg, 4 kg for all systems and structural components. Furthermore a contingency of 2 kg was taken into account.

Now, the design has become more detailed and the exact masses of the components that are going to be used, can be used in the mass budget breakdown. Since this is the mass breakdown of the final design, a contingency of 15% of the estimates MTOW of the preliminary design has been used, which equals 0.15 kg. The contingency is to account for the weight which inevitably is added during production, or the dirt and moisture that accumulates during operations. Furthermore, an estimation was made for the weight of the pitot tube and wiring, as these could not be retrieved.

Power Budget

In Table 5.8 the power budget allocation is shown. The estimated electrical power consumptions were multiplied with the time in which they are deployed to obtain the energy consumed, which is used to size the battery. As described in Section 4.1.2 a 40% contingency was introduced to provide for a margin of safety.

[55] What is noise? Accessed on June 12, 2015: `noiselimiters.co.uk`

[56] Hobby King, accessed on June 15, 2015: `http://www.hobbyking.com/hobbyking/store/__41608__FrSky_X8R_8_16Ch_S_BUS_ACCST_Telemetry_Receiver_W_Smart_Port.html`

Table 5.7: Mass budget allocation

Description	Component	Weight [kg]
Structure	Fuselage	0.63
	Wing	2.3762
	Booms	0.1767
	Horizontal tail	0.3443
	Vertical tails	0.2952
Propulsion	Electrical motor	0.0660
	Propeller	0.0157
	Electronic Speed Controller	0.0140
UAV Systems	Flight controller	0.0380
	GPS Module	0.0168
	Pitot tube	0.0100
	Parachute	0.4170
	Transceiver (RF Module)	0.0060
	Antenna	0.0454
	Remote Control Receiver	0.0168
	Plasma actuators	0.3500
	Wiring	0.425
Power	Battery	1.7640
	High-voltage pulse generator and transformers	1.5250
Empty weight		8.81
Payload weight		1.0000
Contingency (15%)		0.150
Maximum Take-Off Weight		9.96

Table 5.8: Power budget

	P_electrical [W]	Time [s]	Energy [Wh]
Climb (propulsion)	242.22	300	20
Loiter (propulsion)	78.47	7200	157
Flight controller	2.5	7500	5
Camera (potential)	2.9	7500	6
Plasma actuators	22.25	7500	46
Subtotal			235
Contingency (40%)			94
Total			329
Peak power	405		
Average power	107.0		

Cost Budget

A requirement of this design project is that it should not exceed € 10.000 including engineering, production of two prototypes and 30 hours of test flights. During preliminary designing, no detailed design choices had been made, so not much could be said about the configuration, used materials, propulsive system, etc. Now, that specific components and materials have been chosen, the actual costs can be determined for the design. These costs can be consulted in Table 5.9. Within this cost budget it is accounted for the fact that certain items required for production (i.e. vacuum pump, safety goggles, etc.) can be provided by the TU Delft facilities or another sponsor company. The prices in the table below are in Euro. A Dollar to Euro conversion rate of 0.89[57] and a Pound to Euro conversion rate of 1.38[58] were used.

[57] Currency value on June 16, 2015
[58] Currency value on June 16, 2015

Table 5.9: Cost budget allocation

Description	Components	Costs [€]
UAV Systems	Electrical motor	102.26
	Propeller	49.61
	Electronic Speed Controller	32.00
	Antenna	26.70
	Transceiver (RF Module)	138.84
	Remote control and Receiver	209.15
	Pitot tube	97.88
	GPS module	190.18
	Parachute	958.00
	Flight controller	355.98
	Full-Bridge board	980.00
	Plasma actuators	89.00
Power	Transformer (ignition coils)	597.96
	Battery	341.52
Structure	Materials and Production (Sec. 5.2)	5,216.01
Payload	Payload	variable
Total		9,355.09

5.5 Risk

This section discusses the possible risks that may be encountered after the design phase has been completed of the plasma controlled UAV. This means that the events may all occur during the operational phase of the UAV, i.e. during flight. The risk analysis that applies to the design phase of the UAV can be found in the MTR [12]. There are two ways to increase the reliability of a UAV [65]:

1. Fault Tolerance
2. Fault Avoidance

Using hardware redundancy, fault tolerance can be achieved. This means that multiple hardware devices are used in order to tolerate the failure when it occurs. Examples of these are duplicated data links, propulsion and flight controls. However, hardware redundancy is not easily added for small UAVs, since it takes up additional space, requires more power and adds to the weight. For small UAVs, fault avoidance is therefore a better approach. Approximately 80% of the UAV failures are a consequence of a fail in the propulsion control system, flight control system or due to human factors [66]. Fault avoidance can therefore be accomplished by improving the reliability of these three components. A risk analysis and a according risk map may show the events that are the most critical for avoidance.

5.5.1 Risk Analysis

The first step of the risk analysis is to identify and list the events. The likelihood of occurring is scaled in three categories: low, possible and probable. Then, the likelihood of occurring is evaluated and the severity of consequence for each event which is also scaled in three categories: negligible, moderate and severe consequence. For each of the seven items in the following list of events, a brief argumentation is given on their risk evaluation:

1. The UAV encounters problems with the flight controller.
A flight controller can be seen as the nerve centre of the UAV; it makes sure that the UAV can be flown exactly the way the user wants. The input for the flight controller is either done by a manual remote controller, or by pre-programming the UAV and let it fly over certain way-points. However, if this flight controller experiences problems, the UAV will not be able the perform a controlled flight. Flight controller failures are one of the three that account for 80% of all UAV failures [66], so the likelihood is probable. Also, the UAV will not be able to fly as wished by the user, and it might have to be replaced for a new flight, so the consequence is considered to be severe.

2. The UAV has an empty battery.
The plasma controlled UAV is electrically propelled. This means that in case of an empty battery, the battery will not provide a high enough voltage in order to propel the UAV. The consequence of an empty

battery is moderate: the flight cannot be continued though a parachute landing can be made. Also, the battery just has to be replaced by a charged one (or the one on board has to be charged) and it is ready for a new flight. The likelihood of this event is probable. An endurance of 2 hours might be long for a small UAV, though it can be reached rather easily, especially when performing multiple short flights.

3. The UAV flies out of the telemetry range.

In order to have the two way telemetry, there should be a data-link between the UAV and the manual remote controller on the ground. However, when the UAV flies out of the 16 km telemetry range, the data-link will be gone. This way, it is not possible to fly the UAV via a manual controller. Only a pre-programmed flight path with e.g. way-points can be flown when out of the telemetry range. Since the UAV will still be able to fly and the UAV does not have to land in order to replace a system or component, the consequence is negligible. The likelihood that the UAV flies out of the 16 km telemetry range is possible.

4. The UAV encounters a structural failure.

Any damage or failure to the structure (cracked foam or de-lamination) of the UAV affect the flight performance of the UAV by compromising its structural integrity. Even though the configuration is rather robust, structural failures can always occur due to e.g. fatigue, bad manufacturing or environmental impacts such as bird strikes or landings gone wrong. If the failure is such that it cannot fly as preferred, the consequence is severe. It involves repair, which delays new flights and increases costs. The likelihood of such an impact is considered to be low, because the moving parts which are normally most critical to damage are not applicable in this plasma controlled UAV.

5. The UAV encounters a plasma actuator failure.

The UAV will be controlled by means of plasma actuators integrated on the wing and the empennage. The dielectric barrier between the two electrodes can burn out if e.g. the voltage is too high. Also, when not installed correctly to the wing, the strip of plasma actuators might not stay attach during flight and therefore be useless. This will lead to an uncontrollable UAV, which might be dangerous. The consequence of this event is therefore severe, also because it will be unable to use for flight as long as the plasma actuators will not be repaired. The likelihood however is low, since the amount of voltage is tested under which no burn outs occur. Also the actuators have been made before so the way of constructing these is familiar.

6. Human factors influence the flight performance of the UAV negatively.

Human factors apply to the person using the manual controller. These factors might be fatigue, inadequate training, misjudgements or excessive workload. The consequence of human influences is moderate; the UAV will still be able to use one of its fail safe procedures as explained in Section 5.3. As mentioned before, human factors have a large contribution to UAV failures. The likelihood is therefore considered as probable.

7. The manual controller does not have enough battery power to work.

As mentioned before, the manual remote controller gives data input to the flight control computer on board of the UAV. If the battery of this controller is low of power, it will not be able to send any data and have a data-link with the UAV. The UAV will still be able to fly, however it will not react to any inputs on the manual controller. The consequence is therefore assumed to be negligible. The likelihood of this event is considered possible, since the user might forget to charge the batteries of the controller or replace them.

The risk for each event is equal to the product of the likelihood of probability of occurring and the severity of consequence. The risk can then be plotted in a risk map with the likelihood of event on the $x-$axis and the consequence of event on the $y-$axis, as shown in the risk-map in Fig. 5.19.

Consequence of event				
	Severe	4, 5		1
	Moderate			2, 6
	Negligible		3, 7	
		Low	Possible	Probable
		Likelihood of occuring		

Figure 5.19: Risk map of the UAV during operation

5.5.2 Risk Mitigation

Events in top right of the risk map (Fig. 5.19) pose the highest threat in accomplishing the objective. In order to most effectively reduce risk, resources should be used to mitigate the risk of these events. The mitigation can be achieved by either decreasing the probability of occurring (fault avoidance) of the event or diminishing the severity of the consequence (fault tolerance). For the most critical risks an approach for mitigation is given in this subsection.

1. The UAV encounters problems with the flight controller

Mitigating the risk of a flight controller that does not work could be handled in two ways. The problem is probably not that it actually breaks downs, but just that it doesn't function in the way it should. Fault tolerance would lead to an extra flight controller, though this does not mean that the other controller does function in the way the user wants. Therefore, fault avoidance is a better way of risk mitigation for this event. Repeatedly service and maintenance will lower the likelihood of the event to occur and therefore minimize the risk.

2. The UAV has empty batteries.

The batteries take up a large part of the UAV and because of constraints to both weight and space in the fuselage it is not a suitable option to just double the batteries on board. Fault avoidance can easily be achieved by making sure that the batteries is always fully powered before taking off. This can be done by charging the battery before the flight and by having a second set of charged batteries at the ground station.

6. Human factors influence the flight performance of the UAV negatively.

Human factors might influence the flight performance of the UAV in a negative way, though the factors are very diverse. It is not possible to achieve any fault tolerance or avoidance that takes out all risk that it might account for. However, it is possible to take away some of them such as via the manual controller. By making it user friendly and easily controllable, the UAV is less prone to human error. Also, in order to avoid faults the user can be trained to fly the UAV.

5.5.3 Fail Safe Modes

For the UAV, two fail safe modes are available. The first is a landing with a parachute. As mentioned in Section 4.1.3, a Skycat X68 Series, all-in-one package is installed in the fuselage. It is tethered on the centre of gravity, in order to obtain a vertical landing when unfolding the parachute. In this way the landing causes minimal damage when hitting the ground. When the parachute unfolds, the propeller stops directly in order to prevent the parachute wires and straps to get tangled into the propeller. A parachute landing should only be used in emergencies, so when the UAV is not able to fly anymore. This might be caused by a structural failure, a failure in the plasma actuators or a lack of battery power, resulting a loss of propulsion.

The second safe mode makes the UAV fly back into the telemetry zone (Home), which is at the location where the last data link had been made. This mode should be pre-programmed in the autopilot, which means that when starting this mode it is not possible to use the manual remote controller anymore. It is therefore a good option to use when the UAV is out of the telemetry range or when the manual controller either lacks of battery power or breaks down. Also, when encompassing failures to the parachute and its mechanism, this is the only safe mode that works in order to make a safe landing. Table 5.10 gives a summary and shows what safe mode can be used best per event.

Table 5.10: Fail safe modes for each event

Event	Description	Fail Safe Mode
1	The UAV encounters problems with the flight controller	Parachute
2	The UAV has an empty battery	Return Home
3	The UAV flies out of the telemetry range	Return Home
4	The UAV encounters a structural failure	Parachute / Return Home
5	The UAV encounters a plasma actuator failure	Parachute
6	Human factors influence the flight performance of the UAV negatively	Parachute
7	The manual controller does not have enough battery power to work	Parachute

Chapter 6 - Conclusion and Discussion

The final chapter of the report discusses the conclusions that can be drawn from the current design and a discussion of these conclusions. This discussion is then combined with other experiences from the design process to make some recommendations for future work on the plasma UAV prototype. Finally, this chapter contains a critical reflection on the purpose of this project, and it is discussed whether plasma control will ever become the new standard for small UAV control.

6.1 Conclusion

This report presents the result of a 10 week design exercise of a plasma controlled UAV. Research has shown that the implementation of plasma actuators in small UAV's has a lot of potential, but before this can be implemented on a large scale a proof of concept is needed.

The aim of this project was therefore to implement plasma control on a UAV. In the 10 week design project, a UAV that used plasma actuators for control, was to be designed by 10 students. The control performance of the vehicle was however not supposed to suffer from this novel type of control. In addition, the wing span could not be more than 3.0 meters and the UAV was supposed to fly for 2.0 hours and have a range of 10 km, all while carrying a 1.0 kg payload.

The result is a 9.96 kg, electrically propelled UAV. It contains a large battery to comply with the endurance and range requirements and a high voltage generator in the fuselage for the plasma actuation mechanisms. The configuration of the UAV is a high-wing with an H-tail and an elevator mounted on top of the vertical tail. The wing has a span of 3 meters and consists of two different airfoils. The NACA63A-915 is a thick cambered airfoil used on the inner section of the wing, ideal to achieve high lift coefficients. At the tips, the symmetrical airfoil NACA64A-015 is used, which is the most optimal for the integration of the plasma actuators. This symmetrical airfoil is used for the entire empennage as well.

Control of the UAV is done fully with plasma actuators, integrated on both the wing and empennage. There are three different flow control mechanisms that are used to roll, pitch and yaw the aircraft. In order to quantify two of these control mechanisms, a windtunnel test was conducted during the project. By combining the results of this windtunnel test with literature on plasma actuator performance, the plasma control forces were known and the control rates of the aircraft were calculated. These control rates were found to be comparable to those of similar UAVs with conventional control surfaces, as fulfilling another top level requirement. The UAV will take-off with a launcher and land with a belly landing. It also contains a parachute in the fuselage for emergency landings, in case the signal is lost or the power system fails. The UAV can be flown with a remote controller or an autopilot with two-way telemetry.

To be able to actually fly the UAV during testing, the standard UAV flight control systems had to be adapted for plasma control. First of all, a high voltage system is implemented, to supply the plasma actuators with the potential difference required to generate plasma. This can be achieved using a full high voltage AC system, however this solution requires the usage of high-voltage switches. This made the design too heavy to fly, and reducing the weight of the high-voltage system proved to be one of the biggest challenges of the project. Eventually, it was decided to use automotive ignition coils to generate a high voltage, with a full bridge-board converting the DC battery signal to an AC signal. In this configuration lightweight low voltage switches can be used, more than halving the weight of the high-voltage system.

Secondly, the flight controller had to be adapted for plasma control. In conventional UAVs the response of a UAV to control inputs is linearly related to the deflection of a control surface. This is rather desirable, since then the magnitude of the control input is variable. Since plasma actuators can only be on or off, the flight controller had to be adapted to keep this linear relationship between control inputs and aircraft attitude. This was achieved by changing the duty cycle of the plasma as a function of the desired control input; for a small attitude change a short duty cycle was used, for a large change a long duty cycle was used. To be able to roll, pitch, yaw and use HLDs, in total 7 different control outputs are required.

Combining this with the four control outputs the rest of the flight system requires, a flight controller with 14 control outputs was selected. All inputs to the flight controller are given by two gyroscopes, a barometer, a magnetometer, a GPS receiver and a pitot tube.

To carry all the loads during flight, a custom composite structure was designed for the UAV. After careful considerations it was opted to make the wings and empennage out of ultra-light TeXtreme®, with a foam airfoil core. The fuselage is made of carbon with an impact-resistant foam inside and the tail booms are made of hollow carbon rods. Even though this material is quite expensive, the weight savings are worth it. The performance of the aircraft was also assessed, to aid in the selection of suitable missions for the UAV and to explore a flight envelope. The engine proved to be strong enough to achieve the desired climb rate, while also being able to turn quickly and in with a small turn radius. After a stability analysis it was also found that the design is stable in all modes, so no control inconveniences will occur while operating within the flight envelope.

Finally a risk analysis was performed, and it was found that most of the possible risks during flight are covered by the design. The presence of the emergency parachute played a large role in this, in case any critical system fails this parachute will prevent the UAV from crashing uncontrollably. Concerning the environmental impact of the UAV, it was found that it is quieter than its competitors. Since the aircraft uses an electric propulsion system the only emissions of the UAV are due to the plasma actuators. When operative, a rather large quantity of ozone is produced, and therefore it is advised to operate the UAV only in well-ventilated areas. Because no harmful materials are used and the propulsion system is very eco-friendly, the design is still considered to be sustainable.

6.2 Discussion and Recommendations

In this section the findings of the conclusion are discussed, together with some of the design choices that were made in the past 10 weeks. Several recommendations for future work follow from these discussions, and schedule for the implementation of these recommendations is made. In addition, the designed UAV is compared to competitor aircraft, to assess how realistic the large-scale implementation of plasma control on small UAVs is.

First of all, during the configuration trade-off it was decided to use a twin-boom mounted 'pi-tail' because the booms would protect the engine blades from possible impacts and the engine could be positioned such that its ground clearance is sufficient. Secondly, it was thought that placing the engine in the back would be favourable with respect to the centre of mass of the aircraft, aiding in the stability and controllability of the aircraft. During the system design it was however found that the engine mass is negligible compared to the rest of the components, especially since it is separated from the battery. The engine-arguments in the trade-off can therefore be given a lower weight, and perhaps a different airframe configuration will be selected as optimal. There are of course also other reasons behind choosing the current configuration, so to thoroughly explore this recommendation a separate design recommendation is needed.

At the end of the design phase with the current configuration, the final mass of the UAV is 9.96 kg, which is a little heavier than the 9.7 kg used in the design iterations. This weight increase is mainly due to a contingency factor that was added for the manufacturing process and estimations of some component weights. Since the increase in weight is only 260 grams, and there are still some small uncertainties in the weight estimations, it is expected that the analysis conducted for the 9.7 kg UAV is still valid. The engine is powerful enough to propel the aircraft and the body moments of inertia and the control rates, which will not change significantly. Only after weighing the produced prototype a proper assessment of the 9.7 kg analysis can be made, but for now it is expected that no problems will occur.

As for the plasma actuator performance, it could be investigated if it is worthwhile to use plexiglass instead of Kapton tape for the DBD plasma actuator. Although this will consume a little bit more power, the durability of plexiglass is higher than that of Kapton tape. The Kapton tape is stuck onto the wing and needs to be replaced after 60 hours of usage, whereas the plexiglass variant can be integrated in the wing which could very slightly decrease drag but increase production complexity. To be able to better asses the different control mechanisms that can be used for plasma control, more extensive windtunnel test could be performed. The novel wing-tip mechanism has for example never been quantified, and the test that were performed resulted in 2D test results. For a comprehensive understanding also of the (electromagnetic) interaction between multiple mechanisms, the full 3D wing model will have to be tested and analysed. This is one of the main points of improvement for a future design.

Concerning the structural design process, the most can be gained in the structural optimization of material thickness. With the current level of knowledge on the structural behaviour of composites it was not possible to thoroughly explore all load cases and fail modes, and therefore no precise quantification of stresses was possible. To ensure that the design would not fail during test flights, it was decided to use the same amount of carbon fibre over the entire wing. The loads in the tip are much lower than the loads in the root however, and using more advanced structural modelling and a longer duration can be used to design the structure on the limit of failure. This will result in a lower weight structure, which will benefit the overall performance of the UAV. As for the fuselage, an aerodynamic modelling program such as VSAERO could be used to give the fuselage structure a more aerodynamic shape. The current project did not facilitate the use of this software, and therefore some compromises had to be made regarding the aerodynamic performance of the fuselage.

Finally, as can be seen in Section 5.4.4, the cost of two two flying design prototypes is very close to the requirement of € 10.000. This is mostly due to the usage of expensive structural materials. If the cost requirement for the UAV turns out to be more critical, the improved structural design of the UAV could be used to reduce production cost or in case heavier (but cheaper) materials are used a new constraint analysis will have to be performed. Depending on customer requirements, a new design iteration might therefore be needed to come up with a design that can be produced at a lower price.

To then test the validity of the overall design, several test flights will have to be performed. During these test the expected performance of the UAV can be performed with the actual performance, which can aid in the design of a future design. In addition, the validity of the hypothetical 3D wing test can be checked during the flight tests, since the windtunnel environment does not fully represent a flight environment. The stability and controllability can also only be assessed properly during a test-flight, and the data from these stability and control tests will be vital for a redesign.

To implement all these recommendations and improvements, a schedule was made for after the DSE time-period. The time-wise arrangement for this second iteration is depicted in Fig. 6.1 in the form of a Gantt-chart. As can be seen from the picture, it is estimated that a total of 46 days is needed. This is mostly taken up by the production and the testing of the design. Another component which takes relatively long is the programming of the flight controller, since it requires quite a bit of adaptations.

Figure 6.1: Gantt chart of post-DSE work

With the design of the UAV complete, the larger scope of the project is considered. At the start of the project, the aim was to give a proof of concept of plasma technology as a means of flight control. In theory the benefits of the plasma actuators were plenty, and it had to be investigated how these benefits translate to real life. During the design process of the UAV, it was found that the implementation of plasma control brings quite some complications with it, some of which were quite severe. The weight of the high-voltage system was for example higher than expected, and as mentioned in Section 5.3 the flight controller required serious modifications. Upon completion of the design it was found that the control rates achieved by the plasma actuators were actually up to par, however sustained flight with plasma actuators will be quite challenging and requires very complicated autopilot software. There is for example no such thing as a trim tab on plasma actuators, and the current prototype uses quite a sophisticated landing procedure. The benefits that plasma actuators bring to the table in theory do translate to practice however, and the fact that the control rates are similar to competitor UAVs is very promising.

If some slight advantages in technology are made, especially high-voltage system technology, the benefits will most definitely outweigh the downsides of plasma control. The issues regarding flight controller software can be solved if enough time is spent on them and several design iterations can be performed to cope with the high-voltage system weight. It is therefore concluded that plasma control is definitely feasible on a commercial scale in the future, and further plasma actuator research on flying models is highly suggested.

Reference List

[1] C. Enloe, T. McLaughlin, R. VanDyken, and K. Kachner, "Mechanisms and Responses of a Single Dielectric Barrier Plasma Actuator: Geometric Effects," *AIAA Journal*, vol. 42, no. 3, pp. 595–604, Mar. 2004.

[2] T. C. Corke, M. L. Post, and D. M. Orlov, "Single dielectric barrier discharge plasma enhanced aerodynamics: physics, modeling and applications," *Experimental Fluids*, vol. 46, pp. 1–26, 2009.

[3] D. Greenblatt, C.Y.Schule, D. Romann, and C.O.Paschereit, "Dieletric Barrier Discharge Flow Control at Very Low Flight Reynolds Numbers," *AIAA Journal*, vol. 46, no. 6, pp. 1528–1541, Jun. 2008.

[4] S. Grundmann and C. Tropea, "Experimental damping of boundary-layer oscillations using DBD plasma actuators," *International Journal of Heat and Fluid Flow*, vol. 30, pp. 394–402, Apr. 2009.

[5] I. Gursul, E. Vardaki, P.Margaris, and Z.Wang, "Control of Wing Vortices," in *Active Flow Control. Papers contributed to the Conference Active Flow Control 2006*, E. Hirschel, W. Schröder, K. Fujii, W. Haase, B. van Leer, M. Leschzinger, M. Pandolfi, J. Periaux, A. Rizzi, B. Roux, and Y. Shokin, Eds., vol. 95, Springer, 2006, pp. 137–151.

[6] E. Moreau, "Airflow control by non-thermal plasma actuators," *Journal of Physics D: Applied Physics*, vol. 40, pp. 605–636, 2007.

[7] S. Walker and T. Segawa, "Mitigation of flow separation using DBD plasma actuators on airfoils: A tool for more efficient windturbine operation," *Renewable Energy*, vol. 42, pp. 105–110, 2012.

[8] P. Zhang, B. Yan, A. Liu, and J. Wang, "Numerical Simulation on Plasma Circulation Control Airfoil," *AIAA Journal*, vol. 48, no. 10, pp. 2213–2226, Oct. 2010.

[9] N. Benard, J. Jolibois, and E. Moreau, "Lift and drag performances of an axisymmetric airfoil controlled by plasma actuator," *Journal of Electrostatics*, vol. 67, pp. 133–139, 2009.

[10] R. C. Nelson, T. C. Corke, C. He, H. Otham, T. Matsuno, M. P. Patel, and T. Terry, "Modification of the Flow Structure over a UAV Wing for Roll Control," in *45th AIAA Aerospace Sciences Meeting and Exhibit*, AIAA, Reno, Nevada, Jan. 2007.

[11] A. Seifert, S. David, I. Fono, O. Stalnov, and I. Dayan, "Roll Control via Active Flow Control: From Concept to Flight," *Journal of Aircraft*, vol. 47, no. 3, pp. 864–874, May 2010.

[12] E. Algera, Y. Bauer, A. van Hauwermeiren, V. van 't Laar, E. Pronk, T. Roos, K. Saß, V. Sonneveld, N. Waars, and S. Wang, "Mid-Term Report - Plasma UAV," Delft University of Technology, Tech. Rep., 2015.

[13] M. Kotsonis, R. Pul, and L. Veldhuis, "Influence of circulation on a rounded-trailing-edge airfoil using plasma actuators," *Experimental Fluids*, vol. 55, no. 1772, 2014.

[14] D. H. Neuhart and J. Odis C. Pendergraft, "A Water Tunnel Study of Gurney Flaps," *NASA Technical Memorandum 4071*, p. 7, Nov. 1988.

[15] P. Zhang, A. Liu, and J. Wang, "Aerodynamic Modification of a NACA 0012 Airfoil by Trailing-Edge Plasma Gurney Flap," *AIAA Journal*, vol. 47, no. 10, pp. 2467–2474, Oct. 2009.

[16] J. Anderson, *Fundamentals of Aerodynamics*, 4th. McGraw-Hill, 2007.

[17] Inspectie Leefomgeving en Transport, *Informatiebulletin lichte onbemande luchtvaartuigen UAS - unmanned aircraft systems*, Ministerie van Infrastructuur en Milieu, Jan. 2015.

[18] E. Gill, *AE3211-I Systems Engineering and Aerospace Design Lecture 2*, PowerPoint Presentation, Feb. 2013.

[19] J. Meyer, F. D. Plessis, and W. Clarke, *Design Considerations for Long Endurance Unmanned Aerial Vehicles*. InTech, 2009.

[20] H. Veerman, "Preliminary multi-mission UAS Design," Master's thesis, Delft Unviersity of Technology, Aug. 2012.

[21] R. C. Agrawal and G. P. Pandey, "Solid polymer electrolytes: materials designing and all-solid-state battery applications: an overview," *Journal of Physics D: Applied Sciences*, vol. 41, no. 22, 2008.

[22] J. Bates, N. Dudney, B. Neudecker, A. Ueda, and C. Evans, "Thin-film lithium and lithium-ion batteries," *Solid State Ionics*, vol. 135, 2000.

[23] T.C.Corke, *Design of Aircraft*, 1st ed. Prentice Hall, 2003.

[24] E. Torenbeek, *Synthesis of Subsonic Airplane Design*. Delft University Press, 1999.

[25] G. J. Alam, M. Mamun, and A. S. Islam, "Improved Aerodynamic Characteristics of Aerofoil Shaped Fuselage than that of the Conventional Cylindrical Shaped Fuselage," *International Journal of Scientific & Engineering Research*, vol. 4, no. 1, Jan. 2013.
[26] T.C.Corke, C.He, and M. Patel, "Plasma Flaps and Slats; An Application of Weakly Ionized Plasma Actuators," in *2nd AIAA Flow Control Conference*, AIAA, Portland, OR, 2004.
[27] R. Whalley and K. Choi, "The starting vortex in quiescient air induced by dielectric-barrier-discharge plasma," *Journal of Fluid Mechanics*, vol. 703, pp. 192–203, Jun. 2012.
[28] T. Brooks, M. Marcoli, and D. Pope, "Airfoil trailing edge flow measurements and comparison with theory, incorporating open wind tunnel corrections," *AIAA Paper*, 1984.
[29] D. Raymer, *Aircraft Design: A Conceptual Approach*. AIAA, 1992.
[30] M.Sadraey, *Aircraft Performance Analysis*. VDM Verlag Dr. Muller, 2009.
[31] J. Mulder, W. van Staveren, J. van der Vaart, E. de Weert, C. de Visser, A. in 't Veld, and E. Mooij, *Flight Dynamics - Lecture Notes*, 3rd ed., Delft University of Technology, 2013.
[32] T. Singhanart, C. Srimontik, and N. Pisitpan, *Design and Analysis of UAV Fuselage*, 2012.
[33] S. Yüksel, "Low Velocity Impact Analysis Of A Composite Mini Unmanned Air Vehicle During Belly Landing," Master's thesis, Middle East Technical University, 2009.
[34] T. H. G. Megson, *Aircraft Structures for Engineering Students*, 4th. Elsevier Aerospace Engineering Series, 2007.
[35] B McGinty, *Von Mises Stress*, `http://www.continuummechanics.org/cm/vonmisesstress.html`, 2012.
[36] P. Grant and C. Q. Rousseau, *Composite Structures Theory and Practice*. ASTM International, 2001.
[37] R. Austin, *Unmanned Aircraft Systems*. John Wiley and Sons Ltd, 2010.
[38] W. Callister, *Materials Science and Engineering*. John Wiley and Sons, 1985.
[39] K. K.Choi and N.-H. Kim, *Structural Sensitivity Analysis and Optimization 1*. Springer, 2005.
[40] A. Deperrois, *Modal Analysis and Experimental Validation*, XLFR5.
[41] M. Rodzewicz, "Airworthiness Tests of the UAV Structure Fatifue Issues," *Fatigue of Aircraft Structures*, vol. 1, no. 1, pp. 82–93, Mar. 2012.
[42] H. Thorsen, "Low-Velocity Impact Simulation Using an Explicit Finite Element Method," Master's thesis, Chalmers University of Technology, 2013.
[43] D. Wille, *Ecolizer 2.0*. OVAM, 2009.
[44] R. Curran and W. Verhagen, *AE3211-I Systems Engineering and Aerospace Design Lecture 8*, PowerPoint Presentation, 2013.
[45] R. J. Vidmar and K. R. Stalder, "Air Chemistry and Power to Generate and Sustain Plasma: Plasma Lifetime Calculations," in *41st Aerospace Sciences Meeting and Exhibit*, AIAA, Reno, Nevada, Jan. 2003.
[46] Unknown, *XTend®OEM RF Modules*, Digi International Inc., 2014.
[47] ——, *XStream®OEM RF Modules*, Digi International Inc., 2014.
[48] G. Zhao, Y. Li, H. Liang, M. Han, and Y. Wu, "Flow separation control on swept wing with nanosecond pulse driven DBD plasma actuators," *Chinese Journal of Aerodynamics*, vol. 28, no. 2, pp. 368–376, Mar. 2015.
[49] B. DeBlauw, E. Lazar, N. Kale, N. Glumac, G. Dutton, and G. Elliott, "Flow an Thermal Properties Induced by Electric Arc Plasma Actuators," in *49th AIAA Aerospace Sciences Meeting including the New Horizons Forum and Aerospace Exposition*, Orlando, Florida: AIAA, Jan. 2011.
[50] D. Tillotson, "Drag Reducation and Directional Control of a Projectile Using Plasma Actuators," Master's thesis, Graduate School of the University of Notre Dame, 2009.
[51] V. Narayanaswamy, N. Clemens, and L. Raja, "Method for aquiring pressure measurements in presence of plasma-induced interference for supersonic flow control applications," *Maseurement Science and Technology*, vol. 22, 2011.
[52] S. van Leeuwen, "Electromagnetic Interference on Low Cost GPS Receivers," National Aerospace Laboratory NLR, Tech. Rep., 2008.
[53] Y. Utkin, S. Keshav, J. Kim, J. Kastner, I. Adamovich, and M. Samimy, "Development and use of localized arc filament plasma actuators for high-speed flow control," *Journal of Physics D: Applied Physics*, vol. 40, pp. 685–694, Jan. 2006.
[54] D. Griffiths, *Introduction to Electrodynamics*. Prentice Hall, 1999.
[55] A. Tsaliovich, *Electromagnetic Shielding Handbook for Wired and Wireless EMC Applications*. Boston: Kluwer Academic Press, 1999.

[56] E. Peers, H. Xun, and L. Xinfu, "A Numerical Model of Plasma-Actuator Effects in Flow-Induced Noise Control," *IEEE Transactions on Plasma Science*, vol. 37, no. 11, pp. 2250–2256, Nov. 2009.
[57] G. Ruijgrok, *Elements of Airplane Performance*. VSSD, Aug. 2009.
[58] B. Miller, C. Warnock, C. Valoria, and J. Coutlee, "Lightweight Unmanned Aerial Vehicle Launcher," Aerojet Rocketdyne, Tech. Rep., Aug. 2012.
[59] G. Ruijgrok, *Elements of Aviation Acoustics*. Delft University Press, Dec. 1993.
[60] Anon, *Prediction Procedure for Near Field and Far Field Propeller Noise*, AIR, 1977.
[61] E.-L. Bertsch, "Noise Prediction within Conceptual Aircraft Design," Master's thesis, TU Braunsweig - Campus Forschungsflughaven/Deutsches Zentrum für Luft- und Raumfahrt, Institut für Aerodynamik und Strömungstechnik, Braunschweig, May 2013.
[62] K. Fidler, "Subsystem Acoustic Testing of A Vertical Takeoff and Landing Ducted Propeller Unmanned Aerial Vehicle," Aviation, Missile Research, Development, and Engineering Center, Tech. Rep., Mar. 2004.
[63] The European Parliament and Council, "Directive 2002/3/CE relating to ozone in ambient air," The European Parliament and Council, Tech. Rep. OJ L67, Mar. 2002, pp. 14–30.
[64] D. Hong, H. Rabat, J. Bauchire, and M. Chang, "Measurement of Ozone Production in Non-thermal Plasma Actuator Using Surface Dielectric Barrier Discharge," *Plasma Chem Plasma Process*, no. 34, pp. 887–897, Feb. 2014.
[65] B. J. de Oliveira Martins Franco and L. C. S. Goes, "Failure Analysis Methods in Unmanned Aeroial Vehicle (UAV) Applications," in *International Congress of Mechanical Engineering*, COBEM, vol. 19, Nov. 2007.
[66] M. Peck, Ed., *Pentagon Unhappy About Drone Aircraft Reliability, Rising Mishap Rates of Unmanned Vehicles Atributed to Rushed Deployments*, National Defense Magazine, May 2003.

Appendix A - Division of Tasks

This appendix shows a table of the different parts in the report and which group members worked on the respective part or reported on it.

Chapter	Part	Name
Summary	Summary	Tim
Introduction	Introduction	Emilie, Amber, Vincent
Project Overview	Literature study	Amber, Tim
	Mission analysis	Vincent, Amber
UAV Design Description	Constraint analysis	Yorrick
	Configuration Description	Emilie, Konstantin, Vincent
Technical UAV design	Propulsive System	Konstantin
	Power System	Siying, Victor, Amber
	Parachute	Konstantin, Amber
	Fuselage Layout	Victor, Siying, Yorrick
	Plasma actuator integration	Amber, Tim, Emilie
	Wind tunnel test	Emilie, Tim
	Aerodynamics	Emilie, Tim, Yorrick, Amber
	Structural Design	Vincent Niels, Edze
	Stability and Control	Siying, Tim
	Validation	Tim
	CAD Drawings	Yorrick, Victor
Operational Details	Sustainable Development	Vincent, Yorrick
	RAMS Analysis	Edze, Tim, Konstantin, Emilie
	Production Plan	Vincent
	Avionics	Victor, Siying
	Performance Analysis	Emilie, Konstantin, Tim
	Risk Analysis	Emilie
Conclusion and Discussion	Conclusion	Niels, Tim
	Discussion	Vincent, Konstantin, Tim

Appendix B - Personal Appendices

B.1 Edze Algera - 4158326

The Design Synthesis Exercise has been a very interesting project. A challenging objective, an extremely motivated team, dedicated academic staff and a full 10 weeks time offered me an experience I never had before. Designing a new kind of vehicle really put all the learned theory to practice and showed more than any other project what actual design is about. In a relatively large group of ten students it proved quite a task to distribute work while keeping personal preferences in mind. Personally I chose this subject for my interests in aerodynamics, on which I also worked the first few weeks. After that most of my time was devoted to structures and materials, as I also quite enjoyed the course on Structural Analysis and Design. The great amount of code needed for this part, required me to really improve on programming in Matlab, as I was used to Python. That proved to be cumbersome at times but in the end was a fruitful aspect of the project. Another interesting aspect was the trade-off in the design that sometimes led to discussion between different parts of the team. For example, a change in landing operations caused an alteration in tail-boom dimensions which influenced stability issues. These discussions are really interesting and give insight in how to best handle in such situations, how to get a point across and how to keep discussions to the point. Gaining knowledge in new fields really motivated me. I also liked the positive and helpful attitude of Marios, Andrea, Wei and Joost. Asking any questions to them or other academic staff was no problem and always gave interesting insight. I really enjoyed the project and look forward to another thesis at this faculty.

B.2 Yorrick Bauer - 4210654

The past 11 weeks of DSE have formed an excellent excercise to integrate all knowledge obtained in the bachelor and work effectively in a design team. This team was very capable and enthousiastic as this project was the first choice for everyone, leading to a professional work environment. Additionally, the cooperative and constructive feedback of the mentors was very helpful. The real novelty was not to design a UAV, as this is done quite straightforwardly following design books; it was to implement the plasma actuators into the design, which was unfamiliar for the whole team. Finally, I think the wind tunnel test required a more practical approach than most other DSEs, and gave a better understanding of the plasma.

B.3 Amber E. van Hauwermeiren - 4171616

The project was a perfect experience in many ways. For starters, we were working with seemingly futuristic technology. Also, I have the feeling that we were actually innovating some fields (plasma control mechanisms, high voltage signal generation, dealing with integration issues like electromagnetic interference and weight), which makes all the effort feel worthwhile.

The design could not have been realised without the good project group we had. In contrast to most projects, everyone was interested into the subject and serious about obtaining a design ready for production. The whole team took to heart the advice of Marios as well, to 'not forget to have fun', which made the 10 weeks way more bearable than they could have been.

The tutoring and external help were really helpful. To produce a valid design, the feedback on academic level concerning the aerodynamics was vital and much appreciated. Although only on a BSc level, the project gave a hint of what it is like to perform a masters thesis.

A big challenge for me in this DSE, was to make sure everyone was doing useful work and keep everyone going in the right direction. The hardest part was to find a design process that left room for out-of-the-box ideas.

Although the wind tunnel test provided some really nice practical experience, more than we could have hoped for in a DSE, I still find it a shame that no test model was and probably will be built in the end. Maybe MAVLab?

B.4 Vincent C. van 't Laar - 4144481

At the beginning of the project the team started with very good motivation and team effort. Everyone contributed how they could. I immediately mentioned not being good with literature studies due to my dyslexia, so I helped elsewhere where possible. Throughout almost the entire project the team kept a friendly environment. It was pleasant to be here and work on the thesis with everyone since the atmosphere was almost always positive. The coaches did a good job at informing us with respect to plasma and aerodynamics (especially Marios and Andrea), however maybe a bit more help with respect to designing a UAV would have been useful since the bachelor focusses on aircraft design.

I don't think that many things in the DSE were new to me apart from anything to do with plasma, and the most challenging part was writing the structural code with Niels. I learned some new commands with MatLab and LaTeX, and I learned more about group dynamics. The most frustrating part was doing the final checks for the report before handing it in since it is hard to know when it is 'good enough'.

B.5 Emilie Pronk - 4094018

The thing that I found most interesting is the fact that we had a project where something new had to be made, instead of most projects where something existing has to be improved or be adjusted. It was a totally new concept, making it a very original project. The concept of plasma actuator mechanisms was new for me, I had never even heard of those things before, which made it stimulating to both design a UAV and integrate those actuators. The most difficult and challenging part of the project was probably the fact that we had to work with ten students together. In the beginning, meetings and discussions took a long time, but throughout the project we started to get more organized. About the coaching, I was glad that we even had four coaches, which gave us good feedback and tips. Also it was nice that we could just ask anybody from the TU for help and they would be there for you to give advice as well. I mostly worked on the aerodynamics and the integration of the plasma actuators the past ten weeks. I found this the most exciting part of the project and in the end I can say that I have learned a lot!

B.6 Tim Roos - 4209648

I think this DSE project was one of the most interesting ones available, since it covered a concept that was new to everyone, plasma actuator. This meant that all of us had to call on our theoretical knowledge and literature study abilities, which I think was very educative. Since the top level requirements were so basic and broad I think the group struggles a little bit in the beginning with where we had to start, but I think that the weekly meetings with the tutors helped in this. The novelty of the plasma actuator was definitely calling but also stimulating, I really wanted to gain a proper understanding and deliver a true proof of concept. I liked the fact that the coaching was very open, we were given a lot of room to do what we wanted to which was very liberating.

I think the entire group worked well together, and we all brought quite a lot of varying expertise to the table. We made sure to work within those areas of expertise, which helped the overall quality of the design. As for the coaching, like I mentioned before I liked the fact that we had a lot of freedom in the design. I feel that on some parts a little bit more guidance could have been given, mainly regarding the systems design since a lot of the knowledge we gained during the undergraduate phase was not applicable to small UAVs. We were however given a lot of names of people within the university with expertise so we were able to contact the right people in the end.

B.7 Konstantin Saß - 4131916

During the past DSE project, I highly enjoyed the fact that we were to implement one specific technology into a UAV, instead of having to design a technological advancement in several disciplines, which would make it a rather generic DSE. I think the most difficult moments were those in which we had to make a big next step. With that I mean for example going from the requirements to an initial sizing. This was difficult because not only the entire group had to be on the same wavelength, but also since all the parts are interrelated. I think the group dynamics of a DSE group was different than those in regular projects. Not only because we work every day, but because it was more important to interact and communicate with each other. Moreover, I think that it gave me definitely some new insights since the knowledge of ten different people is shared with each other. In that way I think that we had a good group: everyone

had sufficiently differentiated knowledge and preferences. Regarding the coaching, I think that there was a nice and good way of communication. The aerodynamics part was obviously the part on which more or less the most work was put into and therefore it was nice to have aerodynamic tutors.

B.8 Victor C. Sonneveld - 4218426

Out of all the projects in the bachelor I definitely enjoyed the DSE most. This was due to the fact that a lot of disciplines meet and you really have to negotiate between these. Going through the entire process of design and iteration was really interesting and was the opportunity to apply a lot of knowledge gained in the bachelor phase. I also enjoyed the fact that we were really free in the design. We did not have many requirements and the amount of deliverables were limited. Although I sometimes thought that meeting our tutors once a week was not sufficient, we actually learned to make more decisions ourselves. Additionally, we had good communications with our coaches using email and skype.

Being in a project with ten colleagues means that the group is bound to have many discussions. I think that the group learned in the process to discuss things in a more efficient way, by sticking to the point and in meetings with the entire group only discuss what really needs to discussed.

Finally, the planning that we had for the project turned out to be very helpful and allowed us to meet all the deadlines without stress.

B.9 Niels Waars - 4226275

The DSE project has been a great experience. The unique opportunity to work full-time on a design project for eleven weeks greatly improved my experience on teamwork and the design process. During previous projects the way to go was much more fixed than during the DSE project. We had really a lot of freedom in our decisions and it was nice to see how the decisions you make in an early stage of the DSE work out over time. Especially because we were provided with a short list of requirements, we had a lot of freedom in our design. Also the group discussions we had in the early stage are a good experience. I think we learned how we could be more efficient in those discussions and that we have improved our discussions a lot.

Personally I chose this project because of my interest in aerodynamics. However, during the project I did not work a lot on aerodynamics. Only at the start of the project I worked on the literature study on plasma actuators. After all, my work on the structures and materials parts was also interesting and I think all the team members were content with their part. The guidance of the project was adequate, the communication was good and the tutors helped us without pushing us in a certain direction.

B.10 Siying Wang - 4224671

The past 11 weeks has been a great experience to me and I've learnt a lot from the group and the DSE project. I chose this project because plasma actuators are newly developed concept and the challenge in controlling the UAV is also fascinating to me. I really enjoyed the fact that I had the change to fully dive into the stability analysis. At the beginning, the project was a bit frustrating because most of the time was spent on system engineering and planning although I do understand that system engineering is essential to the design. After the mid-term review, the project shifted its focus to the technical design. The mentors helped us a lot during the project, especially in aerodynamics and arranging for the wind-tunnel test. We maintained good communication and made use of the feedback from the mentors. It would be better though, if there could be another mentor available in design and system engineering, since aircraft/spacecraft design is always an important part in every project.